HHS Public Access

Author manuscript

Nat Metab. Author manuscript; available in PMC 2022 January 11.

Published in final edited form as:

Nat Metab. 2020 November ; 2(11): 1284–1304. doi:10.1038/s42255-020-00298-z.

CD38 ecto-enzyme in immune cells is induced during aging regulating NAD+ and NMN levels

Claudia C.S. Chini[a], **Thais R. Peclat**[a], **Gina M. Warner**[a], **Sonu Kashyap**[a], **Jair Machado Espindola-Netto**[a], **Guilherme C. de Oliveira**[a], **Lilian S. Gomez**[a], **Kelly A. Hogan**[a], **Mariana G. Tarragó**[a], **Amrutesh S. Puranik**[a,#], **Guillermo Agorrody**[a], **Katie L. Thompson**[a], **Kevin Dang**[b], **Starlynn Clarke**[b], **Bennett G. Childs**[c], **Karina S. Kanamori**[a], **Micaela A. Witte**[a], **Paola Vidal**[a], **Anna L. Kirkland**[a], **Marco De Cecco**[d,$], **Karthikeyani Chellappa**[e], **Melanie R. McReynolds**[f], **Connor Jankowski**[f], **Tamara Tchkonia**[g], **James L. Kirkland**[g], **John M. Sedivy**[d], **Jan M. van Deursen**[c], **Darren J. Baker**[c], **Wim van Schooten**[b], **Joshua D. Rabinowitz**[f], **Joseph A. Baur**[e], **Eduardo N. Chini**[a,*]

[a]Signal Transduction and Molecular Nutrition Laboratory. Kogod Aging Center, Department of Anesthesiology and Perioperative Medicine, Mayo Clinic College of Medicine, Rochester, MN 55905, USA

[b]Teneobio Inc., 1490 O'Brien Drive, Menlo Park, CA 94025, USA.

[c]Department of Biochemistry and Molecular Biology, Mayo Clinic, Rochester, MN 55905, USA.

[*]To whom correspondence should be addressed: 222 3rd Ave. SW, 55905, Phone: (507) 284-6696, chini.eduardo@mayo.edu.
[#]Current address for A.S.P. is Division of Rheumatology, Department of Medicine, NYU Langone Health, NY 10016
[$]Current address for M.D.C is Astellas Institute for Regenerative Medicine, 33 Locke Drive, Marlborough, MA 01752

Author Contributions

E.N.C., C.C.S.C generated the original hypothesis and concept of the manuscript. All authors contributed to the development of the hypothesis and experimental approaches. C.C.S.C., T.R.P., and K.A.H. performed cell isolations and experiments. M.G.T., G.C.O., J.M.E.N, T.R.P., S.K., K.T., G.A., J.M.S. and M.D. designed and performed animal studies. B.G.C., D.J.B., and J.M.vD. established the INK-ATTAC cohort, treated mice with AP or Vehicle, and prepared tissues for expression analyses. J.K. and T.T. contributed with reagents and design for senescence experiments. C.C.S.C., E.N.C., M.G.T., T.R.P., J.M.E.N., K.S.K., G.C.O., L.S.G, G.A., M.A.W., P.V., A.L.K., K.C., M.R.M., C.J., J.D.R., and J.A.B. designed, performed, and interpreted enzymatic analyses and nucleotide measurements. A.S.P. and S.K. performed flow cytometry. S.K. and G.M.W. performed immunohistochemistry. K.A.H., G.M.W., and L.S.G. performed PCR analyses. K.A.H. performed cytokine measurements. C.C.S.C., M.A.W., and G.M.W made CD38 constructs. W.vS., K.D., and S.C. developed and screened the anti-CD38 antibodies. J.M.E.N developed the method used to measure NMN in the serum. All authors contributed to the writing of the manuscript.

Competing Interests Statement

Dr. Chini holds a patent on the use of CD38 inhibitors for metabolic diseases that is licensed by Elysium health. E.N.C is a consultant for TeneoBio, Calico, Mitobridge and Cyokinetics. E.N.C is on the advisory board of Eolo Pharma (Santa Fe, Argentina) W.v.S. is the Chief Scientific Officer of Teneobio, a company interested in the development of therapeutic antibodies. W.v.S, K.D., E.N.C, and S.C own stocks of Teneobio. J.L.K., T.T., J.M.vD., and D.J.B. have a financial interest related to this research: patents on transgenic animals capable of being induced to delete senescent cells are held by Mayo Clinic. J.L.K., T.T., D.J.B. and J.M.v.D. are co-inventors on patent applications licensed to or filed by Unity Biotechnology, a company developing senolytic medicines, including small molecules that selectively eliminate senescent cells. J.M.v.D. is a co-founder of Unity Biotechnology. J.M.S. is a cofounder of Transposon Therapeutics, Inc., serves as Chair of its Scientific Advisory Board, and consults for Astellas Innovation Management LLC, Atropos Therapeutics, Inc. and Gilead Sciences, Inc. J.D.R. is a member of the Rutgers Cancer Institute of New Jersey and of the University of Pennsylvania Diabetes Research Center; a co-founder and stockholder in VL54, Sofro, and Raze Therapeutics; and advisor and stockholder in Agios Pharmaceuticals, Kadmon Pharmaceuticals, Bantam Pharmaceuticals, Colorado Research Partners, Rafael Pharmaceuticals, and L.E.A.F. Pharmaceuticals. J.B. has intellectual property related to the use of NAD precursors in liver regeneration. All other authors declare no conflict of interest. This research has been reviewed by the Mayo Clinic Conflict of Interest Review Board and is being conducted in compliance with Mayo Clinic Conflict of Interest policies.

[d]Center on the Biology of Aging, and Department of Molecular Biology, Cell Biology and Biochemistry, Brown University, 70 Ship Street, Providence, RI 02903, USA.

[e]Department of Physiology and Institute for Diabetes, Obesity, and Metabolism, Perelman School of Medicine, University of Pennsylvania, Philadelphia, PA 19104, USA.

[f]Lewis-Sigler Institute for Integrative Genomics, Department of Chemistry, Princeton University, Princeton NJ

[g]Robert and Arlene Kogod Center on Aging, Mayo Clinic, Rochester, MN 55905, USA

Abstract

Decreased nicotinamide adenine dinucleotide (NAD^+) levels have been shown to contribute to metabolic dysfunction during aging. NAD^+ decline can be partially prevented by knockout of the enzyme CD38. However, it is not known how CD38 is regulated during aging, and how its ecto-enzymatic activity impacts NAD^+ homeostasis. Here we show that increases in CD38 in white adipose tissue (WAT) and liver during aging is mediated by accumulation of $CD38^+$ immune cells. Inflammation increases CD38 and decreases NAD^+. In addition, senescent cells and their secreted signals promote accumulation of $CD38^+$ cells in WAT, and ablation of senescent cells or their secretory phenotype decrease CD38, partially reversing NAD^+ decline. Finally, blocking the ecto-enzymatic activity of CD38 can increase NAD^+ through a nicotinamide mononucleotide (NMN)-dependent process. Our findings demonstrate that senescence-induced inflammation promotes accumulation of CD38 in immune cells that through its ecto-enzymatic activity decreases levels of NMN and NAD^+.

Keywords

CD38; NAD^+; aging; senescence and inflammaging

Introduction:

NAD^+ is a critical nucleotide involved in oxidation-reduction reactions[1–4] and is a substrate to a group of diverse enzymes, including PARPs and sirtuins, involved in several aspects of cellular homeostasis[1–4]. NAD^+ levels decrease during aging and in progeroid states, contributing to metabolic dysfunction and decline in overall fitness[5–14]. Several mechanisms have been proposed to explain this NAD^+ decline. For example, levels of NAMPT, the rate-limiting enzyme of the NAD^+ salvage pathway, may decline during aging[15–17]. Another hypothesis proposes that the DNA repair enzyme PARP1 consumes and depletes NAD^+ during aging[10,11]. Finally, levels and activity of the NADase CD38 increase during aging, leading to NAD^+ decline[5,12], and CD38 inhibition preserves tissue NAD^+ during chronological aging[5,12]. Yet, several aspects of CD38 biology remain open questions in the aging field, including: 1) which cells express CD38 during aging; 2) what drives CD38 expression; and 3) what role does its ecto-enzymatic activity play in the regulation of tissue nucleotides.

A prevailing explanation for the aging process is the “inflammaging” hypothesis[18]. Accumulation of senescent cells with a secretory phenotype promotes chronic sterile

inflammation that leads to age-related dysfunctions[18–21]. Interestingly, CD38 is expressed mostly in immune cells[22], and it is possible that inflammaging could induce CD38 accumulation in tissues. Indeed, secreted factors from radiation-induced senescent cells *in vitro* induce CD38 expression in macrophages[23]. However, a possible mechanistic link between senescent cells, inflammation, CD38, and tissue NAD^+ decline *in vivo* during aging has never been explored.

Another unique characteristic of CD38 is its cellular localization. The majority of CD38 has a type II membrane orientation, with the catalytic site facing the outside of cells[24–27], functioning as an ecto-NADase[24–26,28,29]. However, CD38 has also been observed in intracellular membranes[30–33], and in soluble intra- and extracellular forms[34,35]. The specific role of the ecto-enzymatic activity of CD38 in NAD^+ homeostasis has not been defined. In fact, how this ecto-enzyme impacts levels of NAD^+, which are predominantly intracellular, is known as the CD38 "topological paradox"[36].

Here we show that $CD38^+$ inflammatory cells accumulate in tissues during chronological aging. This increase is mediated, in part, by the "inflammaging" induced by senescent cells. Furthermore, we demonstrate that the ecto-enzymatic activity of CD38 regulates nicotinamide nucleotides levels *in vivo*, and that this is partially mediated by the extracellular degradation of the NAD^+ precursor NMN.

Results:

Accumulation of $CD38^+$ immune cells in tissues during aging

CD38 is expressed mainly in immune cells, tissue resident macrophages (Kuppfer cells), endothelial cells, and immune precursor cells[12,24,30,31,37–41]. Although we reported that CD38 levels increase during aging[5,12], it is unclear which cells express CD38 during this process. Because aging is considered a pro-inflammatory state, we hypothesized that the cells expressing CD38 during aging would be mostly immune cells. Thus, we performed immunohistochemistry and flow cytometry on white adipose tissue (WAT) and liver from young and aged mice (Fig. 1 and Extended Data Fig. 1). The frequency of total $CD38^+$ cells increased in WAT and liver of 28–32 month-old mice when compared to 3–4 month-old mice (Figure 1a-d). Furthermore, the frequency of $CD45^+/CD38^+$ cells in mouse WAT and liver increased with aging (Fig. 1a-d and Extended Data Fig. 1). No increase in $CD38^+/CD45^-$ or in $CD38^+$ endothelial cells ($CD38^+/CD31^+$) were found in WAT or liver (Fig. 1b,d and Extended Data Fig. 1a). Indeed, the $CD38^+/CD45^-$ population decreased in liver (Fig. 1d). $CD38^+/CD45^+$ cells could be found in immune clusters in both WAT and liver of older mice (Fig. 1a,c). Further characterization demonstrated an increase mostly in $CD38^+$ macrophages/monocytes in both WAT and liver, and T cells ($CD8^+$ and $CD4^+$) and granulocytes in liver of extremely old mice compared to young mice (Fig. 1e-g). An increase in $CD38^+$ cells was also observed when comparing 3–4 month-old with 22 month-old mice (Extended data Fig. 1b-c,e). In isolated immune cells, we confirmed that M1 macrophages, T cells, and NK cells possess CD38-NADase activity (Fig. 1h), with M1 macrophages having the highest activity (Fig. 1h).

In addition to an increase in the percent of $CD38^+$ cells with aging, we also observed a shift to higher fluorescence intensity, suggesting an increase in the amount of CD38 per cell (Fig. 1e, right panel and Extended Data Fig. 1c-d). Then, we explored whether cells from aged mice expresses more CD38 in response to inflammatory stimuli than cells from young mice. We focused on macrophages since pro-inflammatory stimuli induce CD38 NADase activity in these cells[23,39,40], and also because M1 macrophages have the highest CD38 activity compared to other immune cells (Fig. 1h). Interestingly, CD38 has been shown to be a marker of the M1 phenotype[42]. We isolated bone marrow derived macrophages (BMDM) from 3 month-old and 18 month-old mice, treated them with the CD38 inducer LPS, and found that macrophages from 18 month-old mice express more CD38 mRNA and protein and have higher CD38 NADase activity in response to LPS than those from young mice (Fig. 1i-k). Thus, increases in CD38 during aging may be mediated by accumulation of $CD38^+$ immune cells and potentially also by increased expression of CD38 per cell.

Accumulation of $CD38^+$ immune cells in tissues is sufficient to reduce NAD^+

To determine the role of $CD38^+$ immune cells in regulation of tissue NAD^+ homeostasis, we performed bone marrow transplant experiments (Fig. 2 and Extended Data Fig. 2). We also explored the role of inflammation in CD38 accumulation by the administration of LPS. In control experiments we injected LPS in wild type (WT) mice and observed an increase in mRNA levels of *Cd38*, *F4/80*, and *Cd45*, and clusters of $CD38^+/CD45^+$ cells in the adjacent WAT (Extended Data Fig. 2a-b).

CD38 knockout (KO) mice were transplanted with bone marrow cells from WT (WT>KO) or CD38 KO mice (KO>KO) (Fig. 2a). Young animals (3–4 month-old) were used because older animals already have tissue inflammation and do not tolerate bone marrow transplants. As shown in Fig. 2b-g and Extended Data Fig. 2c-h, the WT>KO transplant induced accumulation of $CD38^+$ cells in several tissues. In tissues that normally contain high levels of immune cells, like spleen and intestine, there was an increase in CD38 activity and a decline in NAD^+ that did not depend on the inflammatory status (Extended Data Fig. 2c-d). In fact, in these tissues, CD38 protein levels and total number of $CD38^+$ cells did not change upon LPS treatment (Extended Data Fig. 2e-f).

In contrast, WAT, liver, and pancreas of WT>KO mice had a small or no increase in CD38 expression and activity compared to KO>KO transplant, and no change in NAD^+ levels in the absence of LPS (Fig. 2b-d and Extended Data Fig. 2g-h). This indicates that $CD38^+$ immune cells have a negligible contribution to NAD^+ homeostasis under normal (non-inflammatory) conditions in these tissues of young mice.

Induction of inflammation by LPS in transplanted mice increased *Cd45* and *F4/80* mRNA, and CD45 positive cells in WAT independent of the bone-marrow donor cell type (Fig. 2e-f). Similarly, in *in vitro* experiments using BMDM from WT and CD38 KO mice, we saw that both genotypes responded similarly to LPS (Extended Data Fig. 2i-j). In fact, with the exception of CD38-specific enzymatic activity and CD38 expression, markers of the M1 phenotype were strongly increased in macrophages from both genotypes in response to LPS, with no statistical differences between WT and CD38 KO with respect to the expression of *Mcp1, Nos1,* or *Il6* (Extended Data Fig. 2i-j). Furthermore, markers of the M2

phenotype were similarly decreased upon LPS in WT and CD38 KO (Extended Data Fig. 2j). Consequently, CD38 is not necessary for either the LPS-induced M1 phenotype *in vitro,* or the LPS-induced immune infiltration *in vivo*.

LPS-induced inflammation caused tissue NAD^+ decline in WAT, liver, and pancreas of WT>KO, but not KO>KO mice (Fig. 2g and Extended Data Fig. 2g-h). Tissue NMN levels also decreased in WAT of the WT>KO mice treated with LPS, in comparison with WT>KO non-treated (Fig. 2g). These results suggest that inflammation induces accumulation of $CD38^+$ immune cells in tissues such as WAT, leading to disruption of NAD^+ and NMN homeostasis.

Accumulation of CD38 during aging is induced by cellular senescence

Accumulation of senescent cells plays an important role during aging[19–21,43–47], promoting chronic “sterile” inflammation via their senescence-associated secretory phenotype (SASP)[19,20,47]. Recently, we reported that conditioned medium from radiation-induced senescent cells promotes the M1 phenotype, and increases CD38 expression and activity in cultured mouse BMDM[23]. However, it is still unclear whether senescence plays a role in CD38 expression and NAD^+ homeostasis *in vivo.* Therefore, we investigated whether senescent cells induce accumulation of $CD38^+$ cells and cause NAD^+ decline during aging.

First, we examined whether senescent cells and $CD38^+$ cells were enriched in WAT of old mice. Senescent cells were identified by loss of lamin B1 and gain of ORF1 staining, as previously reported[48]. Indeed, $CD38^+$ cells and lamin $B1^-/ORF1^+$ cells were enriched in WAT from old mice (Fig. 3a-b). Furthermore, we found more $CD38^+/CD45^+$ cells, immune clusters, and $ORF1^+$ senescent cells in WAT of old, compared to young mice (Fig. 3b). $CD38^+$ cells could be found in proximity to, as well as at a distance from senescent cells (Fig. 3a-b). Additionally, $CD38^+$ cells were more widespread in old WAT than senescent cells (Fig. 3a-b). These observations support the hypothesis that senescent cells could be regulating CD38 in part, via their secreted soluble factors (SASP). Through SASP, they could affect immune cells distantly, therefore not requiring a direct interaction between these two cell types.

To study the role of senescence in CD38 regulation *in vivo*, we tested whether ablation of senescent cells in naturally aged mice could decrease CD38 levels and influence tissue NAD^+ decline. For these experiments we used a mouse model in which senescent cells were cleared during the aging process[43,44]. Senescent cells often express high levels of the cell cycle regulator $p16^{Ink4a}$, and the INK-ATTAC transgenic mouse model permits ablation of these $p16^{Ink4a}$-expressing senescent cells through the administration of the otherwise inert compound AP20187[43,44]. Clearance of $p16^{Ink4a}$ positive cells improves health and life-span in mice[43,44]. We tested the effects of AP20187 on the expression and catalytic activity of CD38 in cells. AP20187 did not affect the LPS-induced CD38 expression or activity in macrophages (Extended Data Fig. 3a-b). In light of the absence of direct effects of AP20187 on CD38, we used INK-ATTAC mice to explore the effect of senescence clearance on CD38 regulation in WAT and liver (Fig. 3c-e and Extended Data Fig. 3c-g). Clearance of $p16^{Ink4a}$ senescent cells starting at 12 months of age through 28 months of age decreased the expression of the senescence marker *p16* (Fig. 3d and Extended Data Fig. 3f) and the

amount of immune cells, immune clusters, ORF1$^+$ cells, and the SASP component IL6 in WAT (Extended Data Fig. 3c-d). More importantly, senescent cell clearance decreased CD38 expression in WAT, bringing CD38 expression to levels similar to middle age mice (12 month-old) (Fig. 3d). This suggests that senescence could be a major contributor to the accumulation of CD38 during aging in WAT. Interestingly, clearance of senescent cells in old mice led to only a small recovery of WAT NAD$^+$ and NMN (Fig. 3e and Extended Data Fig. 3e), suggesting that cellular senescence-induced CD38 accumulation is not the only factor responsible for the NAD$^+$ decline observed in WAT during aging. In liver, clearance of senescent cells, as determined by a decrease in *p16*, led to a decrement in *Cd38* expression and, unlike WAT, promoted a larger reversal of tissue NAD$^+$ decline (Extended Data Fig. 3f-g). These data indicate that in liver, the senescence-induced CD38 expression may play a more prominent role in aging-induced NAD$^+$ decline.

It has been proposed that senescent pre-adipocytes accumulate during aging[46], and injection of senescent pre-adipocytes in young animals recapitulates several age-related phenotypes[46]. Therefore, we tested whether injection of senescent pre-adipocytes induces the accumulation of CD38$^+$ inflammatory cells in WAT (Fig. 3f). X-ray treated pre-adipocytes expressed several markers of cellular senescence, such as *p16* and *p21*, and showed increased expression and levels of IL6 and other SASP components such as MCP-1, Eotaxin, GDF15, and FGF (Extended Data Fig. 3h-i). We were unable to detect significant levels of TNF-α, a well-known inducer of CD38, in the CM from either control or senescent mouse pre-adipocytes. Interestingly, induction of senescence by X-ray did not change the expression of *Cd38* in the pre-adipocytes themselves (Extended Data Fig. 3h). Injection of senescent pre-adipocytes, but not non-senescent pre-adipocytes, in WT mice led to an accumulation of CD38$^+$/CD45$^+$ inflammatory cells near senescent cells in WAT (Fig. 3g).

To determine whether the CD38$^+$ cells could be, in part, originating from the periphery, we injected vehicle, non-senescent, or senescent pre-adipocytes intraperitoneally into CD38 KO mice and 2 days later we injected luciferase-expressing peripheral blood mononuclear cells (PBMC) from CD38 WT mice (Fig. 3h). Two days later, WAT was harvested and the accumulation of CD38 was quantified by RT-PCR. There was an increase in accumulation of the luciferase signal and CD38 expression in WAT when senescent cells were injected in comparison to non-senescent cells and PBMC-only injected mice (Fig. 3i-j), indicating that there was an increase in infiltration of circulating CD38$^+$ cells induced by cellular senescence. These data demonstrate that cellular senescence can induce CD38 accumulation in WAT *in vivo*.

Accumulation of CD38 *in vivo* can be induced by SASP

To explore the possibility that changes in CD38 accumulation and NAD$^+$ decline in WAT were driven partially by the SASP, we injected conditioned media (CM) from senescent pre-adipocytes in WAT of mice and measured CD38 expression, CD38-NADase activity, and NAD$^+$ levels *in vivo*. In control experiments we confirmed that CM from senescent mouse pre-adipocytes (CM-SEN) increased CD38 expression and activity in mouse macrophages in culture, compared with CM from non-senescent pre-adipocytes (CM-NS) (Extended Data Fig. 4a-b). Consistent with our hypothesis, CM-SEN increased CD38 activity and caused

tissue NAD^+ decline in WAT collected from the site of the subcutaneous injection (Fig. 4a). Additionally, CM-SEN increased expression of *Cd38* and the inflammatory cell markers *Cd45* and *F4/80* in WAT *in vivo*, compared with CM-NS (Fig. 4b).

We subsequently tested whether inhibition of the SASP *in vivo* decreased expression of CD38 and reversed tissue NAD^+ decline in WAT. Recently, it has been described that during cellular senescence LINE-1 elements (L1s) such as ORF1 become transcriptionally de-repressed and activate late senescence contributing to the maintenance of the SASP[48]. Furthermore, it has been demonstrated that nucleoside reverse transcriptase inhibitors (NRTIs), such as lamivudine (3TC), inhibit the L1 reverse transcriptase (RT) and downregulate age-associated inflammation in WAT via inhibition of the SASP[48]. Hence, 3TC has been categorized as a "senostatic" agent, in contrast to "senolytic" agents that remove senescent cells from tissue. Here we used 3TC as a pharmacological tool to inhibit SASP (Fig. 4c). In control experiments we determined that 3TC did not directly inhibit CD38 activity in macrophages (Extended Data Fig. 4c). We treated aged mice (26 month-old) with and without 3TC for 2 weeks. As previously described[48], 3TC decreased the expression of SASP components, but not the senescent cell marker *p16* in WAT (Fig. 4d). Furthermore, 3TC decreased the expression of the macrophage marker *F4/80* by 40% and *Cd38* by 25% in WAT of aged mice (Fig. 4e). Notably, 3TC increased WAT NAD^+ levels nearly four-fold, in comparison with vehicle-treated mice (Fig. 4f). The incongruity between the magnitude of decrease in *Cd38* expression and increase in NAD^+ levels in WAT suggests that 3TC may regulate NAD^+ levels by a complex mechanism that may include inhibition of CD38 and other NAD^+-consuming enzymes. To investigate this possibility we tested whether 3TC decreased the expression of other NAD^+-consuming enzymes such as PARP1 and SIRT1. Akin to the decrease in *Cd38* expression, 3TC also decreased the expression of *Parp1* by about 25% (Fig. 4e), indicating that the 3TC-induced increase in NAD^+ may be mediated by inhibition of both CD38 and PARP1. In fact, we previously shown that PARP1 inhibition can potentiate the effect of CD38 inhibition in increasing NAD^+ levels in several tissues[5,12], providing an explanation for the robust effect of 3TC in NAD^+ levels *in vivo*, despite the modest inhibition of CD38 expression.

Next, we investigated whether senescent cells, secretory components, and $CD38^+$ cells could be found in proximity in tissues of old animals. As previously mentioned, senescent cells can be identified by loss of lamin B1 and gain of ORF1 staining (Fig. 3a). Senescent cells with the secretory phenotype (SASP) were identified by the presence of IL6 and a lack of lamin B1 (Fig. 4g). We chose IL6 as a marker of SASP based on our *in vitro* experiments showing that IL6 is abundantly secreted by senescent pre-adipocytes (Extended Data Fig. 3h-i). Also, we found that an anti-IL6 antibody, but not an anti-TNF-α antibody, was sufficient to decrease CD38 activity in BMDM induced by the CM-SEN from mouse pre-adipocytes (Extended Data Fig. 4d). Interestingly, an anti-TNF-α antibody blocked the increase in CD38 expression induced by mouse embryonic fibroblast (MEF) CM-SEN in HUVECs (Extended Data Fig. 4e), suggesting that different types of senescent cells may induce CD38 in non-senescent cells via distinct SASP factors.

The abundance of senescent cells and IL6 was increased in WAT of old compared with young mice (Fig. 4g and Extended Data Fig. 3c-d). Interestingly, some of the $CD38^+$

cells could be found near the senescent/SASP (IL6)-secreting cells in old mice (Fig. 4g). However, it is possible that non-senescent cells could also secrete factors that induce/attract $CD38^+$ cells in aged tissue. Collectively, our experiments in Figures 3 and 4 indicate that senescent cells and their SASP play a role in the accumulation of $CD38^+$ immune cells during aging.

CD38 is required for genotoxic/senescence-induced NAD^+ decline

Even though clearance of senescent cells/SASP decreased CD38 levels and prevented tissue NAD^+ decline during aging, we still do not know whether CD38 activity is indeed required for this NAD^+ decline. To address this question, we used an *in vivo* model of chemotherapy-induced cellular senescence. The chemotherapeutic agent doxorubicin cause cellular senescence *in vivo*, and several of the deleterious effects of doxorubicin appear to be mediated by senescent cells[49]. To investigate if senescence-mediated NAD^+ decline was caused by the accumulation of catalytically active CD38, we treated WT and transgenic catalytically inactive CD38 (CD38 CI)[12] mice with a single dose of doxorubicin (15 mg/kg) and 10 days later examined the burden of cellular senescence, levels of inflammatory cytokines, and expression of macrophage markers and *Cd38* (Fig. 5a-c). As previously reported[49], doxorubicin increased expression of the senescence marker *p21*, inflammatory cytokines, and the macrophage activation marker *F4/80,* and *Cd68*, a marker of total macrophage and monocyte lineage in WAT of WT mice (Fig. 5b and Extended Data Fig.5a). In addition, doxorubicin increased *Cd38* mRNA expression, protein levels, and activity in WT mice, and reduced tissue NAD^+ levels (Fig. 5c-f). Doxorubicin also increased the expression of senescent cell and SASP markers, the macrophage markers *F4/80* and *Cd68*, and both mRNA and protein levels of CD38 in WAT of CD38 CI mice (Fig. 5b-d). Importantly, *Cd38* mRNA levels in the CD38 CI mice were reduced in comparison to WT, but CD38 protein levels were similar between the two genotypes, and both mRNA and protein responded to doxorubicin treatment to the same extent in both genotypes (Figure 5c-d). Of note, doxorubicin treatment in the CD38 CI mice did not decrease tissue NAD^+ levels in WAT, indicating that CD38 activity is necessary for doxorubicin-induced NAD^+ decline (Fig. 5e-f). In conclusion, CD38 is downstream of cellular senescence in the cascade of events leading to tissue NAD^+ decline. Importantly, abrogation of CD38 catalytic activity uncouples senescence from tissue NAD^+ homeostasis.

The ecto-enzymatic activity of CD38 regulates NMN availability to cells

Even though we demonstrated that accumulation of $CD38^+$ cells have an important role in inflammation and age/senescence-related NAD^+ decline, it is not known how these $CD38^+$ cells regulate tissue NAD^+ levels. We previously proposed that $CD38^+$ cells regulate NAD^+ in other cells by modulating the availability of NAD^+ precursors[12]. However, it is unclear if this regulation occurs through the ecto-enzymatic activity of CD38. Since NAD^+ levels outside cells are very low or undetectable[50], the fact that the majority of CD38 catalytic activity faces the outside of the cell remains an intriguing element of CD38 biology[22,36].

We first investigated the roles of the ecto-versus intracellular CD38 in the regulation of NAD^+ and its precursors in cells. Our hypothesis was that intracellular CD38 activity regulates NAD^+ levels inside $CD38^+$ cells, and that its ecto-enzymatic activity modulates

the availability of extracellular precursors to other cells. We first transfected 293T cells with different CD38 expression constructs: vector, wild type CD38 (WT), a catalytically inactive CD38 construct (CI), or a truncated CD38 construct that is expressed exclusively intracellularly (Δ49) (Fig. 6a-b)[28]. We confirmed that the majority of the WT and CI CD38 were localized to the plasma membrane, while Δ49 was exclusively intracellular (Fig. 6b). Also, although the majority of WT CD38 was found as an ecto-enzyme in the plasma membrane, there was also intracellular localization of WT CD38, including in the cytosolic fraction (Fig. 6b and Extended Data Fig. 6a-b), mimicking the distribution of endogenously expressed CD38. Furthermore, both WT and Δ49 CD38 decreased NAD^+ levels in transfected cells (Fig. 6c). We next investigated whether it is the ecto- or intracellular activity of CD38 that regulates NAD^+ levels inside these cells. Cells transfected with WT and Δ49 CD38 were treated with: 1) the CD38 antibody isatuximab (SAR650984), which is cell impermeable[51] and inhibits only the ecto-enzymatic activity of CD38, or 2) the small molecule CD38 inhibitor 78c, which is cell-permeable and inhibits both the ecto- and intracellular activities of CD38[12,52]. In whole cell lysates from transfected 293T, isatuximab abolished the enzymatic activity of WT CD38 and Δ49 CD38 (Extended Data Fig. 6c-d). However, when added to intact transfected cells only 78c, but not isatuximab, increased NAD^+ levels in 293T cells expressing WT or intracellular Δ49 CD38 (Fig. 6d). Similar results were observed when cells were treated with NMN (Fig. 6e). Thus, we concluded that the intracellular CD38 activity observed in both WT and Δ49 CD38 transfections is sufficient to regulate intracellular NAD^+ levels, even when cells are treated with NMN. Interestingly, addition of recombinant CD38 to the culture media of untransfected 293T, mimicking a pure ecto-enzymatic activity of CD38, had no effect on baseline NAD^+ levels in these cells but completely prevented the NAD^+ boosting mediated by the addition of extracellular NMN. This effect was reversed by the addition of the blocking antibody isatuximab (Extended Data Fig. 6e), indicating that the ecto-enzymatic activity of CD38 only hydrolyzes substrates extracellularly.

To determine the role of the CD38 activity of one cell in the availability of NAD^+ precursors to other cells that do not express CD38, we performed co-culture experiments between 293T cells transfected with CD38 expression constructs in the upper chamber and AML 12 cells in the lower chamber (Extended Data Fig. 6f). AML 12 cells do not express significant amounts of CD38, but they do appear to express the putative NMN transporter Slc12a8[53]. Interestingly, under basal conditions none of the CD38 constructs expressed in 293T cells regulated NAD^+ levels in the AML 12 cells (Fig. 6f). In contrast, the NMN-mediated NAD^+ boosting in AML 12 cells was blocked by expression of WT CD38 in 293T cells (Fig. 6f). Expression of CI CD38 or Δ49 CD38 in 293T cells did not prevent the NMN-induced increase in NAD^+ in AML 12 cells (Fig. 6f), despite the fact that the Δ49 CD38 decreases NAD^+ and NMN responses in 293T cells expressing this construct (Fig. 6d-e). Furthermore, in co-culture experiments with 293T cells expressing WT CD38, addition of isatuximab reversed the inhibition of NMN-induced NAD^+ boosting in the AML 12 cells (Extended Data Fig. 6g). In conclusion, CD38 has a dual role in NAD^+ homeostasis, where the ecto-enzymatic activity of CD38 controls the availability of NMN to other cells, and the intracellular activity exclusively regulates NAD^+ homeostasis inside that cell.

The ecto-enzymatic CD38 activity of M1 macrophages regulates NMN availability

We next investigated the role of CD38 in NAD^+ homeostasis in immune cells that naturally express CD38, such as macrophages. BMDM treated with LPS to induce CD38 expression and activity had a decline in total cellular NAD^+ levels (Fig. 7a-c). Surprisingly, the CD38 inhibitor 78c did not prevent this NAD^+ decline (Fig 7a-c). LPS also induced NAD^+ decline in CD38 KO macrophages despite the absence of CD38 NADase activity, and this decline was also not prevented by 78c (Fig. 7b). These results indicate that, *in vitro,* LPS-induced NAD^+ decline in BMDM is not regulated by CD38 alone. Interestingly, Minhas et al. have proposed that LPS-induced NAD^+ decline in macrophages is mediated, in part, by LPS-induced PARP1 activation[54]. Thus, we tested whether the PARP1 inhibitor olaparib could prevent LPS-induced NAD^+ decline in macrophages. Akin to CD38 inhibition, PARP1 inhibition alone did not prevent this NAD^+ decline (Fig. 7c). However, combined inhibition of PARP1 and CD38 completely reversed the LPS-induced NAD^+ decline (Fig. 7c). In macrophages treated with the NAD^+ precursor NMN, we also observed that inhibition of CD38 and PARP significantly increased NAD^+ levels over levels in macrophages treated with LPS alone (Fig. 7d). In macrophages, NMN induced a minimal non-significant increase in intracellular NAD^+, likely due to the low level of expression of the putative NMN transporter Slc12a8 in these cells (Fig. 7e). This result contrasts with our observations in AML 12 cells, which express higher levels of Slc12a8 (Fig. 7e-f). Interestingly, expression of the enzyme *Nampt* increases in M1 macrophages, suggesting that these cells may be protected from the high CD38 expression by increasing NAD^+ levels via the salvage pathway (Extended Data Fig. 7a). Because CD38 alone is not sufficient to control intracellular NAD^+ levels or NMN availability to the macrophages themselves, we postulated that the function of the ecto-enzymatic activity of CD38 in M1 macrophages was to modulate the availability of NMN to other cells.

To inhibit the ecto-enzymatic hydrolase activity of mouse CD38 we developed specific heavy chain antibodies t (Extended Data Fig. 7b-g). These antibodies were developed using the UniRat technology, and were validated by binding to CD38 and inhibiting its hydrolase activity (Extended Data Fig. 7b-g). Antibody 68 (Ab68) was used as the prototype inhibitory antibody in our studies. Ab68 differs from clinically approved anti-CD38 antibodies in that it is a heavy chain antibody with an inactivated mouse IgG2a Fc tail, which prevents binding to mouse FcγRs and diminishes toxicity (Extended Data Fig. 7h-j) while still being a potent non-competitive inhibitor of CD38 hydrolase activity (Extended Data Fig. 7g). Indeed, in contrast to the commercially available anti-CD38 antibody NIMR-5, Ab68 is neither internalized by cells nor cytotoxic (Extended Data Fig. 7i-k). The specificity of Ab68 binding was validated using freshly isolated mouse spleen cells from WT and CD38 KO animals. Ab68 binds to WT but not CD38 KO cells (Extended Data Fig. 7f).

Co-culture of LPS-stimulated macrophages with AML 12 cells decreased the NAD^+ boosting effect of NMN in AML 12 cells, an effect that was reversed by Ab68 (Fig. 7f). In control experiments we cultured the AML 12 cells alone and found that NMN-induced NAD^+ boosting was unaffected by LPS or CD38 inhibitors (Extended Data Fig. 7l), indicating that the effects of LPS and Ab68 were dependent on macrophages. Next, we treated LPS-stimulated macrophages with NMN and measured NMN levels in the

media. NMN levels decreased in the media upon treatment of macrophages with LPS, and this effect was reversed by Ab68 (Fig. 7g). Thus, extracellular CD38 activity of M1 macrophages controls availability of NMN to other cells.

To determine the specificity of CD38 for NMN we performed similar experiments using the precursors NR, which is not a direct substrate for CD38[12,55]. NR-induced NAD^+-boosting in AML 12 cells was completely inhibited by co-culture with LPS-treated macrophages (Fig. 7h). However, the effect of LPS-treated macrophages on the NR-induced NAD^+ boosting in AML 12 cells was not reversed by Ab68 (Fig. 7h). This suggests that the effect of CD38 on NAD^+ boosting by extracellular precursors is specific for NMN. Next, we performed co-culture experiments using macrophages isolated from CD38 KO mice and AML 12 cells in the presence of NMN or NR. While LPS treatment of CD38 KO macrophages did not decrease NMN-induced NAD^+ boosting in AML 12 cells, it decreased NR-induced boosting (Extended Data Fig. 7m). Findings in CD38 KO macrophages treated with LPS confirm that the inhibitory effect of M1 macrophages on NMN-induced NAD^+ boosting in co-cultures with AML 12 cells is dependent on CD38. These experiments also indicate that in addition to CD38, M1 macrophages may express an alternative enzyme that modulates the availability of extracellular NR. This enzyme could be CD157/BST1, a gene duplication of CD38 that has been reported to hydrolyze NR, but not NAD^+ or NMN[55]. Indeed, LPS induced expression not only of *Cd38*, but also *Cd157*/*Bst1* in BMDM (Extended Data Fig. 7a).

We also performed co-culture experiments using nicotinic acid (NA). We observed a trend for NA to boost NAD^+ in the AML 12 cells co-cultured with macrophages that was not affected by LPS or CD38 inhibition with Ab68, possibly indicating that the NA effects were not modulated by CD38 (Extended Data Fig. 7n).

Next, we explored the role of secreted factors from senescent cells on BMDM NAD^+ homeostasis. Treatment of macrophages with CM-SEN leads to a three-fold induction of CD38 expression and NADase activity (Extended Data Fig. 4a-b and 7o). However, CM-SEN did not significantly change NAD^+ levels inside BMDM themselves (Fig 7i and Extended Data Fig. 7o). This is likely because CM-SEN is less potent as an inducer of CD38 expression in comparison to LPS (Extended Data Fig. 7o), and may not concomitantly activate PARP1 (Fig. 7a-c)[54,56].

In contrast, induction of CD38 in macrophages by CM-SEN decreased the NAD^+ boosting effect of NMN in AML 12 cells (Fig. 7j). Importantly, the effect of CM-SEN-treated macrophages on NMN-induced NAD^+ boosting in AML 12 cells was completely reversed by inhibition of the ecto-enzymatic activity of CD38 (Fig. 7j). There was also a trend toward decreased NMN levels inside AML 12 cells, which was reversed by treatment with Ab68 in the co-culture experiments with CM-SEN-treated macrophages (Fig. 7k). Therefore, we postulate that $CD38^+$ immune cells, such as M1 macrophages, through their ecto-enzymatic activity, modulate organismal NAD^+ homeostasis via degradation of the extracellular NAD^+ precursor NMN.

The ecto-enzymatic activity of CD38 regulates NAD^+ homeostasis via an NMN-dependent mechanism *in vivo*

Our experiments indicate that accumulation of $CD38^+$ immune cells in tissues such as WAT causes disruption of NAD^+ homeostasis during inflammation and the aging process. Moreover, our *in vitro* data suggest that the ecto-enzymatic activity of CD38 in immune cells may regulate the availability of NMN to cells in the tissue. To explore this possibility *in vivo*, we inhibited the ecto-enzymatic activity of CD38 in mice using our specific CD38 antibody.

Using 4 month-old (young) mice we characterized the effects of antibody Ab68 and the non-inhibitory antibody Ab69 on CD38 activity and NAD^+ levels in several tissues. Administration of the antibody Ab68 *in vivo* decreased CD38 activity and increased NAD^+ levels in WAT of WT mice, whereas control antibody Ab69 had no effect (Fig. 8a-b). In contrast, Ab68 did not raise NAD^+ levels in CD38 KO mice, indicating that the presence of CD38 appears to be required for the effect of Ab68 in NAD^+ levels (Fig. 8b). Similarly, in all other tissues analyzed from Ab68-treated WT mice there was a decrease in CD38 activity and increase in NAD^+ levels induced by this antibody (Extended Data Fig. 8a-b). On the other hand, akin to WAT, in other tissues from CD38 KO mice, Ab68 did not raise NAD^+ levels (Extended Data Fig. 8a-b). Ab68 did not significantly change mRNA expression of *Cd38* or other NAD^+ consuming enzymes in WAT (Extended Data Fig. 8c).

Although our data demonstrate that CD38 ecto-enzymatic activity regulates NAD^+ homeostasis *in vivo*, it is unclear which NAD^+ precursor is the substrate for CD38 in the extracellular space. Levels of free NAD^+ in the extracellular space are expected to be very low[50], therefore, it is possible that the primary substrate for CD38 in the extracellular space is NMN. We investigated whether CD38 regulates levels of NMN in WAT *in vivo*, and observed that NMN levels increase after Ab68 treatment (Fig. 8c). This increase was accompanied by a dramatic decrease in nicotinamide (NAM) levels (Fig. 8c). In contrast, Ab69 had no effect on any of the NAD^+ anabolic or catabolic metabolites (Fig. 8c). Increases in NMN and decreases in NAM were also found in liver and skeletal muscle of Ab68-treated mice (Extended Data Fig. 8d). Moreover, the boost in NMN induced by Ab68 in WT tissues was similar to the differences observed when we compared levels of this nucleotide in WT and CD38 KO mice, without antibody treatment (Fig. 8d and Extended Data Fig. 8d-e).

Treatment of mice with Ab68 had no significant effects on levels of the NAD^+ *de novo* pathway metabolites tryptophan, kynurenine and hydroxykynurenine, or quinolinic acid in WAT (Fig. 8c). Levels of NAM, but not nicotinic acid (NA), were dramatically decreased by treatment with Ab68, indicating that the main substrate for the CD38 ecto-enzymatic activity is NAM nucleotide derivatives and not NA nucleotides (Fig. 8c). WAT levels of NR were undetectable in both vehicle and A68-treated animals (data not shown). Finally, levels of ADPR were also decreased by the treatment with Ab68 (Fig. 8c) demonstrating that, in addition to NMN, NAD^+ is also degraded by the ecto-enzymatic CD38 activity.

To explore the possibility that NMN was required for the NAD^+ boosting effect of Ab68, we blocked the synthesis of NMN using an inhibitor of NAMPT, an enzyme involved in

the synthesis of NMN. As predicted, pre-treatment with FK866 abrogated both NMN and NAD^+ boosting caused by Ab68 in WAT (Fig. 8d), demonstrating that NMN is required for Ab68-induced NAD^+ boosting.

In order to understand the role of CD38 in NMN regulation, we determined the time course of increases in NMN and NAD^+ in WAT after treatment with Ab68 in aged mice. Consistent with our hypothesis, inhibition of CD38 ecto-enzymatic activity led to an increase in NAD^+ levels in WAT that was detected 4 hours after injection of Ab68 and was preceded by a faster and higher increase in NMN (Fig. 8e). In liver, we also detected an earlier increase in NMN followed by an increase in NAD^+ levels (Extended Data Fig. 8f).

We next tested whether inhibition of the ecto-enzymatic activity of CD38 increases NMN levels in the extracellular space. Blood is the only tissue where the concentration of extracellular components is readily available to study. We measured serum NMN in the presence of Ab68 to determine if the antibody could directly regulate NMN extracellular levels. Interestingly, Ab68 treatment promoted a rapid and sizable change in serum NMN levels (Fig. 8f). This result is consistent with the observation that NMN is rapidly metabolized in the extracellular space of mouse whole blood in a CD38-dependent manner (Extended Data Fig. 8g). In fact, the optimal pH for the NMNase reaction is 7.4, the same as extracellular pH (Extended Data Fig. 8h). Levels of NR in serum also increased about 4-fold, likely because of the conversion of NMN to NR (Extended Data Fig.8i).

The role of the ecto-enzymatic activity of CD38 in NMN degradation was also investigated by measuring levels of NMN in the serum after administration of an oral dose of NMN. Orally administered NMN is rapidly metabolized at first passage in the liver, and NMN levels are nearly undetectable after the administration of NMN[57]. Although oral administration of NMN in mice leads to nearly undetectable levels of NMN in the serum, treatment with Ab68 increased baseline NMN and boosted the effect of the administration of exogenous NMN in the serum levels of this precursor (Fig. 8g).

Finally, we compared the effect of Ab68 on NMN-mediated NAD^+ boosting in WAT of young and older animals. In untreated mice, absolute NAD^+ levels were decreased in old compared to young WAT (Fig. 8h). Consistent with the presence of CD38 in tissues of young and old mice, treatment with Ab68 increased NAD^+ in WAT of both ages, leading to similar total levels of NAD^+ in young and old mice (Fig. 8h). However, since the absolute NAD^+ levels in older animals in the control group were about seven times lower than in young animals, the relative (fold) increase induced by Ab68 was several times higher in older than in young mice (Fig. 8h-i). Ab68 also augmented the NAD^+-boosting effects of NMN in both young and old (Fig. 8i). However, the relative changes were much greater in old when analyzed relative to the NAD^+ levels of their respective age-matched controls (Fig. 8i). Since Ab68 increased NAD^+ levels in WAT of old mice, we investigated whether Ab68 regulated mRNA levels of inflammatory markers in old mice. As expected, in WAT of 18 month-old mice, there was an increase in expression of *Cd38*, *Cd45*, and all inflammatory markers tested compared to 3 month-old (young) mice. Treatment with Ab68 did not change the expression of either *Cd38* or *Cd45* in 18 month-old mice (Extended Data Fig. 8j). It did, however, lead to a significant decrease in *Il1b* expression and a decrease in

other inflammatory markers, such as *Mcp1* and *Tnfa*, which was not statistically significant (Extended Data Fig. 8j)

Discussion

Our study uncover a connection between age-related NAD^+ decline and inflammaging partially mediated by a senescence/SASP-induced accumulation of $CD38^+$ inflammatory cells in tissues. We found that multiple subsets of $CD38^+$ inflammatory cells accumulate during aging and are observed in immune clusters. Interestingly, these immune clusters have been described during aging in WAT and liver[58,59]. We further demonstrate that in pro-inflammatory conditions $CD38^+$ cells accumulate in tissues, leading to immune clusters and subsequent tissue NAD^+ decline.

The increase in $CD38^+$ cells during aging was prevented by clearance of senescent cells. Although collectively our results indicate that senescent cells, partially via their SASP, increase CD38 abundance, our findings do not exclude the possibility that other mechanisms could contribute to the increased CD38 accumulation observed during aging. It is possible that CD38 expression in macrophages and T cells may be mediated by an alternative mechanism. For example, it has been demonstrated that senescent cells can express major histocompatibility complex II (MHC-II)[60]. Perhaps, the direct interaction of T cells with the MHC II in senescent cells might increase CD38 expression. It is also possible that the increase in endotoxins observed in aged humans and mice[61,62] may induce CD38 expression. Thus, senescent cells, SASP and endotoxins together could be the driving forces that regulate CD38 expression in aging.

It is possible that non-senescent cells may also secret cytokines and chemokines that could promote recruitment and/or induction of CD38 expression in immune cells. However, because clearance of senescent cells *in vivo* during chronological aging reduced *Cd38* expression, amount of immune cells, immune clusters, $ORF1^+$ cells, and the SASP component IL6, it appears that senescent cells play an important role in the accumulation of $CD38^+$ immune cells in tissues during aging. Furthermore, senescent cells/SASP may promote a positive feedback-loop leading to further accumulation of $CD38^+$ cells. For example, senescent cells could recruit/activate immune cells, which further secrete chemokines and cytokines that amplify pathways leading to accumulation of $CD38^+$ immune cells in aging.

With regard to the role of senescence-induced CD38 accumulation in age-related NAD^+ decline, it appears that this mechanism plays a role in both WAT and liver. Interestingly, although senescent cell clearance in very old mice led to a decrease in *p16* and *Cd38* expression in both liver and WAT to levels comparable to 12 month-old mice (middle age), the effect on NAD^+ was less dramatic in WAT. Clearance of senescent cells in old mice almost completely reversed NAD^+ decline in the liver, but only partially recovered WAT NAD^+ levels, indicating that senescence-induced CD38 accumulation is not the only mechanism involved in age-related NAD^+ decline *in vivo*. It is likely that several mechanisms, additively or synergistically, may interact and contribute to the age-related NAD^+ decline. Indeed, activation of PARP1 has also been proposed to regulate this

process[10,11]. Interestingly, decreases in both CD38 and PARP1 may be responsible for the reversal in NAD^+ decline detected in our experiments of mice treated with the "senostatic" agent 3TC.

It is also important to highlight the studies proposing that decreases in expression of NAD^+-synthetic pathways may play a role in aging-related NAD^+ decline. The group led by Shi Imai has shown that NAMPT decreases during aging and regulates aging-related NAD^+ decline[14–17]. QPRT, an enzyme of the NAD^+ *de novo* synthetic pathway was also shown to decrease during aging[54]. Therefore, it appears that a complex interaction between several enzymes and pathways is responsible for aging-related NAD^+ decline.

The *in vivo* experiments performed with Ab68 allowed us to better understand the role of the ecto-enzymatic activity of CD38. Although our experiments indicate that presence of CD38 is required for the binding and NAD^+-boosting effect of Ab68, as with other pharmacological tools, we cannot completely exclude off-target effect that occur independent of CD38. For example, the observation that Ab68 treatment of WT mice increases NAD^+ levels in WAT and liver to levels higher than CD38 KO mice could suggest a possible off-target effect of this antibody, or alternatively, that CD38 KO mice develop an adaptation to prevent chronic high levels of NAD^+. In any case, the development of inhibitory anti-CD38 antibodies may provide valuable tools to understand important biological questions in the NAD^+ field. For example, historically, the ecto-enzymatic activity of CD38 has been considered a "topological paradox"[22]. Our data with Ab68 support the view that the ecto-enzymatic activity of CD38 plays a critical role in the regulation of nicotinamide nucleotides in cells and *in vivo*.

One key finding from our studies is that NMN is one of the major substrates for CD38, and that the ecto-NMNase activity of CD38 regulates cellular NAD^+ levels by controlling availability of NMN. These results are consistent with an emerging model showing that part of the metabolism of nicotinamide nucleotides occurs in the extracellular space, where the availability of NAD^+ precursors to cells regulates NAD^+ homeostasis. We cannot exclude the possibility that the ecto-NADase activity of CD38 is also degrading a small amount of NAD^+ that is secreted or leaks from cells. In fact, we observed that inhibition of the ecto-enzymatic activity of CD38 with Ab68 *in vivo* leads to a decrease in the levels of the NAD^+ degradation product ADPR. Furthermore, in some cells the intracellular localized CD38 may directly degrade cellular NAD^+.

One interesting question is why inflammatory cells express CD38 upon activation. We postulate that the main function of CD38 is to degrade extracellular nicotinamide nucleotides such as NMN and possibly NAD^+. However, the physiological role of the CD38 ecto-enzymatic activity is complex and may include the regulation of extracellular paracrine molecules such as adenosine, nicotinamide, and cADPR. In particular, the generation of adenosine by coupling of CD38 with another ecto-enzyme such as CD73 may have a significant impact on the regulation of tissue inflammation in situations such as cancer and infections[25,26,63]. Finally, the "sterile" inflammation of aging could lead to a similar deleterious scenario wherein $CD38^+$ inflammatory cells promote the decrease of extracellular NAD^+ precursors, such as NMN, which are important for intracellular NAD^+

homeostasis (Fig. 9 and Supplementary Fig. 9). In fact, during aging, levels of NAMPT have been reported to decrease in some tissues[14–17]. This indicates that during aging cells may have decreased capacity to generate intracellular NAD^+ from nicotinamide through the salvage pathway, and may rely on extracellular NAD^+ precursors such as NMN and NR.

In summary, senescent cells within aging tissues play an important role in driving the accumulation of $CD38^+$ inflammatory cells, which is one of the mechanisms that contributes to age-related NAD^+ decline. Complete elucidation of all the mechanisms leading to age-related NAD^+ decline will require future studies investigating the complex interactions between the multiple pathways involved in organismal NAD^+ homeostasis.

Methods

Ethical Compliance

All protocols requiring use of animals were approved by the Mayo Clinic Institutional Animal Care and Use Committee (IACUC) and studies were conducted in adherence to the NIH Guide for the Care and Use of Laboratory Animals. Mice were housed in standard cages at regulated temperature (ranging from 68 to 72 °C) and humidity (30–70%) with 12 hour light-dark cycles, and were maintained on a normal chow diet (ND) (PicoLab 5053 Rodent Diet 20; Lab Diets) *ad libitum.* Male and female mice were used for these experiments.

Reagents

The following reagents were used: AP20187 (Clontech), 78c (Calbiochem), Olaparib (LC Laboratories), type II collagenase (Worthington Biochemical), QuikChange Site-Directed Mutagenesis Kit (Agilent Technologies), CellTracker CM-DiI dye (Invitrogen), recombinant mouse FcγR I and FcγR IV (Acro Biosystems), Isatuximab (TeneoBio), UniAb clone ID 337468 and 337469 (TeneoBio), MabSelect SuRe resin, Superdex 200i 10X300GL column, ADH, Diaphorase, 3TC, and HISTOPAQUE-1077 were from Sigma-Aldrich. Recombinant human and mouse CD38 proteins, NMNAT1, anti-mouse TNFα- and IL6-neutralizing antibodies, and Luminex Premixed Multi-Analyte Magnetic Luminex Assay Kit were from R&D Systems. αMEM, DMEM, DMEM:F12, fetal calf serum, glutamine, ITS, penicillin/streptomycin, and Lipofectamine 3000 were from Life Technologies. When not specified, reagents and chemicals were purchased from Sigma-Aldrich.

Mouse Models

Experiments were performed using the following mouse lines: C57BL/6 (WT), CD38 KO, CD38 CI, and INK-ATTAC mice. The CD38 KO mice have been described previously in Partida-Sánchez *et al.* and Maier *et al.*[41,64] The CD38 CI mice have been described previously in Tarrago *et al.*12 The INK-ATTAC mice have been described previously in Baker *et al.*[43,44] All KO and transgenic lines are on a C57BL/6 background. No littermates were used in this study. All controls used for comparisons with CD38 KO and CD38 CI were WT mice on a C57BL/6 background, as recommended by the Jackson Laboratory.

Animals used in our studies were classified as young adult (3–4 months), middle age (12 months), old (18–22 months) and extremely old (26–32 months). The specific age in months is described for each experiment in the text and figures.

Anti-CD38 Mouse Antibodies

The V_H regions of heavy chain-only antibodies (HCAbs) form the smallest active antibody fragment. These V_H regions are ideal building blocks for a variety of antibody-based biologics because they are capable of fusing to other molecules and may also be attached in series to construct multispecific antibodies without requiring proper heavy and light chain pairing. Production of human HCAbs has been impeded by the fact that natural human V_H regions require light chain association and display poor biophysical characteristics when expressed in the absence of light chains. Here, we present an innovative platform for the rapid development of diverse sets of human HCAbs which have been selected *in vivo*. Our unique approach combines antibody repertoire analysis with immunization of transgenic rats called UniRats. They produce HCAbs with fully human V_H domains in response to an antigen challenge. UniRats express HCAbs from large transgenes representing the entire productive human heavy chain V(D)J repertoire; mount robust immune responses to a wide array of antigens; exhibit diverse V gene usage; and generate large panels of stable, high affinity, antigen-specific molecules.

HCAbs occur naturally in camelids (V_HH) and cartilaginous fish (V_{NAR}), where they form a functional paratope using only the heavy chain variable domain without light chain pairing[65–68]. Since the initial discovery of V_HHs in 1993, extensive research has demonstrated that HCAbs have both therapeutic applications and characteristics equivalent to conventional antibodies[69–72]. Furthermore, HCAbs are smaller than standard Ig molecules because they lack light chains, which may facilitate targeting of epitopes not readily accessible to classic antibodies including narrow protein clefts and enzyme active sites[66,73,74].

Development of UniRat Transgenic Animals

Previously identified, characterized and, in part modified BACs (bacterial artificial chromosomes) and YACs (yeast artificial chromosomes) accommodate human heavy chain variable region genes and rat constant region genes[75]. To enable heavy-chain antibody expression, a rat constant region BAC was reassembled by replacement of Cμ and adjacent 3′ regions with Cγ2α as the first C gene followed by Cγ1 and Cγ2b; with removed C_H1 exons. Locus functionality was retained by including 5′ and 3′ control regions with the downstream hs elements (3′αE) following Cε and Cα in natural configuration. Heavy-chain-only expression was then enforced by silencing the endogenous heavy and light chain (kappa and lambda) loci. The discovery workflow combines antibody repertoire deep sequencing and custom bioinformatics analysis with a high-throughput gene assembly, recombinant expression, and screening[73]. Endogenous rat heavy chain, kappa, and lambda loci have been knocked out.

Immunizations, Next-Generation Sequencing, Clonotype Analysis, and Cloning

Methods described in Harris *et al.*73 were used to identify antigen-specific UniAbs. In brief, UniRat animals were immunized using standard adjuvants along with recombinant protein antigens. After approximately 7 weeks of immunization, draining lymph nodes were harvested and total RNA was isolated. cDNAs encoding heavy chain only antibodies highly expressed in lymph node cells were selected for gene assembly and cloned into an expression vector. Subsequently, these heavy chain sequences were expressed in HEK293 cells as UniAb heavy chain only antibodies (CH1 deleted, no light chain).

UniAbs do not associate with light chains and their human V_H regions are functional as single domains. The antigen binding site of UniAbs is significantly smaller than the binding site of conventional antibodies and uniquely suited to bind small pockets in proteins.

Next-Generation Sequencing (NGS) of the Ab repertoire was used to rapidly identify stable, high affinity UniAbs using methods recently described by Harris *et al.*73 In brief, lymph nodes of 6 UniRats immunized with recombinant murine CD38 protein (R&D Systems) were isolated, washed, and cell pellets frozen. Total RNA was harvested from each cell pellet, and cDNA synthesized by first strand cDNA synthesis and 5'RACE by PCR amplification of the full Ig heavy chain. Samples were multiplexed on a single next-generation sequencing run by adding index labels to each sample by primer extension. The resulting indexed samples were pooled to create a library which was sequenced using the Illumina MiSeq platform with 2 × 300 paired-end reads. Each sample was covered by ~100,000 paired reads on average, and only those sequences that showed permissive alignment of at least 20 nucleotides to a human Ig locus were kept. Forward and reverse reads were paired when possible and merged reads covering entire VH regions were translated into relevant open reading frames. Framework and CDR regions were determined using IGBLAST (https://www.ncbi.nlm.nih.gov/igblast/), then agglomerative clustering was used to cluster the full set of CDR3 protein sequences for each sample at an 80% similarity threshold. The total number of reads in each cluster was recorded for clonotypes represented by five or more paired sequence reads. A clonotype is defined as a group of CDR3 protein sequences clustered at 80% similarity. Polarization of CDR3 clonotypes was measured by calculating the percentage of total reads in a sample that was contained in each CDR3 clonotype. Clonotypes were ranked by abundance for each sample and those most highly represented were prioritized for functional screening. Two hundred eighteen heavy chain variable regions were individually cloned into an expression vector containing an Fc tail. Each heavy chain vector was transfected into HEK293 cells in 96-well format and, after allowing for expression, cell culture supernatant was harvested and clarified by centrifugation. Thirty UniAbs bound to CHO cells that were transfected with an expression vector for mouse CD38 demonstrated inhibition of the CD38 hydrolase activity by at least 20%. Selected UniAbs were transfected into Expi-CHO cells according to manufacturer's instructions (ThermoFisher). Antibodies were expressed for these experiments with either a human IgG1 Fc region or an inactivated murine IgG2a Fc tail. The first capture step employed a MabSelect SuRe (Sigma-Aldrich) resin. After the first capture step, the protein pool was concentrated and loaded on to a Superdex 200i 10X300GL column (Sigma-

Aldrich) equilibrated with PBS for further polishing to remove any high molecular weight species. Fractions were collected and the most homogenous fractions were pooled.

Binding to $CD38^+$ cells was assessed by flow cytometry (Guava easyCyte 8HT, EMD Millipore) using CHO cells stably expressing mouse CD38. Briefly, 100,000 target cells were stained with a dilution series of purified UniAbs for 30 minutes at 4°C. Following incubation, the cells were washed twice with flow cytometry buffer (1X PBS, 1% BSA, 0.1% NaN_3) and stained with goat $F(ab')_2$ anti-human or mouse IgG conjugated to R-phycoerythrin (PE) (Southern Biotech) to detect cell-bound antibodies. After a 20 minute incubation at 4°C, the cells were washed twice with flow cytometry buffer and then mean fluorescence intensity (MFI) was measured by flow cytometry.

To measure inhibition of CD38 hydrolase activity, mouse CD38-expressing CHO cells (125,000 cells/well) were incubated with each purified anti-CD38 UniAb in hydrolase activity buffer (40 mM Tris, 250 mM Sucrose, 25 μg/mL BSA, pH 7.5) for 15 minutes at room temperature. After incubation, ε-NAD^+ (BioLog) was added to a final concentration of 150 μM. Production of a fluorescent product was measured at 1 hour (ex 300 nm/em 410 nm) using a Spectramax i3x plate reader (Molecular Devices). Hydrolase enzyme inhibition was assessed by comparing signal from UniAb-treated wells to the percent of total enzymatic activity observed in absence of UniAbs.

UniAbs ID323037 (human IgG1 Fc tail) and ID337468 (inactivated mouse IgG2a Fc tail) have identical VH regions, but different CH2 and CH3 domains. UniAbs ID322967 (human IgG1 Fc tail) and ID 337468 (inactivated mouse IgG2a Fc tail) also have identical VH binding sites. The following mutations were introduced into the CH2 and CH3 domains of mouse IgG2a to render them functionally silent, namely: L235A/G237A/P238S/E268A/Q309L/A330S/P331S. Antibodies with silenced mouse IgG2a Fc tails have normal *in vivo* half-lives. Binding to mouse CD38 and hydrolase blocking activities were identical between UniAbs with identical VH regions; Fc tails did not affect specificity and hydrolase blocking potency.

UniAb Purification

Soluble UniAb was expressed in CHO cells using protein free media supplemented with L-Glutamine (Invitrogen). Cell harvest was clarified by centrifugation and 0.2 μm PES filtration. During purification, the first capture step employed a MabSelect SuRe (Sigma-Aldrich) resin. The column was equilibrated with PBS and the clarified harvest loaded onto the column. A post load wash with PBS occurred, followed by elution with 50 mM Acetic Acid, 10% Glycerol, 10% Sucrose, pH 3.6. The elution pool was immediately neutralized to approximately pH 6.5 with 2 M Tris, pH 9. After the first capture step, the protein pool was concentrated and loaded on to a Superdex 200i 10X300GL column (Sigma-Aldrich) equilibrated with PBS for further polishing to remove any high molecular weight species. Fractions were collected, and the most homogenous fractions were pooled.

Binding affinities of anti-mouse CD38 antibodies (Ab68 and Ab69) and a mouse control antibody OKT3

Both antibodies UniAb clone ID337468 (Ab68) and UniAb clone ID337469 (Ab69) are expressed on a silenced mouse IgG2a background, whereas OKT3 (Acro Biosystems) is on a wild-type IgG2a background. Ab68 is an inhibitor of mouse CD38 cyclase and hydrolase activity. Ab69, which does not inhibit mouse CD38 enzyme functions, was used as a negative control. Affinities were measured by BioLayer Interferometry, using an Octet QK384 instrument (Fortebio Inc) in kinetics mode, essentially as previously described[76]. In this label-free dip and read assay format, antibodies are immobilized via anti-mouse-Fc sensors. During the binding step antibody-loaded sensors are dipped into wells containing recombinant mouse FcγR IV (mouse FcγR IV -FC4-M52H3, Acro Biosystems), recombinant mouse FcγR I (mouse FcγR I -CD4M5227, Acro Biosystems), or recombinant mouse CD38 (mouse CD38– 50191-M08H, Sino Biological). Next, sensors are placed into wells containing only buffer for real-time assessment of dissociation rates for each antibody/recombinant protein pair.

Ab68 binding to freshly isolated mouse cells.

Ab68 was labeled with FITC using the FluoReporter®FITC Protein Labeling Kit (Thermo fisher) according to manufacturer's instructions. The molar ratio of dye to protein used during the labeling reaction was 30:1. The efficiency of labeling was determined to be 5.4 dye molecules/antibody molecules. Labeling of FITC-Ab68 to freshly isolated splenocytes was determined by flow cytometry. Non-specific IgG was used as a blank control.

Ab68 internalization Assay

Both antibodies Ab68 and control antibody NIMR-5 (Novus Biologicals) are on a silenced IgG2a background. Briefly, antibodies are labeled with Zenon pHrodo iFL IgG Labeling Reagent (Thermo fisher) according to manufacturer's instructions. CHO cells stably transfected to express murine CD38 are added to each well at final concentration of 0.5×10^6 cells/mL and incubated at 37°C and 7% CO_2 for 0.75, 1.5, and 3 hours. After incubation, the cells are analyzed by flow cytometry to measure antibody-mediated internalization.

Antibody and Drug Treatments *in vivo*

Anti-CD38 mouse antibodies.—The antibodies UniAb clone ID 337468 (Ab68) (TeneoBio) and UniAb clone ID 337469 (Ab69) (TeneoBio) were used *in vivo*. Four-month-old C57BL/6 (WT) and CD38 KO mice were treated with PBS (vehicle), Ab68, or Ab69. Mice were given intraperitoneal injections (i.p., 5 mg/kg/dose) at day 1 and day 5. At day 8, mice were sacrificed and tissues were harvested for assays. In other experiments, 18 or 22 month-old C57BL/6 mice (Aged Rodent Colony, National Institute on Aging) were given a single i.p. injection (5 mg/kg) of Ab68 or vehicle. Mice were sacrificed at different time points and tissues were collected for further analysis. All mice used for these experiments were male.

Anti-CD38 mouse antibody and NMN.—Three-month-old and 18-month-old C57BL/6 mice were treated with single dose of PBS (vehicle) or Ab68 (i.p., 5 mg/kg). At day 3, mice were given an oral gavage with NMN (500 mg/kg) or vehicle PBS, sacrificed 6 hours later, and tissues and serum were collected for further analysis. Male and female mice were used for this experiment.

Anti-CD38 mouse antibody and FK866.—Four-month-old C57BL/6 mice were treated with vehicle (1% hydroxypropyl-β-cyclodextrine and 12% propylenglycol) or FK866 (25 mg/kg) by i.p. injection once a day for 8 days. At day 5, mice received a single dose of PBS (vehicle) or Ab68 (i.p., 5 mg/kg). When 8 days of FK866/vehicle treatment were completed, the mice were sacrificed and tissues were harvested for further analysis. In these experiments we used young mice to avoid the higher mortality observed in older mice treated with the NAMPT inhibitor FK866. All mice used for this experiment were male.

B/B Homodimerizer (AP20187).—A equal size cohort of 12-month-old INK-ATTAC mice were treated with vehicle (control group) or AP20187 (AP; B/B homodimerizer, Clontech) by i.p. injection (2 mg/kg/dose) twice a week for 16 months. Mice were sacrificed at 28 months of age, and tissues were collected for further analysis. Due to the increase in life-span induced by AP treatment, there were more animals remaining at the time of sacrifice (28 months) in the AP group versus vehicle group. Male and female mice were used for this experiment.

Lamivudine (3TC).—26 month-old C57BL/6 mice were treated with 3TC (Sigma-Aldrich) dissolved in drinking water (2.0 mg/mL). Controls received drinking water without drug. Mice were treated for 2 weeks and euthanized for tissue collection and analysis. Male and female mice were used for this experiment.

Doxorubicin.—12 month-old WT C57BL/6 and CD38 CI mice were treated with vehicle (Ctrl) or a single dose of doxorubicin (i.p., 15 mg/kg), and WAT was harvested 10 days later for analyses. All mice used for this experiment were male.

Bone Marrow Transplant

Three to 4-month-old CD38 KO recipient mice were irradiated using a Cesium irradiator with 2 dosages of 5 Gray radiation 24 hours apart. Bone marrow cells were isolated from tibias and femurs of 6 to 8-week-old WT or CD38 KO donor mice. After the second dosage of irradiation, recipient mice were injected with approximately 1×10^6 donor cells by retro-orbital injection. Transplant mice were given sulfamethoxazole (95 mg/kg/24hr) in drinking water starting at 3 days before the first irradiation through 2 weeks post-transplant. Engraftment was confirmed by staining blood cells for CD38. Twelve weeks post-transplant, mice received daily subcutaneous injections of, either LPS (300 μg/kg) or vehicle PBS for 5 days. At day 5, mice were sacrificed and tissues were harvested. Male and female mice were used for this experiment.

Preparation of PBMCs

Peripheral blood mononuclear cells (PBMCs) were prepared from whole blood of C57BL/6 and CAG–luc (Jackson Laboratory, #025854) mice using HISTOPAQUE-1077 to separate white and red blood cells according to the manufacturer (Sigma-Aldrich). Briefly, blood was layered over an equal volume of HISTOPAQUE-1077 and centrifuged at room temperature for 30 minutes at 1600 rpm. The interface containing PBMCs was removed and treated with red blood cell lysing buffer (Sigma-Aldrich) for approximately 2 minutes. PBMCs were washed and re-suspended in PBS (pH 7.4).

Senescent cell and PBMC transplantation

Senescent and control mouse pre-adipocytes were labelled with cell tracker CM-DiI dye according to the manufacturer's instructions (ThermoFisher Scientific). One year-old CD38 KO mice were injected IP with vehicle, senescent pre-adipocytes or 1 million control pre-adipocytes. After 48 hours, mice received approximately 700,000 luciferase positive PBMCs by retro-orbital injection. Forty eight hours later, mice were imaged for detecting the luciferase positive PBMCs using a Xenogen IVIS 200 system (Caliper Life Sciences, Hopkinton, MA). 3mg D-Luciferase in 200 μl PBS was injected IP into each animal before the imaging. The abdominal cavity of the animals were opened just before the imaging and the exposure for the images was set at 3 min. The mice were sacrificed following imaging and tissues were harvested. Male and female mice were used for this experiment.

293T and AML 12 Cell Lines: Culture, Transfection, and Treatments

HEK293T cells (ATCC) were cultured in DMEM with 10% FBS and 1% penicillin/streptomycin (Life Technologies). AML 12 cells (ATCC) were grown in DMEM:F12 media with 10% FBS, 1% penicillin/streptomycin, 40 ng/mL dexamethasone, 0.005 mg/mL insulin, 0.005 mg/mL transferrin, and 5 μg/mL selenium (ITS, Gibco). The human CD38 plasmid and the E226D catalytically inactive mutant have been previously described[5,12]. The Δ49 mutant was generated by site-directed mutagenesis using the QuikChange Kit (Agilent Technologies). The Δ49 mutant has a deleted amino-terminal tail and transmembrane domain, and is localized intracellularly[28]. Transfections were performed using Lipofectamine 3000 (Life Technologies) according to the manufacturer's instructions. HEK293T cells were transfected for 48 hours. We used 293T cells for transfections because they do not appear to express endogenous CD38 and, upon transfection, they demonstrated adequate transfection efficiency (as determined by immunoblotting) and remained viable. Drug and antibody treatments were performed 20 hours after transfection began. HEK293T were treated with 0.5 μM 78c or 5 μg/mL isatuximab (TeneoBio) in the presence or absence of 400 μM β-nicotinamide mononucleotide (NMN). 293T and AML 12 cells were treated with drugs and antibodies in their respective base media with addition of 1% FBS and 1% penicillin/streptomycin. Dexamethasone and ITS were removed from AML 12 medium during treatments. For the co-culture experiments, AML 12 cells were plated in the lower chamber and HEK293T or macrophages were plated in the upper chamber. Transfections of 293T with CD38 plasmids were performed as described above. Twenty hours after transfection, 200 μM NMN was added to the upper chamber. Four hours later, both chambers were incubated together for an additional 20 hours. Then, AML 12 cells were

collected for NAD^+ measurements. In experiments where 293T cells were incubated with human recombinant CD38 (hrCD38, R&D Systems) in the cell culture medium, the first step involved incubation of the hrCD38 (100 ng/mL) with 5 μg/mL isatuximab for 30 minutes at 37°C in cell culture media containing 1% FBS. The recombinant protein-antibody mixture was then added to the cells and 150–300 μM NMN was added. After 18 hours, 293T cells were collected for NAD^+ measurements.

Primary cells

Mouse splenic CD49b NK cells, CD11b microglia, $CD4^+$ T cells, and $CD8^+$ T cells were obtained from C&M LABPRO. Cells were thawed in RPMI-1640 containing 10%FBS before CD38 activity was measured.

Mouse pre-adipocytes: isolation, treatments, induction of senescence, and collection of conditioned media

Mouse pre-adipocytes (mPA) were prepared from subcutaneous WAT isolated from C57BL/6 mice according to Cartwright *et al.*[77] Pooled WAT was minced for 5 minutes, followed by a 1 hour digestion in type II collagenase (Worthington) at 37 °C (3 mg enzyme/1 g WAT). Samples were vortexed every 10 minutes. Following digestion, mPA were centrifuged for 10 minutes at 1200 rpm at room temperature. The pellet was re-suspended in αMEM (Gibco) with 10% fetal calf serum (FCS, Gibco). Cells were plated in 60 mm cell culture plates (cells from 1 mouse/plate) and expanded prior to reaching confluence. Drug treatments were performed in αMEM with 10%FCS.

To induce senescence, mouse pre-adipocytes were exposed to 10 Gy x-ray irradiation (Rad Source Technologies). Cells were maintained for 20 days with changes of media every 3–4 days. Twenty days after irradiation, cells were collected and analyzed for expression of senescence markers. Conditioned media from senescent cells (CM-SEN) was collected on day 20 (3 days after last media change). Prior to analysis, conditioned media was centrifuged for 5 minutes at 1200 rpm to remove cell debris. Control conditioned media from non-senescent cells (CM-NS) was collected from proliferating pre-adipocytes that had been growing for 3 days without media change.

Quantification of the secretory phenotype of mouse pre-adipocytes

Secreted factors from conditioned media of mouse pre-adipocytes (mPA) were measured using the Mouse (17 and 3 plex) Premixed Multi-Analyte Kit (R&D Systems) and analyzed by MAGPIX instrument (Luminex Corporation) according to the manufacturer. This assay provided simultaneous detection of secreted factors from conditioned media. Samples were normalized to cell count and diluted two-fold. Values reported as pg protein/mL medium. The lowest average value of the standard curve across batches was considered the limit of detection (LOD): IL6 9.744 pg/mL; Eotaxin 3.068 pg/mL; GDF-15 3.872 pg/mL; GROα 11.270 pg/mL; IL-1α 10.058 pg/mL; MIP-1α 0.269 pg/mL; MIP-3α 39.553 pg/mL; MIP-1β 57.94 pg/mL; MCP-1 70.97; FGF-basic 19.48 pg/mL; GROα 11.270 pg/mL. Analytes below LOD include: IL-2; IFNγ; IL-1β; MIP-3β; IL-13; IL-7; GM-CSF; TNFα; MIP-3β; IL-4; A2M.

Quantification of IL6 by ELISA in WAT of mice

IL6 was measured by ELISA (R&D Systems, IL6 Elisa kit. M6000B) in tissue extracts as recommended by manufacturer.

BMDMs: Preparation and Treatment with Conditioned Media

Mouse BMDMs were isolated as previously described in Matalonga *et al.*40. Briefly, bone-marrow-derived macrophages were obtained from bone marrow precursors differentiated for 6–7 days in DMEM supplemented with 20% heat-inactivated fetal bovine serum (FBS) and 30% L929 cell conditioned medium. Both female and male mice were used indistinctively for generation of primary macrophages. When macrophages from old mice were isolated, we used 18 month-old mice for these studies, rather than 28–34 month-old, because macrophages from the latter had poor viability and could not be cultured reliably.

BMDMs were seeded at 6 million cells per 60 mm dish and cultured for 20 hours with LPS in DMEM +2%FBS or conditioned media (CM) collected from senescent or non-senescent mPA cultivated in α-MEM containing 10% FCS. During these treatments macrophages were also incubated with the following antibodies or inhibitors: 5 μg/mLAb68 (TeneoBio), 5 μg/mL mouse TNF-α antibody and mouse IL6 antibody (R&D Systems), 0.5 μM 78c (Calbiochem), and 5 μM Olaparib (LC Laboratories). When macrophages were cocultured with AML12 cells, 1.5×10^6 macrophages were plated in coculture inserts (6 well inserts, 0.4 μm, greiner bio-one) and incubated with 100 ng/mL LPS or CM for 18 hours before addition of 5 μg/mL Ab68. 3 hours later, 200 μM NMN was added for 4 hours. Then, macrophages were incubated with AML12 cells (plated in 6 well plates) for an additional 20 hours before collection of AML 12 cells.

MEFs: Preparation, Induction of Senescence, and Collection of Conditioned Media

Primary mouse embryonic fibroblasts (MEFs) were generated as previously described[78]. Briefly, embryos were harvested at day 13.5 post conception, mechanically disaggregated and digested in trypsin/EDTA (0.25%) for 1 hour. Cells were cultivated in medium containing DMEM with 10% FBS, sodium pyruvate, glutamine, nonessential amino acids, and antibiotic in a humidified incubator with 5% CO_2 at 37°C.

Senescence was induced in MEFs that had reached approximately 75% confluence by administering 10 Gy in a cesium irradiator. Media was subsequently changed at days 4 and 7 post-irradiation. Conditioned media (CM) was harvested at day 10 following incubation of cells for 24 hours with serum-free DMEM. CM was centrifuged prior to use.

HUVECs: Treatment with Conditioned Media from MEFs

Human umbilical venous endothelial cells (HUVECs - ATCC® PCS100013™) were cultured in Vascular Cell Basal Medium supplemented with Endothelial Cell Growth Kit VEGF (ATCC PCS100041). Exposure of HUVECs for 36 hours to CM from senescent and proliferating MEFs was performed between passage 4 and 6 at 90–100% confluence. Before treatment 2% FBS was added to MEF CM. A 2 hour pre-incubation of CM with TNFα-neutralizing antibody (5 μg/mL) was performed before CM was added for 20 hours to HUVECs.

Immunoblotting

Immunoblotting assays for whole cell lysates of cells and tissues were performed as previously described in Tarrago *et al.*[12] Tissues or cells were homogenized and lysed in NETN buffer (20 mM Tris-HCl, pH 8.0, 100 mM NaCl, 1 mM EDTA, 0.5% Nonidet P-40) supplemented with 50 mM β-glycerophosphate, 5 mM NaF, and a protease inhibitor cocktail (Roche). After 30 min of incubation at 4°C, the samples were centrifuged at 12,000 rpm for 10 min at 4°C. When cytosolic fractions were prepared, cells were lysed in 2–5 volumes of 10 mM HEPES pH 7.4, 10 mM KCl, 0.05% NP40. Cells were incubated on ice for 20 minutes with lysis buffer and then centrifuged at 14,000 rpm at 4 °C for 10 minutes. The supernatant contained the cytoplasmic proteins. Protein concentrations in the supernatants were determined by BioRad protein assay. Lysates were separated by SDS-PAGE, and electrophoretically transferred to PVDF membranes (Immobilon-P; Millipore). Enhanced chemiluminescence detection was performed using SuperSignal West Pico or Femto Chemiluminescence Substrate (Thermo Scientific). Films were scanned and densitometry was performed using ImageJ. The following antibodies were used for immunoblotting: human CD38 (Abcam – ab108403, 1:1000), mouse CD38 (R&D Systems–AF4947, 1:1000), Slc12a8 (Aviva Systems Biology-ARP44039, 1:1000), Actin (Cell Signaling Technology – 8457, 1:5000), Tubulin (Abcam – ab15568, 1:4000).

Measurement of NAD^+ levels by Cycling Assay

Detection of NAD^+ was performed as described before using a cycling assay[5,12]. To determine intracellular NAD^+ levels, 3×10^6 cells or approximately 20 mg of tissue was homogenized in 10% trichloroacetic acid (TCA). Samples were centrifuged at 12,000 rpm for 2 min at 4°C. The supernatants were collected, and the pellets were resuspended in 0.2 N NaOH for protein determination. TCA was removed with organic solvents (3 volumes 1,1,2-trichloro-1,2,2-trifluroethane: 1 volume trioctylamine) in a ratio of 2 volumes of organic solvent to 1 volume of sample. After phase separation, the top aqueous layer containing NAD^+ was recovered and the pH was corrected by addition of 1M Tris pH 8.0.

For the cycling assay, samples were diluted in 100 mM sodium phosphate buffer pH 8 in a volume of 100 μL/ well and added to white 96 well plates. Next 100 μL of reaction mix (0.76% ethanol, 4 μM FMN, 27.2 U/ mL alcohol dehydrogenase (ADH), 1.8U/ mL Diaphorase, and 8 μM resazurin) was added to each well. 96-well plates were read in a fluorescence plate reader (Molecular Devices, SpectraMax® Gemini™ XPS) in an excitation wavelength of 544 nm and an emission wavelength of 590 nm. We have previously demonstrated that the NAD^+ cycling assay is as sensitive and specific as the UPLC-mass spectroscopy assay[5].

NMN Measurement in Serum by Cycling Assay

To determine serum NMN levels, serum was deproteinated by addition of 10% trichloroacetic acid (TCA). Samples were centrifuged at 12,000 rpm for 2 minutes at 4°C. The supernatants were collected, and the pellets were re-suspended in 0.2 N NaOH for protein determination. TCA was removed with organic solvent (3 volumes 1,1,2-trichloro-1,2,2-trifluroethane: 1 volume trioctylamine) in a ratio of 2 volumes of organic solvent to 1 volume of sample. After phase separation, the top aqueous layer containing

NMN was recovered and the pH was corrected by addition of 1M Tris pH 8.0. NMN concentration was measured by fluorescence of resazurin redox reaction using a coupled assay with NMNAT1 (R&D −5865NT), ADH and Diaphorase (Sigma-Aldrich).

NAD^+, NMN and other metabolite measurement by HPLC-Mass Spectroscopy

NAD^+ precursors were measured as described in Tarrago *et al.*[12]. For nucleotide measurements, the HPLC was at a flow rate of 0.25 mL/min with 99% buffer A from 0–3 min, a linear gradient to 99% buffer A/1% buffer B (100% methanol) from 3–20 min, 80% buffer A/20% buffer B from 20–21 min, a linear gradient to 30% buffer A/70% buffer B from 21–28 min at 0.35 mL/min, 99% buffer A/1% buffer B from 28–31 min, and a linear gradient to 99% buffer A from 31–37 min at 0.25 mL/min. Concentrations were quantitated based on the peak area compared to a standard curve and normalized to protein content in the tissue sample.

Enzymatic Activities

CD38 hydrolase activity was measured using 50 μM nicotinamide 1,N6-ethenoadenine dinucleotide (ε-NAD) as a substrate in 0.25 M sucrose and 40 mM Tris-HCl (pH 7.4). Fluorescence was measured at an excitation wavelength of 300 nm and an emission wavelength of 410 nm.

NMNase assay measured the nicotinamide produced in the assay using a yeast nicotinamidase (PNC1). Samples were incubated in assay buffer containing 250 mM Tris-Cl pH 8, 1.37 M NaCl, 27 mM KCl, 10 mM $MgCl_2$ and 2 μg purified PNC1 (mybiosource) for 1 hour at 37 °C. Next, OPT developer (10 mM OPT [ortho-pthalaldehyde], 10 mM DTT in 100% ethanol) was added, and samples were incubated in a shaker for 1 hour at room temperature in the dark. Samples were read in a black 96-well plate in a fluorescent plate reader with an excitation wavelength of 413 nm and an emission wavelength of 476 nm.

Quantification of mRNA

RNA was isolated from cells and mouse tissues using TRIzol or Qiagen RNeasy kits. cDNA was synthesized using the Qiagen QuantiTect or ABI High Capacity cDNA Reverse Transcription kit. Quantitative real-time PCR was performed using commercially available TaqMan gene expression probes (Applied Biosystems), according to the manufacturer's instructions on a BioRad CFX384 thermal cycler. The relative mRNA abundance of target genes was calculated by the $2^{(-ddCq)}$ method. Expression changes were calculated relative to control. TaqMan probes used in this study are described in Supplementary Information Table 1.

Immunostaining

Cells: 293T cells transfected with different constructs were seeded on ibidi μ-Slide VI 0.4, Poly-L-Lysine chamber slides (ibidi). After 40 hours of transfection cells were first stained with membrane staining dye CellBrite fix (Biotium Inc) at 37 °C for 15 minutes. After membrane staining, cells were immunostained after fixation and permeabilization with anti-CD38 primary antibody (1:200 Novus Biologicals-NBP1–95323) followed by AlexaFluor 568 tagged secondary antibody (1:500). Confocal images were taken using

LSM 780 confocal microscope at 40X magnification. The images were processed with Zen software.

Tissues: For liver, OCT-embedded tissue was cryosectioned at 10 μm thickness, fixed in MeOH:acetone (1:1) for 5 minutes at −20°C. Sections were blocked with 10% normal donkey serum in PBS-T for 1 hour at RT, and then incubated overnight at 4 °C with fluorescently tagged primary antibodies in 1% donkey serum. For WAT, whole tissue was fixed in 1% paraformaldehyde for 30 minutes followed by blocking and permeabilization using 5% BSA in PBS with 0.1% saponin for 1 hour at RT. Samples were incubated with primary antibodies overnight at 4°C and secondary antibody for 2 hours at RT. The following antibodies from BD Biosciences were used for both liver and WAT: CD38 AF647 (562769), CD45 FITC (553080), IgG2aκ AF647 isotype control (557690), and IgG2bκ isotype control (553988), 1:100 dilution for all. Additional antibodies used for WAT are Lamin B1 AF488 (Santa Cruz – sc37415, 1:200), IL6 (Cell Signaling Technology – 12912, 1:200), ORF1p (Abcam – ab216324, 1:100) and, anti-rabbit AF568 (Invitrogen – A-11011, 1:100). Nuclei were stained with Hoechst 33342. Images were obtained with an LSM 780 confocal microscope, and image capture was performed with ZEN 2.1 black software (Zeiss) using standardized exposure settings.

Liver and White Adipose Tissue (WAT) Flow Cytometry Analysis

For liver analysis, flow cytometry preparation and staining was done as described previously in Camacho-Pereira *et al.*[5] Mouse liver tissue was minced and digested with liberase (Sigma) at 37° C for 15 minutes to make single cell suspensions. Cells were incubated with FC-receptor block (Miltenyi), and stained with antibodies for 45 min at 4° C. The cells were stained with the following antibodies: Ter119 APC-Cy7 (1:50), CD45 BV786 (1:33), B220 PE-Cy7 (1:50),CD19 PE-Cy7 (1:50), CD19 BUV395 (1:50), CD3 BUV395 (1:50), CD4 BV650 (1:50), CD8 BB515 (1:50), CD11c PE-CF594 (1:25), and CD11b BV711 (1:33) were from BD Biosciences; Ly6G FITC (1:50), NK1.1 APC (1:50), F4/80 BV421(1:25), Ly6c AF700 (1:50), CD43 BV510 (1:20), and CD38 PE (1:50) were from BioLegend; CD3 PerCP-EF710 (1:50) was from Invitrogen; and live-dead Ghost 780 Near IR was from (Tonbo Biosciences). Flow cytometry analysis was performed on LSR-II (BD Biosciences). Flow cytometry analysis was done using FlowJo (FlowJo, LLC).

For WAT tissue, single cell suspension was prepared by mincing the tissue with scissors followed by 0.1% w/v collagenase II digestion (Gibco) at 37 °C for 60 minutes. The digested tissue was filtered through a 70 μm cell strainer. The RBCs were lysed with ACK lysis buffer (Gibco).The cells were then blocked with FcR blocking reagent (1:10, Miltenyi Biotec) in staining buffer for 10 minutes on ice. After washing, cells were stained with PE anti-CD38 (1:66) and FITC anti-CD45 (1:200). Propidium iodide (Invitrogen) was used for the live dead exclusion. The samples were run on MACSQuant Analyzer 10 (Miltenyi Biotec). After gating on FSCxSSC, single cells were gated followed by live dead exclusion gates. The $CD38^+$ cells were gated on live cells followed by $CD45^+$ or $CD45^-$. Flow cytometry analysis was done using FlowJo (FlowJo, LLC).

For 22 months WAT samples, after ACK lysis the cells were stained with near IR live dead dye (Invitrogen) for 30 minutes in PBS at room temperature. After washing, cells were stained with PE anti-CD38 (1:66), BV786 anti-CD45 (1:66), BV510 anti-F4/80 (1:50). The samples were run on LSR II (BD Biosciences). Flow cytometry analysis was done using FlowJo (FlowJo, LLC).

Spleen and jejunum single cell preparation and flow cytometry

To isolate splenocytes, the spleen was placed on the 70μm cell strainer held on a 50 mL falcon. Using the plunger end of the syringe, spleen was gently pressed through the cell strainer and was rinsed with RPMI media. Cells were centrifuged at 350g for 5 minutes. After supernatant aspiration, cells were suspended in ACK lysis buffer for 5 minutes and then 15 mL PBS was added. Cells were centrifuged at 350g for 5 minutes.

For single cell isolation from jejunum, the tissue was first minced and then digested in 20 mL RPMI complete media containing enzyme cocktail of collagenase type 4 (0.6 mg/mL), DNase (9 U/mL) and hyaluronidase (0.06 mg/mL) for 25 minutes at 37ºC with 250 rpm. The digested tissue was passed through the 100 μm cell strainer. The flow through was centrifuged for 7 minutes at 1600 rpm and pellet was collected and kept on ice. The remaining tissue on the cell strainer was digested again as described earlier. The two pellets were pooled together and the percoll gradient separation was performed using 44 % and 67% percoll to isolate the immune cells.

The single cells suspension from spleen and gut was then stained with live dead dye. Following live dead staining, cells were incubated with FcR block for 10 minutes on ice. Next, cells were stained with specific markers in cell staining buffer for 1 hour on ice. The cells were fixed with 2% paraformaldehyde and samples were run on LSR II.

Statistical Analysis

Data are mean ± SEM, analyzed by unpaired two-sided t-test as specifically described in the figure legends. When large data sets were included SD is shown in the figure. Analyses were performed using Microsoft Excel 2010 and GraphPad Prism 6.

Data collection

Data collection was performed using Microsoft Excel 2010.

Code availability

No custom codes or mathematical algorithms that are deemed central to the conclusions of our manuscript were used in our studies.

Data availability

The data that supports the findings of this study are available from corresponding author upon reasonable request. Source data are available online.

Further information on research design is available in the Nature Research Reporting Summary linked to this article

Extended Data

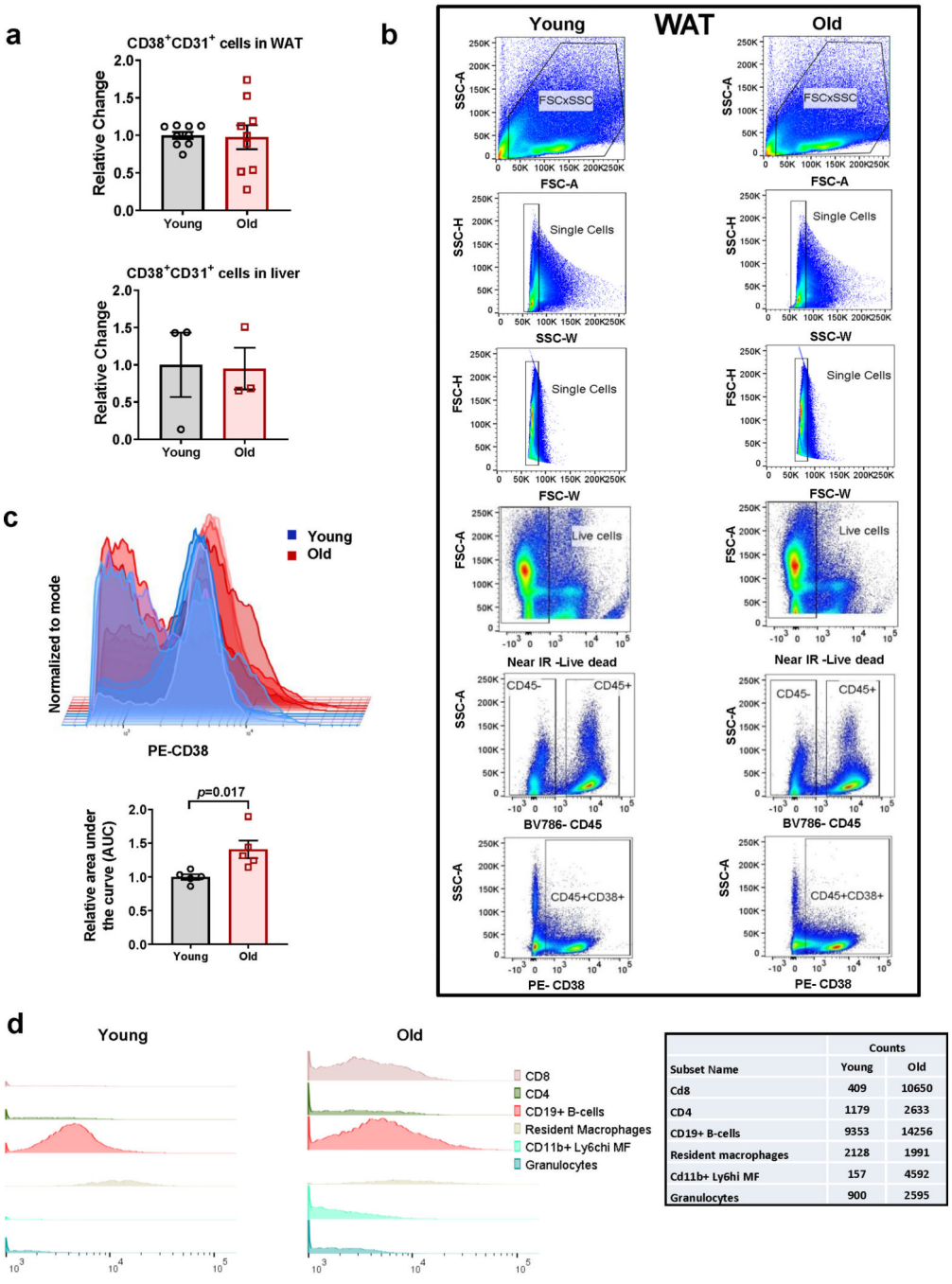

Subset Name	Counts	
	Young	Old
Cd8	409	10650
CD4	1179	2633
CD19+ B-cells	9353	14256
Resident macrophages	2128	1991
Cd11b+ Ly6hi MF	157	4592
Granulocytes	900	2595

Extended Data Fig. 1. CD38^{+} cells increase in tissues with aging.

(**a**) Graphs show no change in CD38^{+}CD31^{+} cell population in WAT and liver tissues between young (4 month-old) and old (32 month-old) mice (n=3 for liver and n=9 mice for WAT). (**b**) Gating strategy used to show the CD45^{+}CD38^{+} population in WAT of young (4 month-old) and old (22 month-old) mice. (**c**) Histograms of CD38^{+} population in young (4 month-old) and old (22 month-old) WAT showing the shift in CD38 expression. The graph

shows the relative area under the curve (AUC) for young and old (n=5 mice per group). (**d**) Histograms showing the CD38 expression in different immune cells in young (4 month-old) and old (32 month-old) liver. Table shows cell counts for each subset of immune cells, the data are representative of n=5 mice per group. (**e**) Gating strategy for $CD45^+$ immune subsets in $CD38^+$ liver cells in young (4 month-old) and old mice (32 month-old). Data are mean ± SEM, analyzed by unpaired two-sided *t*-test.

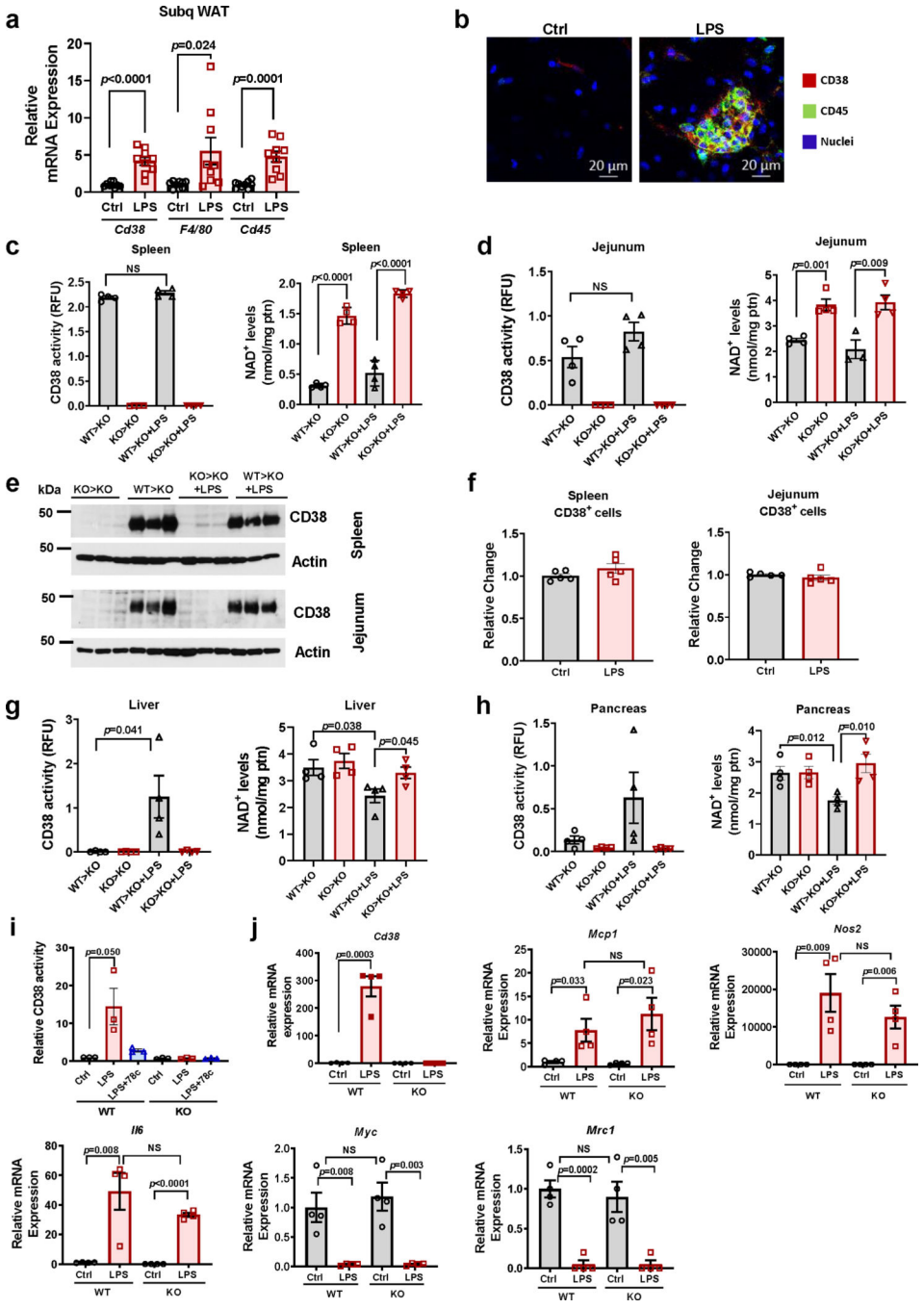

Extended Data Fig. 2. CD38 increases in tissues after LPS administration, bone marrow transplant of WT cells into CD38 KO mice, and in activated macrophages.

(**a-b**) 12 month-old mice received daily subcutaneous injection of vehicle (Ctrl) or LPS (300 μg/kg) for 5 days (n=9 mice per group). (**a**) mRNA expression of *Cd38*, *F4/80*, and *Cd45* in subcutaneous WAT (Subq WAT) measured by qRT-PCR analysis and expressed relative to Ctrl. (**b**) Immunofluorescent staining for CD38 (red) and CD45 (green) in Subq WAT, showing accumulation of $CD38^+CD45^+$ cells with LPS treatment. Images are representative of 6 mice per group. (**c-h**) Sub-lethally irradiated CD38 KO mice were subjected to bone marrow transplant (BMT) with 1×10^6 bone marrow cells (BMC) per animal from either WT (WT>KO) or CD38 KO donors (KO>KO). Twelve weeks after transplantation, mice were subcutaneously injected with LPS (300 μg/kg) or vehicle daily for 5 days and harvested at day 5. (**c**,**d**) CD38 activity and NAD^+ levels in spleen and jejunum (n=4 mice per group). (**e**) CD38 expression by immunoblot (n=3 mice per group). (**f**) Number of $CD38^+$ cells by flow cytometry was measured in spleen and jejunum with and without LPS treatment (n=5 mice per group). (**g**,**h**) CD38 activity and NAD^+ levels in liver and pancreas (n=4 mice per group). (**i**) CD38 activity was measured in macrophages isolated from WT or CD38 KO mice and treated or not with LPS (100 ng/mL) with and without the CD38 inhibitor 78c (0.5 μM) for 24 hours. CD38 activity is relative to Ctrl WT (n=3 biologically independent samples). (**j**) Macrophages isolated from WT or CD38 KO mice were treated or not with LPS (100 ng/mL) for 24 hours and mRNA expression of *Cd38* and other markers of macrophage activation were measured. Expression was measured by qRT-PCR analysis and expressed relative to Ctrl WT (n=4 biologically independent samples). Data are mean ± SEM, analyzed by unpaired two-sided *t*-test, NS=non-significant.

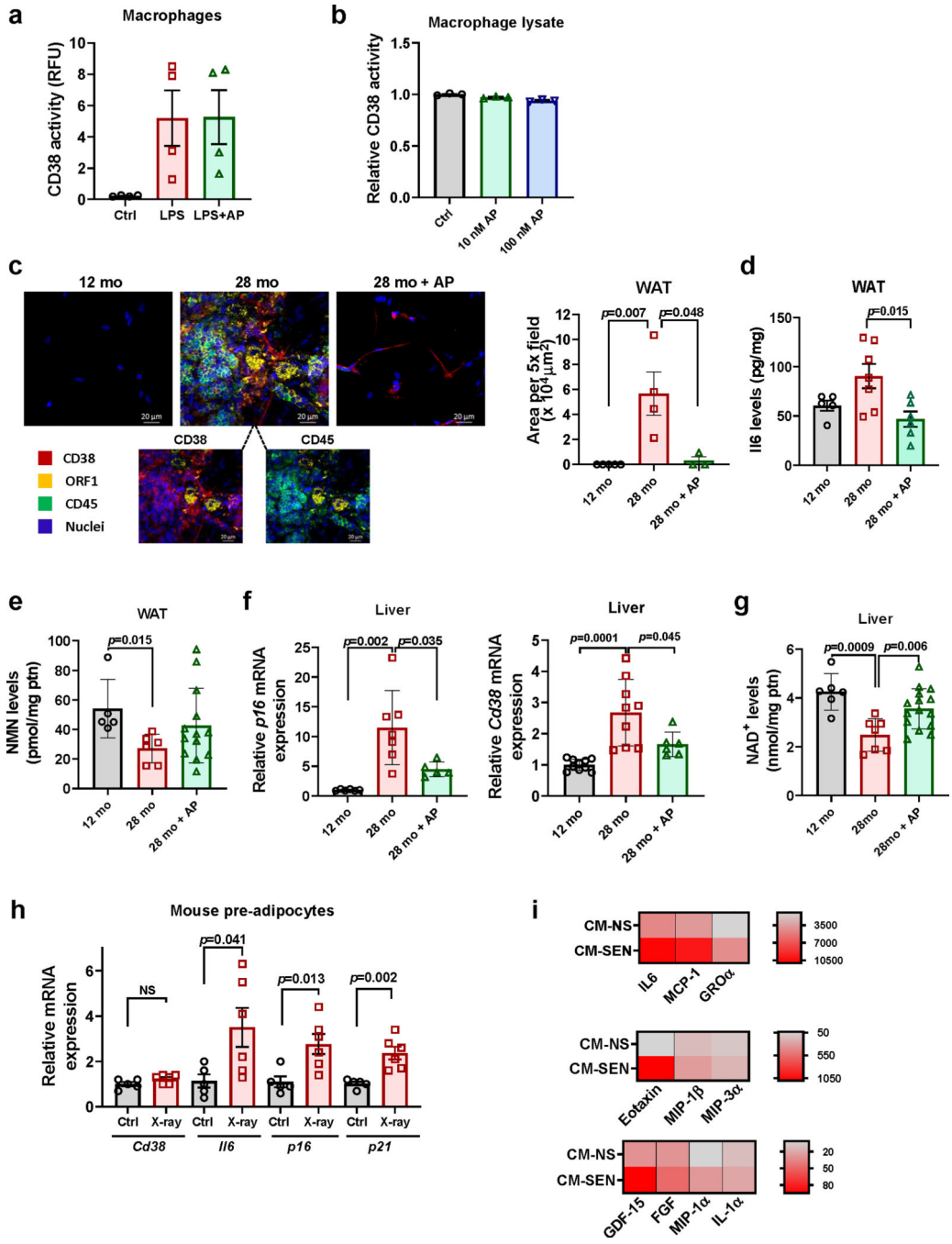

Extended Data Fig. 3. Senescence regulates CD38 *in vivo*.

(**a**) WT macrophages were incubated with LPS (100 ng/mL) in the presence or absence of 100 nM AP20187 for 20 hours. CD38 activity was measured in cell lysates (n=4 biologically independent samples). (**b**) WT macrophages were treated with LPS (100 ng/mL) for 20 hours and cell lysates were prepared. Lysates were incubated with or without AP20187 for 15 min before CD38 activity was measured (n=3 biologically independent samples). (**c**-**g**) 12 month-old INK-ATTAC mice were treated with vehicle or with AP20187 for 16 months (28 month-old groups) and were compared with 12 month-old animals. (**c**) Representative

images of immunofluorescent staining for CD38 (red), ORF1 (yellow), and CD45 (green) in WAT. Insets show the image of 28 month-old WAT with removal of green color channel CD45 signal (left) and with removal of red color channel CD38 signal (right) to show accumulation of $CD38^+$ $CD45^+$ cells near $ORF1^+$ cells. Graph shows quantification of $CD45^+$ immune clusters in WAT, based on 20 5x fields per sample (12 mo, n=5; 28 mo, n=4; 28 mo+AP, n=3 mice). (**d**) IL6 levels in WAT detected by ELISA (12 mo n=5; 28 mo n=7; 28 mo+AP n=6 mice). (**e**) NMN levels measured in WAT (12 mo n=5; 28 mo n=6; 28 mo+AP n=13 mice). (**f**) Relative mRNA levels of *p16* (12 mo n=6; 28 mo n=7; 28 mo+AP n=5 mice) and *Cd38* (12 mo n=10; 28 mo n=9; 28 mo+AP n=6 mice) detected by qRT-PCR analysis in liver. Levels are relative to 12 month-old mice. (**g**) NAD^+ levels in liver (12 mo n=6; 28 mo n=7; 28 mo+AP n=15 mice). (**h**) Relative mRNA levels of inflammatory and senescence-related genes in X-ray irradiated WT mouse pre-adipocytes determined by qRT-PCR. Levels are relative to control non-senescent cells (Ctrl) (Ctrl n=5; X-ray n=6 biologically independent samples). (**i**) Quantitative analysis of cytokines/chemokines in conditioned media harvested from irradiated (CM-SEN) or non-senescent (CM-NS) mouse pre-adipocytes. Heat maps reflect analytes (pg/mL) measured in 3–25-plex Luminex assays. Heat map shows average of 5 biologically independent samples. Data are mean ± SEM, except letters e-g that are mean ± SD, analyzed by unpaired two-sided *t*-test.

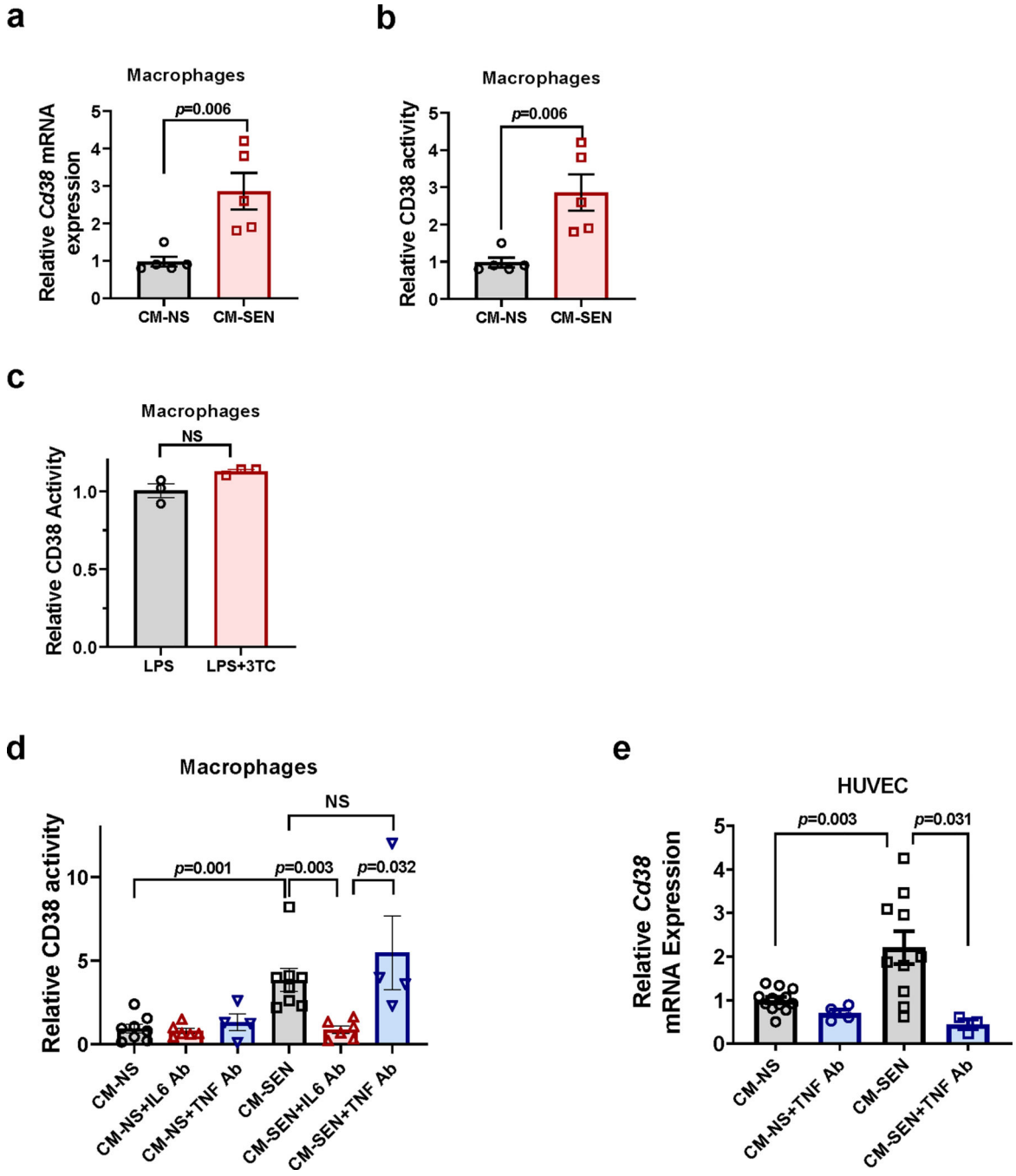

Extended Data Fig. 4. The senescence-associated secretory phenotype (SASP) increases CD38 accumulation.

(**a**-**b**) WT macrophages were incubated with conditioned media from senescent (CM-SEN) and non-senescent (CM-NS) mouse pre-adipocytes for 20 hours. CD38 expression and activity are relative to CM-NS. (**a**) *Cd38* mRNA expression in the macrophages was measured by qRT-PCR analysis. (n=5 biologically independent samples). (**b**) Relative CD38 activity in macrophage lysates (n=5 biologically independent samples). (**c**) WT macrophages were treated with LPS (100 ng/mL) with and without 3TC (10 μM) for 20 hours and

CD38 activity was measured in cell lysates (n=3 biologically independent samples). (**d**) WT macrophages were incubated with conditioned media from senescent (CM-SEN) and non-senescent (CM-NS) mouse pre-adipocytes for 20 hours. Conditioned media was pre-incubated for 2 hours with or without IL6 or TNF-α antibody (5 μg/mL) before addition to the macrophages. CD38 activity was measured in cell lysates, and expressed relative to CM-NS (CM-NS and CM-SEN n=8; CM-NS+IL6 Ab and CM-SEN+IL6 n=6; CM-NS+TNF Ab and CM-SEN+TNF n=4 biologically independent samples). (**e**) HUVECs were treated with conditioned media from senescent (CM-SEN) and non-senescent (CM-NS) mouse embryonic fibroblasts for 20 hours. CM was pre-incubated for 2 hours with or without TNF-α antibody (5 μg/mL) before addition to the HUVECs. *Cd38* mRNA expression was measured by qRT-PCR analysis (CM-NS n=12; CM-NS+TNF Ab n=4; CM-SEN n=10; CM-SEN+TNF Ab n=4 biologically independent samples). Data are mean ± SEM, analyzed by unpaired two-sided *t*-test.

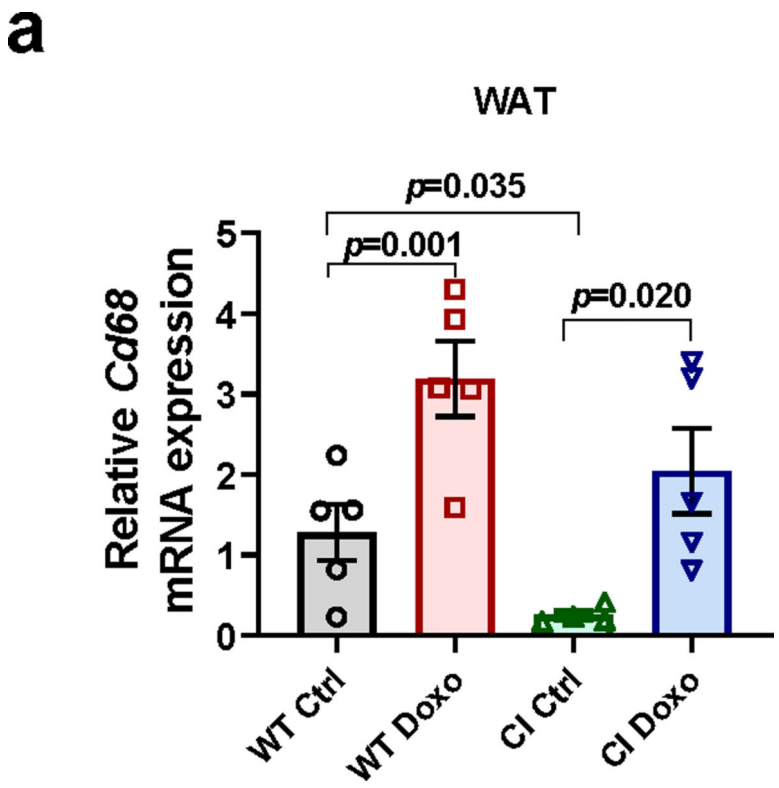

Extended Data Fig. 5. CD38 is required for genotoxic/senescence-induced NAD$^+$ decline.
(**a**) *Cd68* mRNA expression measured by qRT-PCR (n=5 mice per group, except for CI Ctrl where n=4 mice). Data are mean ± SEM, analyzed by unpaired two-sided *t*-test.

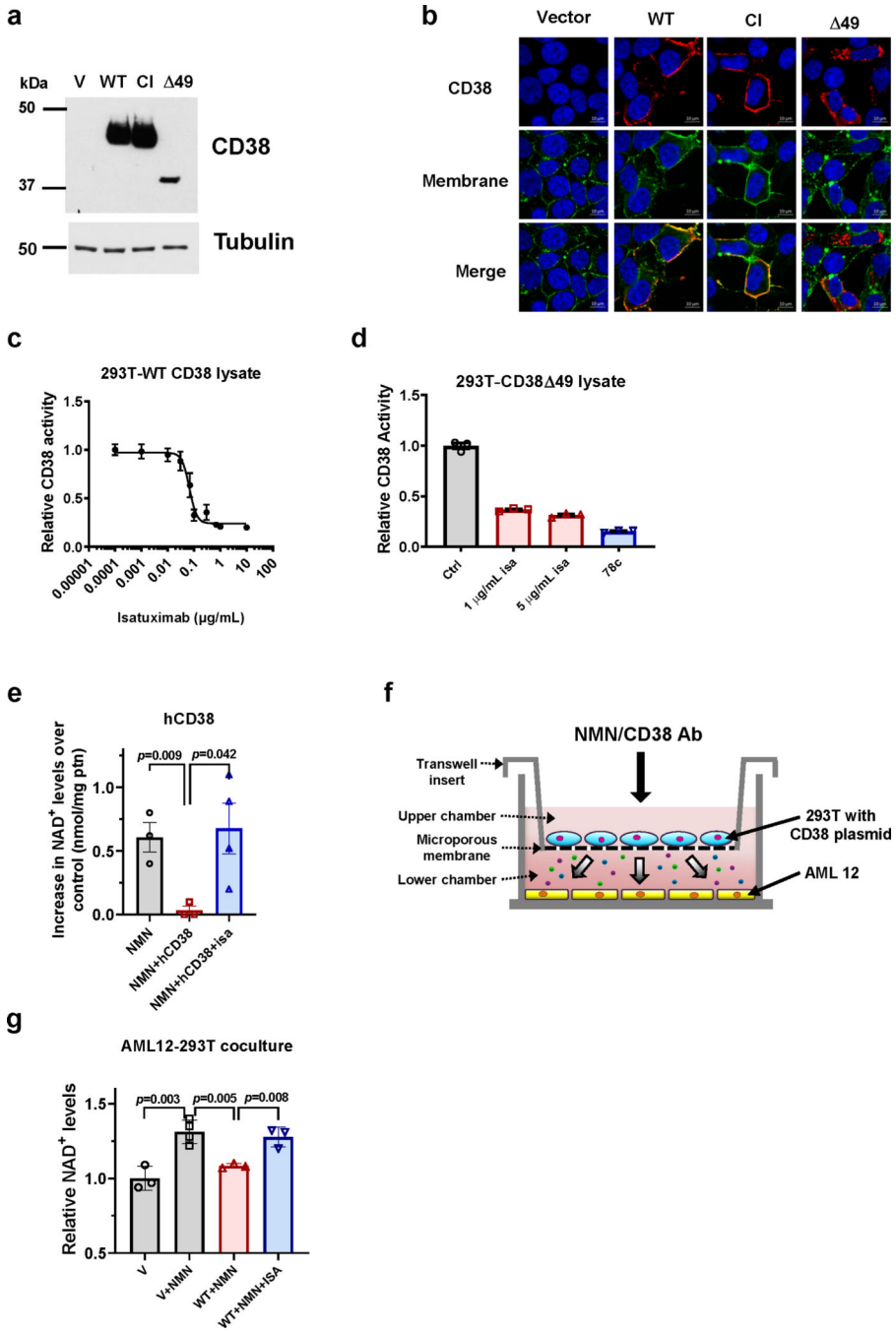

Extended Data Fig. 6. Characterization of the inhibitory CD38 antibody in human cells.

(**a**) 293T cells were transfected with vector (V), CD38 WT (WT), CD38 CI (CI) or CD38 Δ49 (Δ49). Representative immunoblotting of 4 independent experiments showing CD38 expression in cytosol of 293T cells transfected with CD38 plasmids. (**b**) Immunofluorescence of fixed 293T cells transfected with CD38 plasmids. Images are representative of 3 independent experiments. Cells were labeled with CD38 antibody and a membrane dye, followed by Hoechst staining. Images show separate CD38 and membrane staining. (**c**-**d**) Lysates of transfected 293T cells were incubated with varied concentrations

of the human CD38 antibody isatuximab (isa) or 0.5 μM 78c for 15 min before CD38 activity was measured. Activity is relative to control (no antibody). (**c**) Lysates of 293T transfected with CD38 WT plasmid (n=4 biologically independent samples). (**d**) Lysates of 293T transfected with CD38 Δ49 plasmid (n=3 biologically independent samples). (**e**) Human recombinant CD38 (hCD38) (100 ng/mL) was incubated with and without isatuximab (5 μg/mL) for 2 hours and then added to 293T cells together with NMN (300 μM). Control samples had no CD38 and no NMN. 293T were incubated with NMN and hCD38 for 20 hours and NAD^+ levels were measured in the 293T cells. Values show the difference from untreated control (n=3 except for NMN+hCD38+isa where n=4 biologically independent samples). (**f**) Scheme representing the coculture model. (**g**) NAD^+ levels in AML 12 cells co-cultured with 293T cells expressing vector or CD38 WT. 293T cells were treated with and without 200 μM NMN 20 hours after transfection in the presence or absence of 5 μg/ml isatuximab. AML 12 cells were collected 20 hours after incubation with 293T cells (n=3 except for V+NMN where n=4 biologically independent samples). Levels are relative to vector-transfected cells. Data are mean ± SEM, analyzed by unpaired two-sided *t*-test.

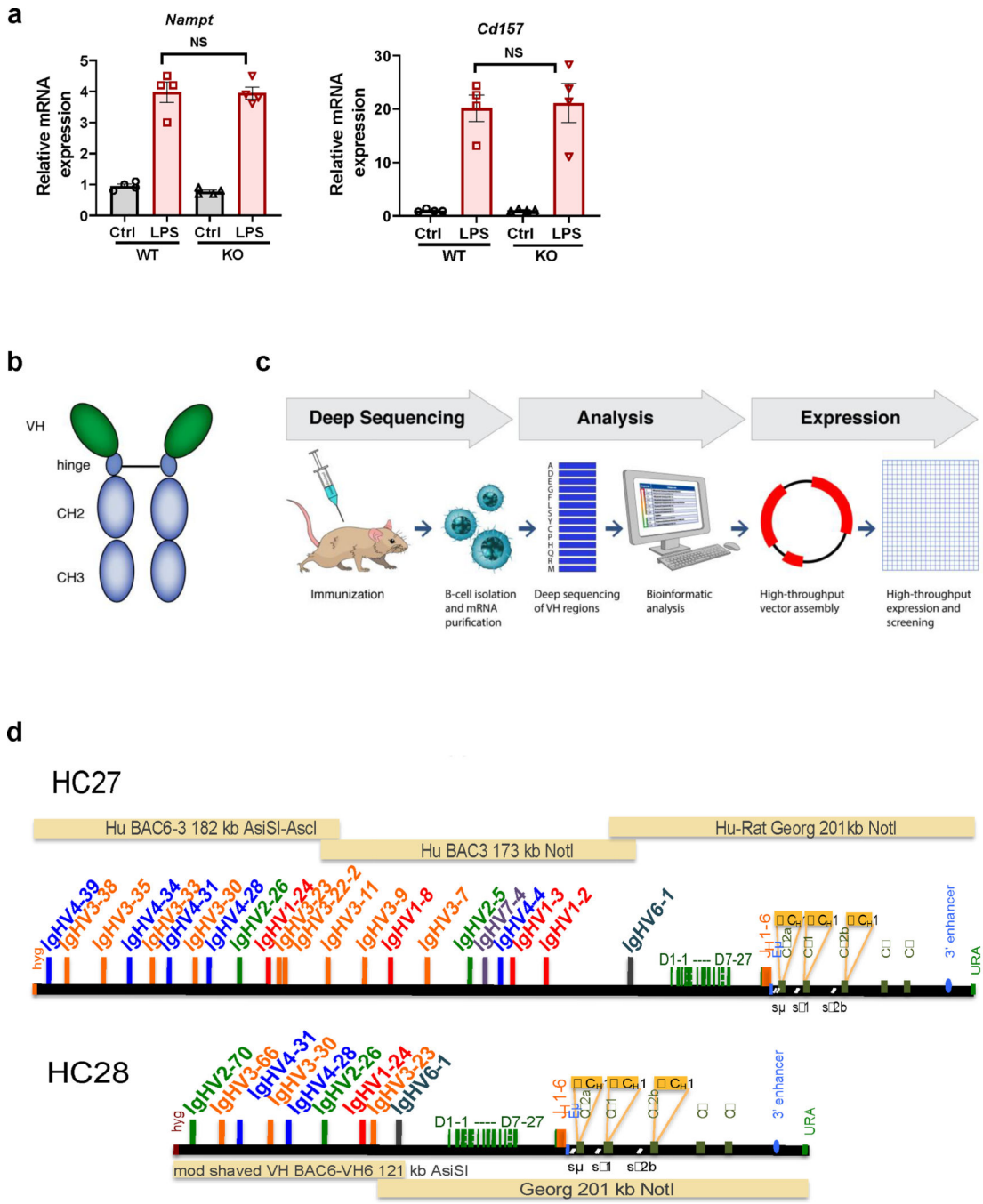

Extended Data Fig. 7. Characterization of the ecto-enzymatic activity of CD38 in BMDMs.

(**a**) Relative mRNA expression of *Nampt* and *Cd157* after treatment of BMDMs of WT and CD38 KO mice with and without 100 ng/mL LPS for 24 hours. Expression, assessed by qRT-PCR, is relative to Ctrl WT (n=4 biologically independent samples). (**b-g**) Characterization of the mouse anti-CD38 antibodies used in this study. (**b**) Schematic representation of a human heavy chain-only antibody (UniAbs). (**c**) Workflow to discover CD38-specific UniAbs. Antibodies were derived from transgenic rats, called UniRats that produce heavy-chain antibodies with fully human V_H domains (UniAbs) in response to an

antigen challenge. (**d**) Development of UniRat transgenic animals. (**e**) Protein and cell-based screens to discover anti-CD38 UniAbs. (**f**) Graph showing the binding of FITC-labeled Ab68 to freshly isolated mouse spleen cells (n=3 biologically independent samples). (**g**) Effect of Ab68 on the rate of CD38 hydrolase activity at different concentrations of substrate (left, n=8; except for no e-NAD where n=4 biologically independent samples and respective Lineweaver-Burk plots (right, n=6 biologically independent samples). (**h**) Table shows the binding affinities (KD) of anti-mouse CD38 antibodies Ab68 and Ab69 and a mouse control antibody OKT3. NB=No Binding. (**i**) Apoptosis of CHO cells stably transfected with mouse CD38 after incubation with antibodies Ab68, Ab69, and NIMR-5 for 24 hours (n=2 samples per concentration). (**j**) Cell viability of WT macrophages treated with LPS (100 ng/mL), with or without Ab68 or Ab69 (5 μg/mL) for 24 hours (n=4 except for LPS+Ab69 where n=3 biologically independent samples). (**k**) Graph shows the internalization of Ab68 compared to control antibody NIMR-5 after 45 minutes and 1.5 hours. (**l**) NAD^+ levels in AML 12 treated with 200 μM NMN in the presence or absence of LPS (100 ng/mL), Ab68 (5 μg/mL), and 78c (0.5 μM). LPS was given for 18 hours, then Ab68 was added, and 3 hours later NMN was added. Cells were collected 20 hours after NMN was added. NAD^+ levels were relative to control (Ctrl) (n=4 biologically independent samples). (**m**) NAD^+ levels in AML 12 cells cocultured with macrophages from CD38 KO mice. LPS was given for 18 hours to the macrophages, then NMN or NR (200 μM) were added for 3 hours. Next, macrophages were incubated with AMLs, and AML cells were collected 20 hours later. NAD^+ levels were relative to control (Ctrl) (n=4 biologically independent samples). (**n**) NAD^+ levels in AML 12 cocultured with macrophages. Macrophages were treated with 200 μM NA in the presence or absence of LPS (100 ng/mL), and Ab68 (5 μg/mL). LPS was given for 18 hours, then Ab68 was added, and 3 hours later nicotinic acid (NA) was added to the macrophages. Three hours after addition of NA, macrophages were incubated with AML cells. AML cells were collected 20 hours later and NAD^+ levels were calculated relative to control (Ctrl) (n=5 biologically independent samples). (**o**) Macrophages were incubated with conditioned media from senescent (CM-SEN) and non-senescent (CM-NS) mouse pre-adipocytes, and with LPS and without (Ctrl) for 20 hours. *Cd38* mRNA expression (CM-NS and CM-SEN n=5; Ctrl and LPS n=4 biologically independent samples), CD38 activity (n=5 biologically independent samples), and NAD^+ levels (n=6 biologically independent samples) were measured in the macrophages. Samples from cells incubated with CM-SEN, were calculated relative to cells incubated with CM-NS. Samples from cells treated with LPS, were calculated relative to vehicle-treated cells (Ctrl). Data are mean ± SEM, analyzed by unpaired two-sided *t*-test, NS= non-significant.

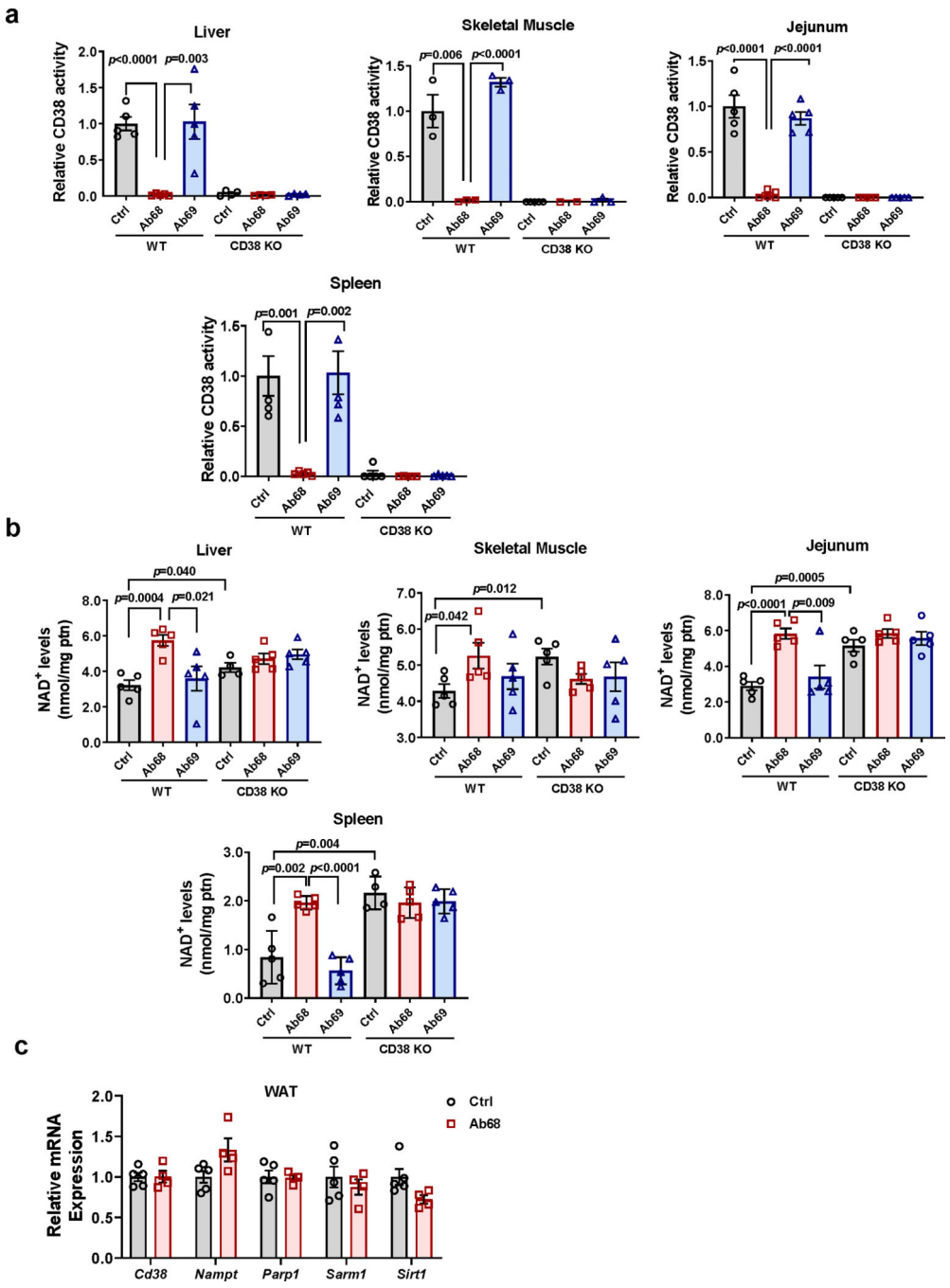

Extended Data Fig. 8. Blocking the CD38 ecto-enzymatic activity regulates NMN, NAD$^+$ levels and CD38 activity *in vivo*.

(**a**-**b**) 4 month-old WT and CD38 KO mice were treated with vehicle (Ctrl), Ab68 (5 mg/kg), or Ab69 (5 mg/kg) on day 1 and day 5, and euthanized on day 8. (**a**) CD38 activity in several tissues (liver n=5 except for Ctrl CD38 KO where n=4 mice; skeletal muscle n=3 except for Ab68 where n=2 mice; jejunum and spleen n=5 mice per group). (**b**) NAD$^+$ levels in several tissues (liver and spleen n=5 mice except for Ctrl CD38 KO where n=4; skeletal muscle and spleen n=5 mice per group). (**c**) 4 month-old WT mice were treated with a

single injection of vehicle (Ctrl) or Ab68 (5 mg/kg). After 3 days, tissues were harvested and gene expression was measured in WAT by qRT-PCR. Values are relative to Ctrl (Ctrl n=5 mice; Ab68 n=4 mice). (**d**) 4 month-old WT mice were treated with vehicle (Ctrl) or Ab68 (5 mg/kg) on day 1 and day 5, and euthanized on day 8. NMN and nicotinamide (NAM) levels were measured in liver and skeletal muscle. Levels are relative to Ctrl (n=5 mice per group). (**e**) Relative NMN levels in WAT, liver and skeletal muscle of 4 month-old WT and CD38 KO mice. Levels are relative to WT mice (n=5 mice per group except for liver CD38 KO where n=3 mice and skeletal muscle CD38 KO where n=4 mice). (**f**) 22 month-old WT mice were injected with a single dose of vehicle (Ctrl) or Ab68 (5 mg/kg). Mice were euthanized at different time points, and NMN and NAD^+ levels were measured in liver. Graphs show the time course of the relative increase of NMN or NAD^+ in vehicle and Ab68-treated over levels at time 0 (n=4 mice per group). (**g**) Graph shows the difference between NMNase activity of CD38 in the blood of WT and CD38 KO mice (n=3 mice per group). (**h**) Human recombinant CD38 enzyme was incubated with NMN at different pHs, and levels of nicotinamide were measured by an enzymatic coupled reaction (n=3 biologically independent samples). (**i**) Relative levels of NAD^+ and NR in the serum of mice injected with a single injection of vehicle (Ctrl) or Ab68 (5 mg/kg). Mice were euthanized 3 days later and NAD^+ and NR levels in the serum were measured (n=6 mice per group). (j) Relative mRNA expression of inflammatory and SASP markers in WAT of 3 month-old (young) and 18 month-old mice (old) treated or not with a single injection of vehicle (Ctrl) or 5 mg/kg Ab68. WAT was collected 3 days after injection of Ab68 (n=5 except for Ctrl old where n=4). Data are mean ± SEM, analyzed by unpaired two-sided *t*-test, except for **(f-g)** where data are analyzed by two-way ANOVA.

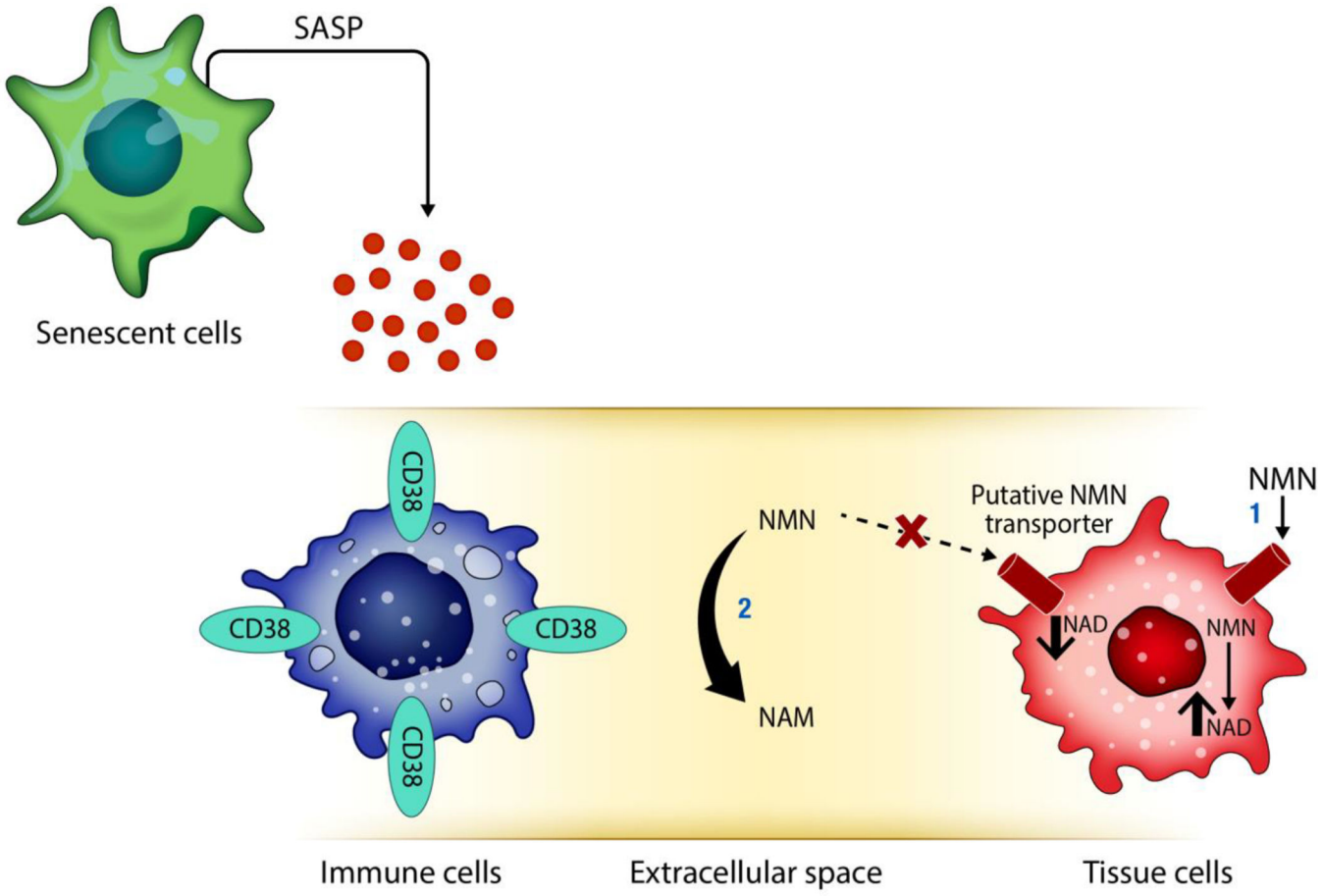

Extended Data Fig. 9. Schematic representation of the role of senescence and sterile inflammation in immune cell CD38 regulation, and the effect of extracellular NMN degradation in the regulation of tissue NAD^+ levels.

The senescence-associated secretory phenotype (SASP) increases the expression/accumulation of CD38 in immune cells in tissues where immune cells appear to regulate tissue NAD^+ levels. It has been proposed that NMN enters the cell through a putative NMN transporter, is converted to NAD^+ intracellularly, and increases intracellular NAD^+ levels (1). In the presence of senescence cells and the sterile inflammation, the levels of the ectoenzyme CD38 appear to increase in immune cells and tissues, degrading extracellular NMN to NAM, and causing a decrease in NMN/NAD^+ levels in tissues (2).

Supplementary Material

Refer to Web version on PubMed Central for supplementary material.

Acknowledgements

This work was supported in part by grants from the Diller Family Foundation, Ted Nash Long Life Foundation, the Glenn Foundation for Medical Research via the Paul F. Glenn Laboratories for the Biology of Aging at the Mayo Clinic (E.N.C, J.M.v.D. and D.B), sponsored research funding from Calico Life Sciences LLC, the Mayo and Noaber Foundations, National Institutes of Health (NIH) National Institute of Aging (NIA) grants AG-26094 (E.N.C), AG58812 (E.N.C.), CA233790 (E.N.C), AG13925 (J.L.K.), AG057493 (J.M.v.D.), AG016694 (J.M.S.), and P01 AG051449 (J.M.S).

National Institute of Diabetes, Digestive, and Kidney disease DK098656 (J.A.B.) Robert J. and Theresa W. Ryan (J.L.K.), and the Connor Group (J.L.K.). A.S.P. would like to thank the Colton Center for Auto-Immunity at NYU Langone for funding support.

References:

1. Hogan KA, Chini CCS & Chini EN The Multi-faceted Ecto-enzyme CD38: Roles in Immunomodulation, Cancer, Aging, and Metabolic Diseases. Frontiers in Immunology 10, doi:10.3389/fimmu.2019.01187 (2019).
2. Katsyuba E, Romani M, Hofer D & Auwerx J NAD+ homeostasis in health and disease. Nature Metabolism 2, 9–31, doi:10.1038/s42255-019-0161-5 (2020).
3. Johnson S & Imai S-I NAD (+) biosynthesis, aging, and disease. F1000Research 7, 132–132, doi:10.12688/f1000research.12120.1 (2018). [PubMed: 29744033]
4. McReynolds MR, Chellappa K & Baur JA Age-related NAD(+) decline. Exp Gerontol 134, 110888, doi:10.1016/j.exger.2020.110888 (2020). [PubMed: 32097708]
5. Camacho-Pereira J et al. CD38 Dictates Age-Related NAD Decline and Mitochondrial Dysfunction through an SIRT3-Dependent Mechanism. Cell Metab 23, 1127–1139, doi:10.1016/j.cmet.2016.05.006 (2016). [PubMed: 27304511]
6. de Picciotto NE et al. Nicotinamide mononucleotide supplementation reverses vascular dysfunction and oxidative stress with aging in mice. Aging Cell 15, 522–530, doi:10.1111/acel.12461 (2016). [PubMed: 26970090]
7. Gomes AP et al. Declining NAD(+) induces a pseudohypoxic state disrupting nuclear-mitochondrial communication during aging. Cell 155, 1624–1638, doi:10.1016/j.cell.2013.11.037 (2013). [PubMed: 24360282]
8. Guan Y et al. Nicotinamide Mononucleotide, an NAD(+) Precursor, Rescues Age-Associated Susceptibility to AKI in a Sirtuin 1-Dependent Manner. J Am Soc Nephrol 28, 2337–2352, doi:10.1681/asn.2016040385 (2017). [PubMed: 28246130]
9. Li J et al. A conserved NAD(+) binding pocket that regulates protein-protein interactions during aging. Science 355, 1312–1317, doi:10.1126/science.aad8242 (2017). [PubMed: 28336669]
10. Mouchiroud L et al. The NAD(+)/Sirtuin Pathway Modulates Longevity through Activation of Mitochondrial UPR and FOXO Signaling. Cell 154, 430–441, doi:10.1016/j.cell.2013.06.016 (2013). [PubMed: 23870130]
11. Scheibye-Knudsen M et al. A high-fat diet and NAD(+) activate Sirt1 to rescue premature aging in cockayne syndrome. Cell Metab 20, 840–855, doi:10.1016/j.cmet.2014.10.005 (2014). [PubMed: 25440059]
12. Tarrago MG et al. A Potent and Specific CD38 Inhibitor Ameliorates Age-Related Metabolic Dysfunction by Reversing Tissue NAD(+) Decline. Cell Metab 27, 1081–1095.e1010, doi:10.1016/j.cmet.2018.03.016 (2018). [PubMed: 29719225]
13. Williams PA et al. Vitamin B3 modulates mitochondrial vulnerability and prevents glaucoma in aged mice. Science 355, 756–760, doi:10.1126/science.aal0092 (2017). [PubMed: 28209901]
14. Yoshino J, Mills KF, Yoon MJ & Imai S Nicotinamide mononucleotide, a key NAD(+) intermediate, treats the pathophysiology of diet- and age-induced diabetes in mice. Cell Metab 14, 528–536, doi:10.1016/j.cmet.2011.08.014 (2011). [PubMed: 21982712]
15. Stein LR & Imai S Specific ablation of Nampt in adult neural stem cells recapitulates their functional defects during aging. Embo j 33, 1321–1340, doi:10.1002/embj.201386917 (2014). [PubMed: 24811750]
16. Johnson S, Wozniak DF & Imai S CA1 Nampt knockdown recapitulates hippocampal cognitive phenotypes in old mice which nicotinamide mononucleotide improves. npj Aging and Mechanisms of Disease 4, 10, doi:10.1038/s41514-018-0029-z (2018). [PubMed: 30416740]
17. Yoshida M et al. Extracellular Vesicle-Contained eNAMPT Delays Aging and Extends Lifespan in Mice. Cell Metabolism 30, 329–342.e325, doi:10.1016/j.cmet.2019.05.015 (2019). [PubMed: 31204283]

18. Franceschi C & Campisi J Chronic inflammation (inflammaging) and its potential contribution to age-associated diseases. J Gerontol A Biol Sci Med Sci 69 Suppl 1, S4–9, doi:10.1093/gerona/glu057 (2014). [PubMed: 24833586]
19. Andriani GA et al. Whole Chromosome Instability induces senescence and promotes SASP. Sci Rep 6, 35218, doi:10.1038/srep35218 (2016). [PubMed: 27731420]
20. Rodier F et al. Persistent DNA damage signalling triggers senescence-associated inflammatory cytokine secretion. Nat Cell Biol 11, 973–979, doi:10.1038/ncb1909 (2009). [PubMed: 19597488]
21. Wiley CD et al. Mitochondrial Dysfunction Induces Senescence with a Distinct Secretory Phenotype. Cell Metab 23, 303–314, doi:10.1016/j.cmet.2015.11.011 (2016). [PubMed: 26686024]
22. Malavasi F et al. Evolution and function of the ADP ribosyl cyclase/CD38 gene family in physiology and pathology. Physiol Rev 88, 841–886, doi:10.1152/physrev.00035.2007 (2008). [PubMed: 18626062]
23. Chini C et al. The NADase CD38 is induced by factors secreted from senescent cells providing a potential link between senescence and age-related cellular NAD(+) decline. Biochem Biophys Res Commun 513, 486–493, doi:10.1016/j.bbrc.2019.03.199 (2019). [PubMed: 30975470]
24. da Silva CP et al. Ectocellular CD38-catalyzed synthesis and intracellular Ca2+-signalling activity of cyclic ADP-ribose in T-lymphocytes are not functionally related. FEBS Lett 439, 291–296 (1998). [PubMed: 9845340]
25. Horenstein AL et al. NAD(+)-Metabolizing Ectoenzymes in Remodeling Tumor-Host Interactions: The Human Myeloma Model. Cells 4, 520–537, doi:10.3390/cells4030520 (2015). [PubMed: 26393653]
26. Horenstein AL et al. Adenosine Generated in the Bone Marrow Niche Through a CD38-Mediated Pathway Correlates with Progression of Human Myeloma. Mol Med 22, 694–704, doi:10.2119/molmed.2016.00198 (2016). [PubMed: 27761584]
27. van de Donk N, Richardson PG & Malavasi F CD38 antibodies in multiple myeloma: back to the future. Blood 131, 13–29, doi:10.1182/blood-2017-06-740944 (2018). [PubMed: 29118010]
28. Sun L et al. A novel mechanism for coupling cellular intermediary metabolism to cytosolic Ca2+ signaling via CD38/ADP-ribosyl cyclase, a putative intracellular NAD+ sensor. Faseb j 16, 302–314, doi:10.1096/fj.01-0705com (2002). [PubMed: 11874980]
29. Mottahedeh J et al. CD38 is methylated in prostate cancer and regulates extracellular NAD(). Cancer Metab 6, 13, doi:10.1186/s40170-018-0186-3 (2018). [PubMed: 30258629]
30. Aksoy P et al. Regulation of SIRT 1 mediated NAD dependent deacetylation: a novel role for the multifunctional enzyme CD38. Biochem Biophys Res Commun 349, 353–359, doi:10.1016/j.bbrc.2006.08.066 (2006). [PubMed: 16935261]
31. Aksoy P, White TA, Thompson M & Chini EN Regulation of intracellular levels of NAD: a novel role for CD38. Biochem Biophys Res Commun 345, 1386–1392, doi:10.1016/j.bbrc.2006.05.042 (2006). [PubMed: 16730329]
32. Liang M, Chini EN, Cheng J & Dousa TP Synthesis of NAADP and cADPR in mitochondria. Arch Biochem Biophys 371, 317–325, doi:10.1006/abbi.1999.1463 (1999). [PubMed: 10545220]
33. Zhao YJ, Lam CM & Lee HC The membrane-bound enzyme CD38 exists in two opposing orientations. Sci Signal 5, ra67, doi:10.1126/scisignal.2002700 (2012).
34. Funaro A et al. Identification and characterization of an active soluble form of human CD38 in normal and pathological fluids. Int Immunol 8, 1643–1650, doi:10.1093/intimm/8.11.1643 (1996). [PubMed: 8943558]
35. Zielinska W, Barata H & Chini EN Metabolism of cyclic ADP-ribose: Zinc is an endogenous modulator of the cyclase/NAD glycohydrolase ratio of a CD38-like enzyme from human seminal fluid. Life Sci 74, 1781–1790, doi:10.1016/j.lfs.2003.08.033 (2004). [PubMed: 14741735]
36. De Flora A, Guida L, Franco L & Zocchi E The CD38/cyclic ADP-ribose system: a topological paradox. Int J Biochem Cell Biol 29, 1149–1166, doi:10.1016/s1357-2725(97)00062-9 (1997). [PubMed: 9438379]
37. Boslett J, Helal M, Chini E & Zweier JL Genetic deletion of CD38 confers post-ischemic myocardial protection through preserved pyridine nucleotides. J Mol Cell Cardiol 118, 81–94, doi:10.1016/j.yjmcc.2018.02.015 (2018). [PubMed: 29476764]

38. Chatterjee S et al. CD38-NAD(+)Axis Regulates Immunotherapeutic Anti-Tumor T Cell Response. Cell Metab 27, 85–100.e108, doi:10.1016/j.cmet.2017.10.006 (2018). [PubMed: 29129787]
39. Lee CU, Song EK, Yoo CH, Kwak YK & Han MK Lipopolysaccharide induces CD38 expression and solubilization in J774 macrophage cells. Mol Cells 34, 573–576, doi:10.1007/s10059-012-0263-3 (2012). [PubMed: 23184288]
40. Matalonga J et al. The Nuclear Receptor LXR Limits Bacterial Infection of Host Macrophages through a Mechanism that Impacts Cellular NAD Metabolism. Cell Rep 18, 1241–1255, doi:10.1016/j.celrep.2017.01.007 (2017). [PubMed: 28147278]
41. Partida-Sanchez S et al. Cyclic ADP-ribose production by CD38 regulates intracellular calcium release, extracellular calcium influx and chemotaxis in neutrophils and is required for bacterial clearance in vivo. Nat Med 7, 1209–1216, doi:10.1038/nm1101-1209 (2001). [PubMed: 11689885]
42. Jablonski KA et al. Novel Markers to Delineate Murine M1 and M2 Macrophages. PLoS One 10, e0145342, doi:10.1371/journal.pone.0145342 (2015). [PubMed: 26699615]
43. Baker DJ et al. Naturally occurring p16(Ink4a)-positive cells shorten healthy lifespan. Nature 530, 184–189, doi:10.1038/nature16932 (2016). [PubMed: 26840489]
44. Baker DJ et al. Clearance of p16Ink4a-positive senescent cells delays ageing-associated disorders. Nature 479, 232–236, doi:10.1038/nature10600 (2011). [PubMed: 22048312]
45. Biran A et al. Quantitative identification of senescent cells in aging and disease. Aging Cell 16, 661–671, doi:10.1111/acel.12592 (2017). [PubMed: 28455874]
46. Xu M et al. Senolytics improve physical function and increase lifespan in old age. Nat Med 24, 1246–1256, doi:10.1038/s41591-018-0092-9 (2018). [PubMed: 29988130]
47. Xu M et al. JAK inhibition alleviates the cellular senescence-associated secretory phenotype and frailty in old age. Proc Natl Acad Sci U S A 112, E6301–6310, doi:10.1073/pnas.1515386112 (2015). [PubMed: 26578790]
48. De Cecco M et al. L1 drives IFN in senescent cells and promotes age-associated inflammation. Nature 566, 73–78, doi:10.1038/s41586-018-0784-9 (2019). [PubMed: 30728521]
49. Demaria M et al. Cellular Senescence Promotes Adverse Effects of Chemotherapy and Cancer Relapse. Cancer Discov 7, 165–176, doi:10.1158/2159-8290.CD-16-0241 (2017). [PubMed: 27979832]
50. Billington RA et al. Emerging functions of extracellular pyridine nucleotides. Mol Med 12, 324–327, doi:10.2119/2006-00075.Billington (2006). [PubMed: 17380199]
51. Deckert J et al. SAR650984, a novel humanized CD38-targeting antibody, demonstrates potent antitumor activity in models of multiple myeloma and other CD38+ hematologic malignancies. Clin Cancer Res 20, 4574–4583, doi:10.1158/1078-0432.ccr-14-0695 (2014). [PubMed: 24987056]
52. Becherer JD et al. Discovery of 4-Amino-8-quinoline Carboxamides as Novel, Submicromolar Inhibitors of NAD-Hydrolyzing Enzyme CD38. J Med Chem 58, 7021–7056, doi:10.1021/acs.jmedchem.5b00992 (2015). [PubMed: 26267483]
53. Grozio A et al. Slc12a8 is a nicotinamide mononucleotide transporter. Nat Metab 1, 47–57, doi:10.1038/s42255-018-0009-4 (2019). [PubMed: 31131364]
54. Minhas PS et al. Macrophage de novo NAD(+) synthesis specifies immune function in aging and inflammation. Nat Immunol 20, 50–63, doi:10.1038/s41590-018-0255-3 (2019). [PubMed: 30478397]
55. Preugschat F et al. A pre-steady state and steady state kinetic analysis of the N-ribosyl hydrolase activity of hCD157. Arch Biochem Biophys 564, 156–163, doi:10.1016/j.abb.2014.09.008 (2014). [PubMed: 25250980]
56. Liu L et al. Lipopolysaccharide activates ERK–PARP-1–RelA pathway and promotes nuclear factor–κB transcription in murine macrophages. Human Immunology 73, 439–447, doi:10.1016/j.humimm.2012.02.002 (2012). [PubMed: 22391342]
57. Liu L et al. Quantitative Analysis of NAD Synthesis-Breakdown Fluxes. Cell Metab 27, 1067–1080 e1065, doi:10.1016/j.cmet.2018.03.018 (2018). [PubMed: 29685734]

58. Lumeng CN et al. Aging is associated with an increase in T cells and inflammatory macrophages in visceral adipose tissue. J Immunol 187, 6208–6216, doi:10.4049/jimmunol.1102188 (2011). [PubMed: 22075699]

59. Singh P et al. Lymphoid neogenesis and immune infiltration in aged liver. Hepatology 47, 1680–1690, doi:10.1002/hep.22224 (2008). [PubMed: 18395842]

60. Yoshimoto S et al. Obesity-induced gut microbial metabolite promotes liver cancer through senescence secretome. Nature 499, 97–101, doi:10.1038/nature12347 (2013). [PubMed: 23803760]

61. Ghosh S et al. Elevated muscle TLR4 expression and metabolic endotoxemia in human aging. J Gerontol A Biol Sci Med Sci 70, 232–246, doi:10.1093/gerona/glu067 (2015). [PubMed: 24846769]

62. Kim KA, Jeong JJ, Yoo SY & Kim DH Gut microbiota lipopolysaccharide accelerates inflamm-aging in mice. BMC Microbiol 16, 9, doi:10.1186/s12866-016-0625-7 (2016). [PubMed: 26772806]

63. Grozio A et al. CD73 protein as a source of extracellular precursors for sustained NAD+ biosynthesis in FK866-treated tumor cells. J Biol Chem 288, 25938–25949, doi:10.1074/jbc.M113.470435 (2013). [PubMed: 23880765]

Methods-only references

64. Maier B et al. Modulation of mammalian life span by the short isoform of p53. Genes Dev 18, 306–319, doi:10.1101/gad.1162404 (2004). [PubMed: 14871929]

65. Detalle L et al. Generation and Characterization of ALX-0171, a Potent Novel Therapeutic Nanobody for the Treatment of Respiratory Syncytial Virus Infection. Antimicrob Agents Chemother 60, 6–13, doi:10.1128/aac.01802-15 (2016). [PubMed: 26438495]

66. Enever C, Batuwangala T, Plummer C & Sepp A Next generation immunotherapeutics--honing the magic bullet. Curr Opin Biotechnol 20, 405–411, doi:10.1016/j.copbio.2009.07.002 (2009). [PubMed: 19709876]

67. Hamers-Casterman C et al. Naturally occurring antibodies devoid of light chains. Nature 363, 446–448, doi:10.1038/363446a0 (1993). [PubMed: 8502296]

68. Konning D et al. Camelid and shark single domain antibodies: structural features and therapeutic potential. Curr Opin Struct Biol 45, 10–16, doi:10.1016/j.sbi.2016.10.019 (2017). [PubMed: 27865111]

69. Holliger P & Hudson PJ Engineered antibody fragments and the rise of single domains. Nat Biotechnol 23, 1126–1136, doi:10.1038/nbt1142 (2005). [PubMed: 16151406]

70. Lauwereys M et al. Potent enzyme inhibitors derived from dromedary heavy-chain antibodies. Embo j 17, 3512–3520, doi:10.1093/emboj/17.13.3512 (1998). [PubMed: 9649422]

71. Wesolowski J et al. Single domain antibodies: promising experimental and therapeutic tools in infection and immunity. Med Microbiol Immunol 198, 157–174, doi:10.1007/s00430-009-0116-7 (2009). [PubMed: 19529959]

72. Yu Y et al. Humanized CD7 nanobody-based immunotoxins exhibit promising anti-T-cell acute lymphoblastic leukemia potential. Int J Nanomedicine 12, 1969–1983, doi:10.2147/ijn.s127575 (2017). [PubMed: 28331319]

73. Harris KE et al. Sequence-Based Discovery Demonstrates That Fixed Light Chain Human Transgenic Rats Produce a Diverse Repertoire of Antigen-Specific Antibodies. Front Immunol 9, 889, doi:10.3389/fimmu.2018.00889 (2018). [PubMed: 29740455]

74. Osborn MJ et al. High-affinity IgG antibodies develop naturally in Ig-knockout rats carrying germline human IgH/Igkappa/Iglambda loci bearing the rat CH region. J Immunol 190, 1481–1490, doi:10.4049/jimmunol.1203041 (2013). [PubMed: 23303672]

75. Vafa O et al. An engineered Fc variant of an IgG eliminates all immune effector functions via structural perturbations. Methods 65, 114–126, doi:10.1016/j.ymeth.2013.06.035 (2014). [PubMed: 23872058]

76. Yoshino J & Imai S Accurate measurement of nicotinamide adenine dinucleotide (NAD(+)) with high-performance liquid chromatography. Methods Mol Biol 1077, 203–215, doi:10.1007/978-1-62703-637-5_14 (2013). [PubMed: 24014409]

77. Cartwright MJ et al. Aging, depot origin, and preadipocyte gene expression. The journals of gerontology. Series A, Biological sciences and medical sciences 65, 242–251, doi:10.1093/gerona/glp213 (2010).

78. Babu JR et al. Rae1 is an essential mitotic checkpoint regulator that cooperates with Bub3 to prevent chromosome missegregation. The Journal of cell biology 160, 341–353, doi:10.1083/jcb.200211048 (2003). [PubMed: 12551952]

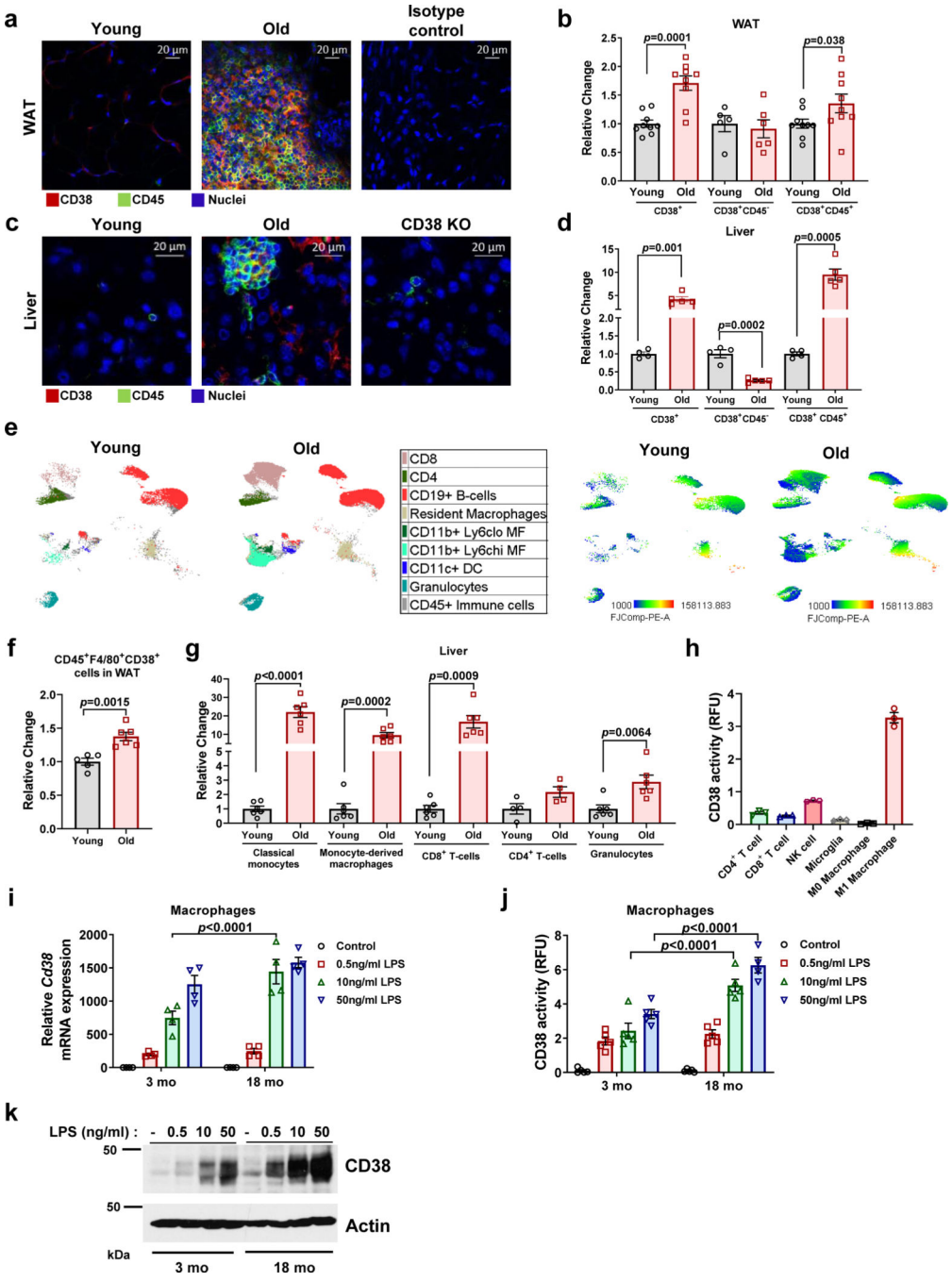

Figure 1. Characterization of CD38$^+$ cell types that accumulate in tissues during aging.

Analysis of WAT (**a**,**b**,**f**) and liver (**c**,**d**,**e**,**g**) of young and old mice. (**a,c**) Representative immunofluorescence image for CD38 (red) and CD45 (green) in WAT and liver of young (3–4 month-old) and old (28–32 month-old) C57BL/6 mice (4 mice per group), compared to isotype control or CD38 Knockout (KO). (**b,d**) CD38$^+$, CD38$^+$CD45$^-$, and CD38$^+$CD45$^+$ cells in young (4 month-old) and old (32 month-old) mice were determined by flow cytometry in WAT (CD38$^+$, CD38$^+$CD45$^+$ n=9 mice per group; CD38$^+$CD45$^-$ n=5 mice for young, 6 mice for old) and liver (young n=4 mice per group; old n=5 mice per

group), changes are relative to young mice. (**e**) In the left panel, flow cytometry-derived color-coded cell clusters of $CD38^+$ immune cell types in liver of young (4 month-old) and old (32 month-old) mice analyzed by Uniform Manifold Approximation and Projection (UMAP). In the right panel, heat maps show CD38 protein expression (lowest in blue and highest in red) in the respective immune clusters (n=4 for young and n=5 for old). (**f**) Graph shows $CD45^+F4/80^+CD38^+$ cell population in WAT of young (4 month-old, n=5 mice) and old mice (32 month-old, n=6 mice). Fold changes are relative to young mice. (**g**) $CD38^+CD45^+$ subsets increase with age in liver tissue (Classical monocytes, monocyte-derived macrophages, $CD8^+$ T cells, and granulocytes n=6 mice; $CD4^+$ T cells n=4 mice). Change is relative to young mice. (**h**) CD38 activity in mouse immune cells isolated from spleen (n=3 biologically independent samples). (**i-k**) Macrophages isolated from 3 month-old and 18 month-old mice were stimulated with different concentrations of LPS for 20 hours. (**i**) *Cd38* mRNA expression measured by qRT-PCR analysis (n=4 biologically independent samples). (**j**) CD38 activity measured in protein lysates (RFU-relative fluorescent units) (n=5, except for 18 mo 50 ng/mL LPS where n=4 biologically independent samples). (**k**) Representative immunoblotting of three biologically independent samples from macrophages treated with different concentrations of LPS. Data are mean ± SEM, analyzed by unpaired two-sided t-test, except for $CD38^+CD45^+$ in Fig 1b, where samples were analyzed by unpaired on-sided t-test.

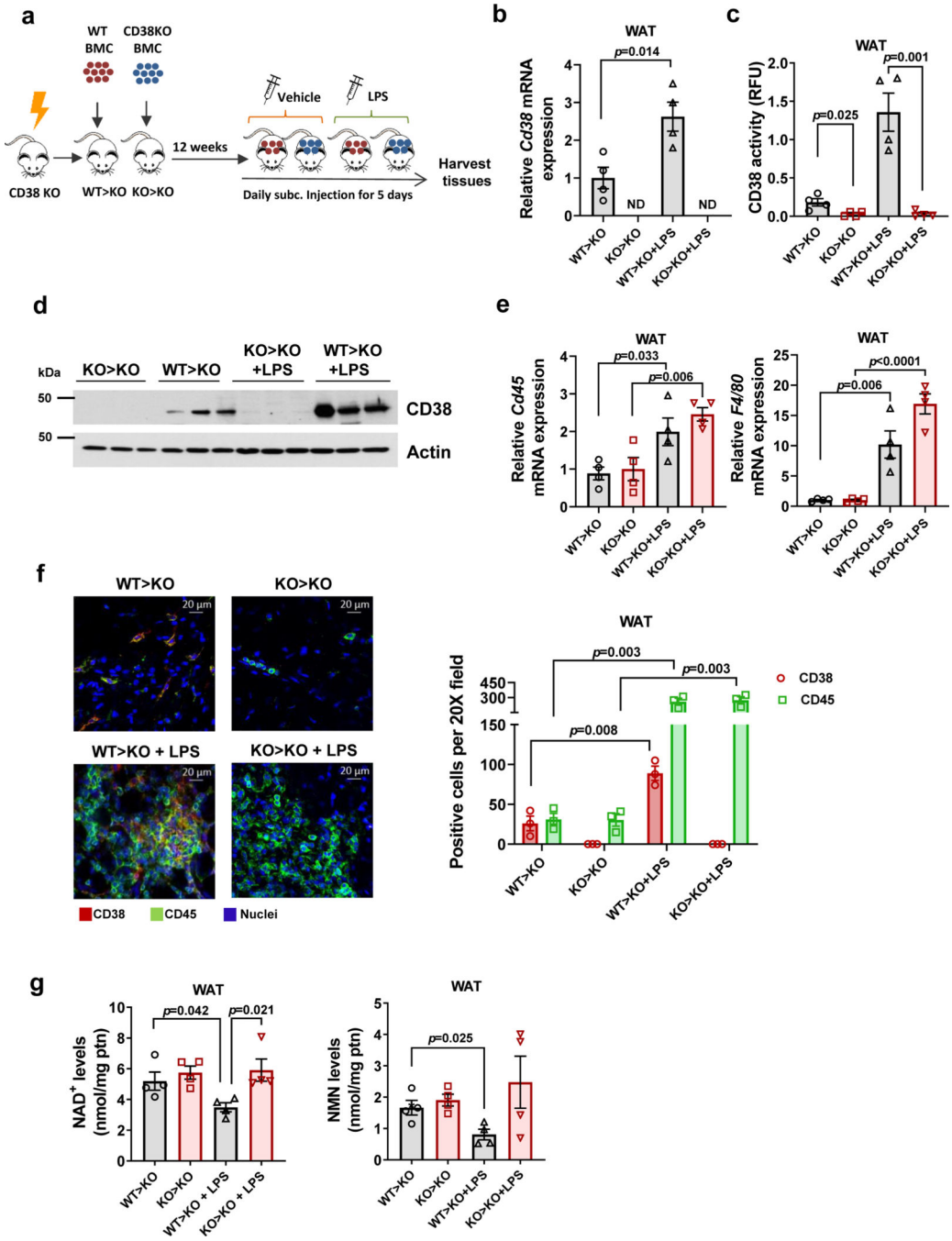

Figure 2. CD38$^+$ inflammatory cells infiltrate WAT and regulate NAD$^+$ levels.

(**a-g**) Sub-lethally irradiated 3 month-old CD38 KO mice were subjected to bone marrow transplant (BMT) with 1×10^6 bone marrow cells (BMC) per animal from either WT (WT>KO) or CD38 KO donors (KO>KO). Twelve weeks after transplantation, µice were subcutaneously injected with LPS (300 µg/kg) or vehicle daily for 5 days and harvested at day 5 (n=4 mice per group). Figure shows analyses in WAT. (**a**) Schematic of experiment. (**b**) Relative *Cd38* mRNA expression measured by qRT-PCR. Expression is relative to WT>KO group. ND denotes non-detectable. (**c**) CD38 activity. (**d**) Representative

immunoblotting showing CD38 levels in 3 mice from each treatment group. (**e**) mRNA expression of *Cd45* and *F4/80* measured by qRT-PCR. Expression is relative to CD38 KO (KO>KO). (**f**) Immunofluorescent staining of CD38 (red) and CD45 (green), representative of 4 mice per group. The graph shows quantification of CD38 and CD45 positive cells from the images (n=3 fields obtained from a representative mouse from each treatment group). (**g**) NAD^+ and NMN levels. Data are mean ± SEM, analyzed by unpaired two-sided t-test.

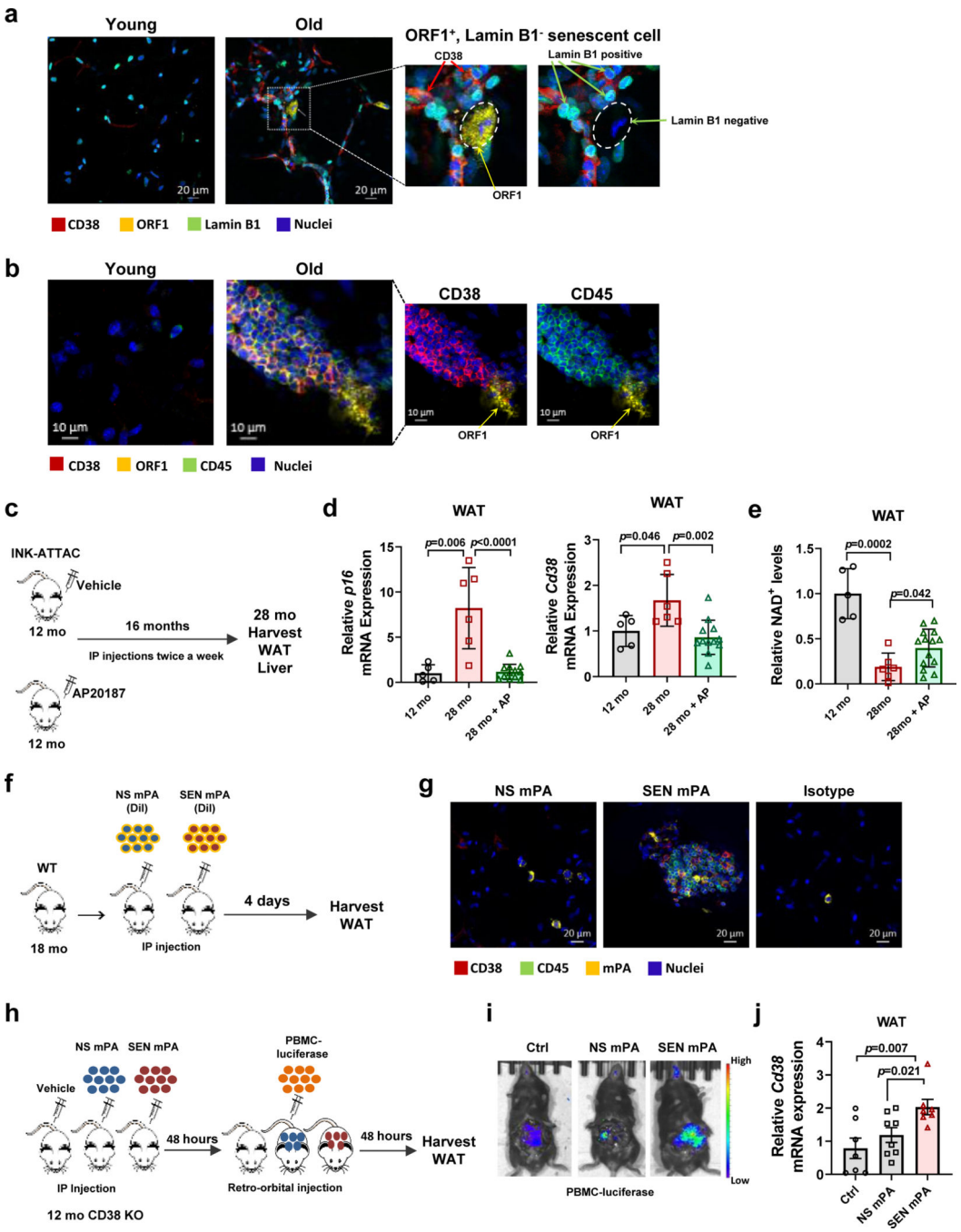

Figure 3. Senescence regulates CD38 accumulation in WAT *in vivo*.

(**a-b**) Immunofluorescent staining of WAT from young (2 month-old) and old (28 month-old) C57BL/6 mice. (**a**) Images of WAT stained with CD38 (red), lamin B1 (green), and ORF1 (yellow), representative of 3 mice per group. Insets show an enlarged portion of old tissue, with and without ORF1 signal, to highlight that $CD38^{+}$ cells are present near $ORF1^{+}$ lamin $B1^{-}$ cells. (**b**) Images of WAT stained with CD38 (red), CD45 (green), and ORF1 (yellow), representative of 6 mice per group. Insets show the image of old WAT with removal of green color channel CD45 signal (left) and with removal of red color channel

CD38 signal (right) to show accumulation of $CD38^+$ $CD45^+$ cells near $ORF1^+$ cells. (**c-e**) 12 month-old INK-ATTAC mice were treated with vehicle or AP20187 for 16 months. At 28 months these mice were euthanized and compared with 12 month-old INK-ATTAC mice. Analyses were performed in WAT. (**c**) Schematic of experiment. (**d**) *p16* and *Cd38* mRNA levels detected by qRT-PCR analysis (12 mo n=5 mice; 28 mo n=6 mice; 28 mo+AP n=12 mice) (**e**) NAD^+ levels (12 mo n=5 mice; 28 mo n=6 mice; 28 mo+AP n=14 mice). (**f-g**) 18 month-old WT C57BL/6 mice were injected IP with DiI-labelled (yellow) senescent (SEN) or non-senescent (NS) mouse pre-adipocytes (mPA) from WT mice. (**f**) Schematic of experiment. (**g**) Immunofluorescent staining of CD38 (red) and CD45 (green) in WAT (representative of n=4 mice per group). Accumulation of $CD38^+$ $CD45^+$ cells was increased when senescent cells were injected. (**h-j**) 12 month-old CD38 KO mice were injected IP with vehicle, senescent (SEN), or non-senescent (NS) mPA from WT mice. 48 hours later, mice were injected with luciferase labeled PBMCs. Control mice received PBMCs only. (**h**) Schematic of experiment. (**i**) Representative images showing increase in $luciferase^+$ PBMCs in mice injected with SEN mPA. (**j**) Relative *Cd38* mRNA levels measured by qRT-PCR in WAT (Ctrl and SEN mPA n=7 mice; NS mPA n=8 mice). Data are mean ± SD (**d,e**) and SEM (**j**), analyzed by unpaired two-sided t-test.

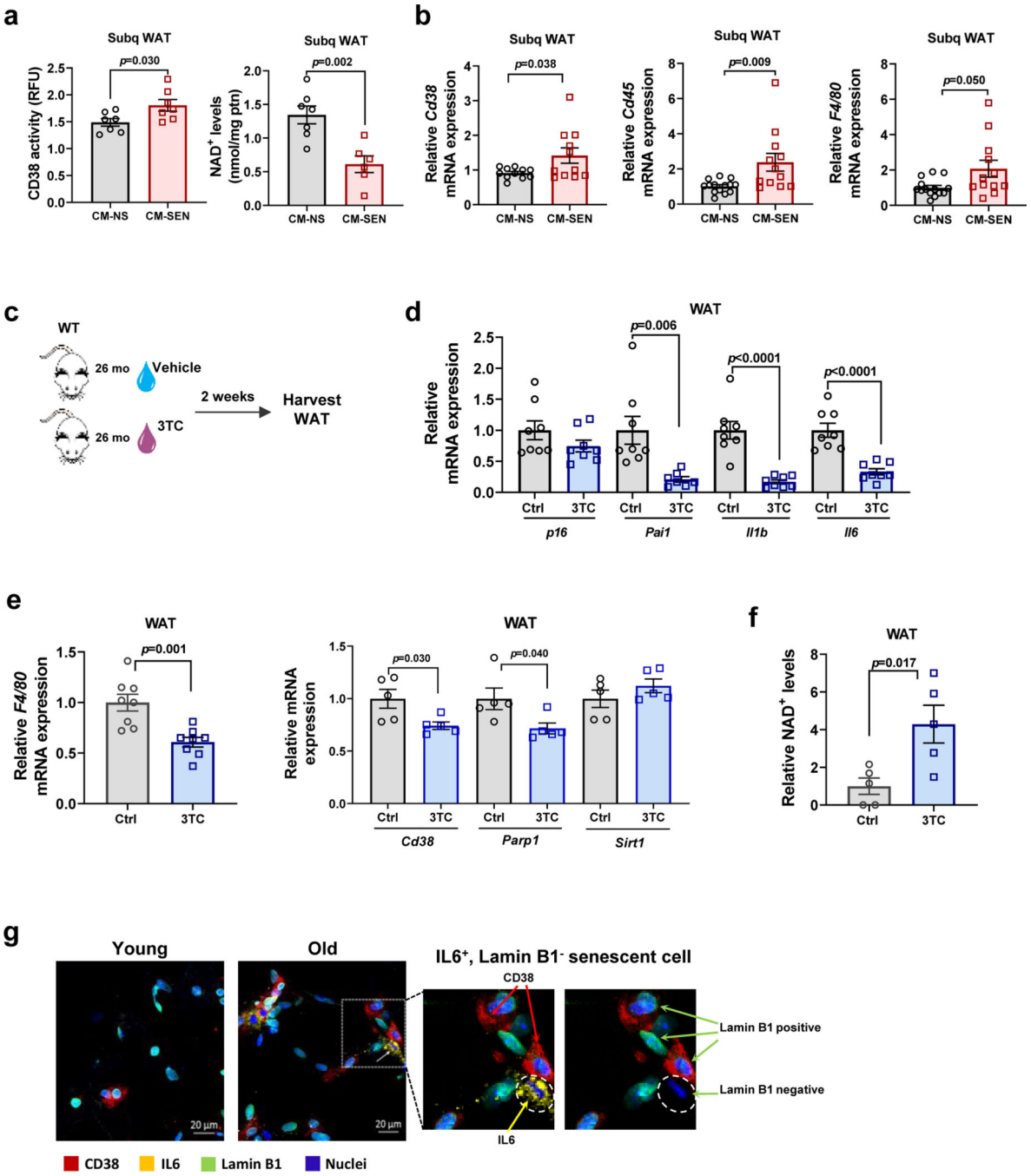

Figure 4. The senescence-associated secretory phenotype (SASP) increases CD38 accumulation and decreases NAD$^+$ levels in WAT *in vivo*.

(**a**-**b**)12 month-old WT mice received daily subcutaneous injection of conditioned media from senescent (CM-SEN) or non-senescent (CM-NS) mouse pre-adipocytes for 5 days, and were harvested at day 5. (**a**) CD38 activity (n=7 mice per group) and NAD$^+$ levels (CM-NS n=7 mice; CM-SEN n=6 mice) were measured in subcutaneous WAT (Subq WAT). (**b**) Relative *Cd38* (n=11 mice per group), *Cd45,* and *F4/80* (CM-NS n=14 mice; CM-SEN n=12 mice) mRNA expression measured by qRT-PCR in Subq WAT. Levels

were relative to CM-NS. (**c-f**) 26 month-old mice were treated with vehicle (Ctrl) or 3TC for 2 weeks. (**c**) Schematic of experiment. (**d**) Relative mRNA levels for *p16* and SASP components measured by qRT-PCR in WAT (n=8 mice per group for all conditions except *Pai1* 3TC where n=7 mice). (**e**) Relative mRNA levels for *F4/80* (n=8 mice per group), *Cd38, Parp1, and Sirt1* (n=5 mice per group) measured by qRT-PCR in WAT. (**f**) Relative NAD^+ levels in WAT (n=5 mice per group). Levels were relative to vehicle-treated mice. (**g**) Immunofluorescent staining of CD38 (red), lamin B1 (green), and IL6 (yellow) in WAT of young (2 month-old) and old (28 month-old) C57BL/6 mice, representative of 4 young and 6 old mice. Insets show enlarged area of old tissue with and without IL6 staining, to highlight that CD38 can be found near $IL6^+$ lamin $B1^-$ cells. Data are mean ± SEM, analyzed by unpaired two-sided *t*-test. Two statistical outliers were identified in the *Cd45* mRNA expression of the CM-SEN-treated animals (with values higher than 16) using the appropriate test in GraphPad Prism 6. These samples were excluded from all the PCR analyses for this experiment. Data were also analyzed by non-parametric Mann-Whitney using the full data set (including the identified statistical outliers) and the *p* value for *Cd45* was 0.002.

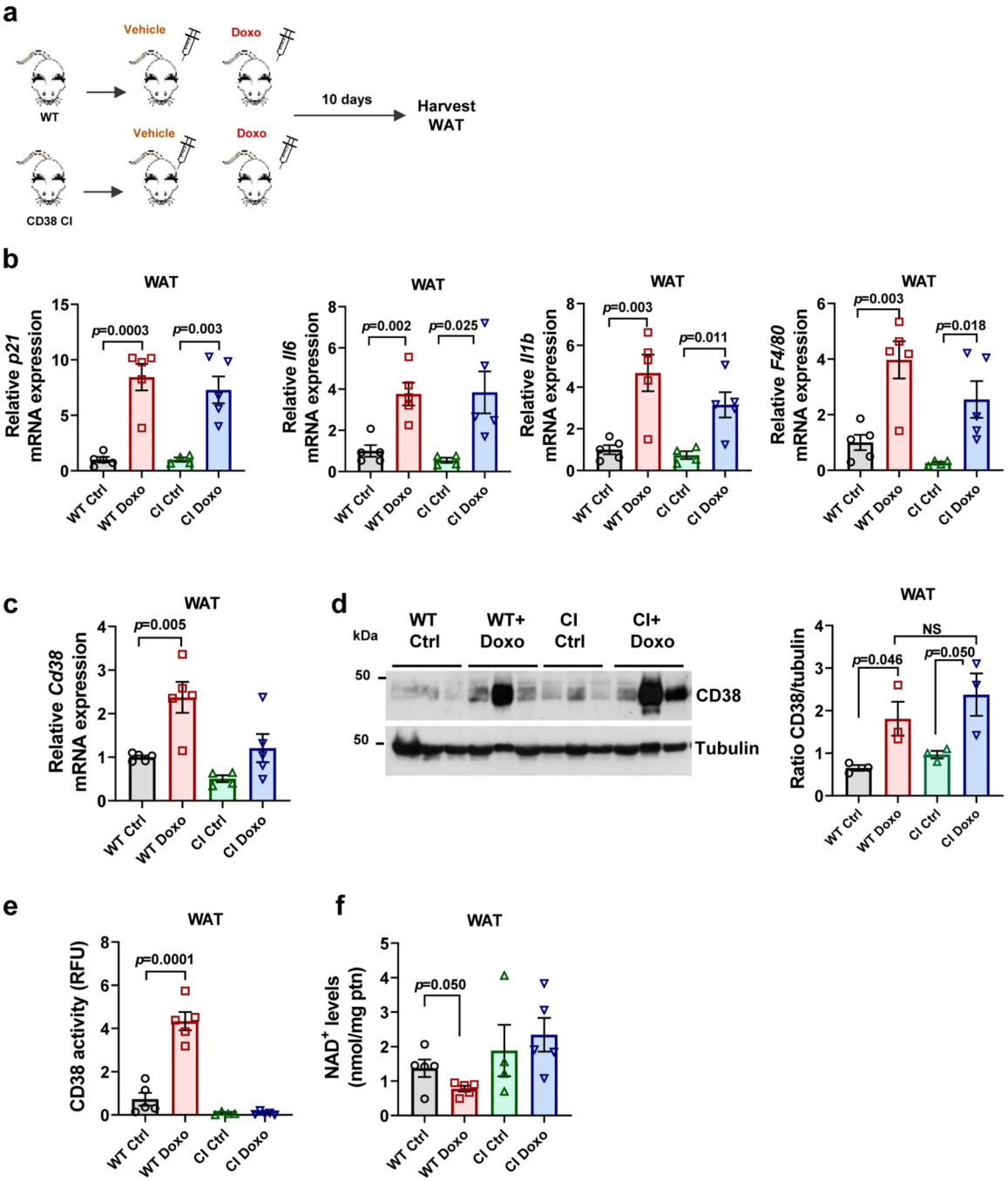

Figure 5. CD38 is required for genotoxic/senescence-induced NAD+ decline.

(**a-f**) 12 month-old WT and transgenic catalytically inactive CD38 (CI) mice were treated with vehicle (Ctrl) or a single dose of doxorubicin (Doxo, 15 mg/kg), and WAT was harvested 10 days later for analyses (CI n=4 mice; WT, WT+Doxo, CI+Doxo n=5 mice per group). (**a**) Schematic of experiment. (**b**) *p21, Il6, Il1b*, and *F4/80* mRNA expression measured by qRT-PCR. (**c**) *Cd38* mRNA expression measured by qRT-PCR. (**d**) Representative immunoblotting of CD38 protein levels and graph showing quantification of CD38 levels. The quantification is a ratio of CD38/tubulin levels (n=3 mice per group).

(**e**) CD38 activity. (**f**) NAD^+ levels. Data are mean ± SEM, analyzed by unpaired two-sided t-test.

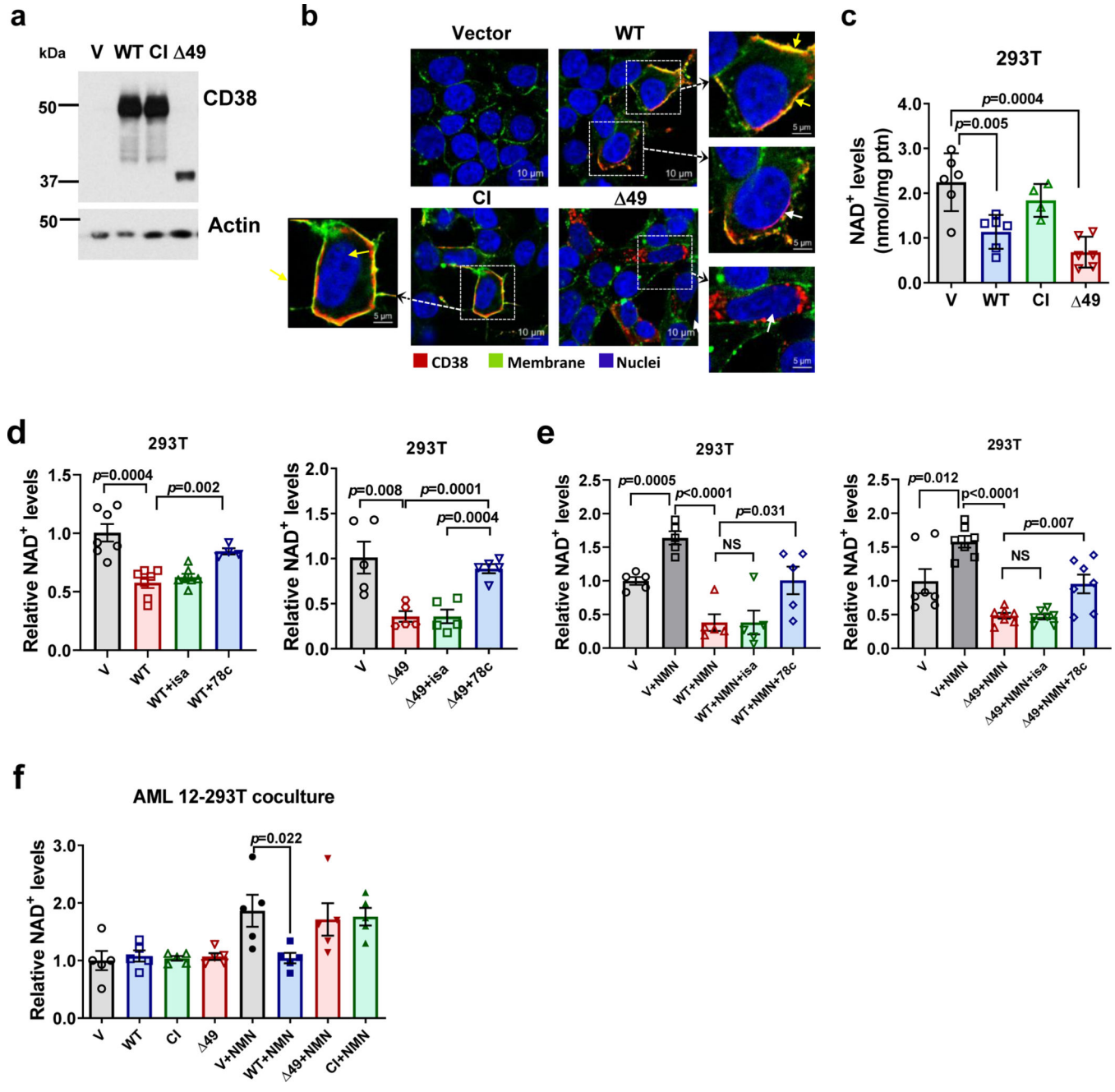

Figure 6. The ecto-enzymatic activity of CD38 regulates availability of extracellular NMN to other cells.

(**a-c**) 293T cells were transfected with vector (V), CD38 WT, CD38 catalytically-inactive (CI), or CD38 Δ49 expression plasmid. (**a**) Representative immunoblotting (of four biologically independent samples) showing CD38 expression in whole cell lysates of 293T cells transfected with CD38 plasmids. (**b**) Immunofluorescence of fixed 293T cells transfected with CD38 plasmids (n=3 biologically independent samples). Cells were labeled with CD38 antibody and a membrane dye, followed by Hoechst staining. Yellow arrows indicate membrane CD38, white arrows show intracellular CD38. (**c**) NAD^+ levels in

transfected 293T cells (V, WT, Δ49 n=6; CI n=4 biologically independent samples). (**d**-**e**) 293T cells were transfected with vector, CD38 WT, or CD38 Δ49 and 20 hours later were incubated with isatuximab (isa, 5 μg/mL) or 78c (0.5 μM). When NMN was added, it was 4 hours after drugs. NAD^+ levels were measured 20 hours after drug treatments (n=5 biologically independent samples). Levels are relative to vector-transfected cells. (**f**) NAD^+ levels in AML12 cells co-cultured with 293T cells expressing CD38 plasmids. 293T cells were treated with and without 200 μM NMN 20 hours after transfection. AML 12 cells were collected 20 hours after addition of NMN (n=5 biologically independent samples). Levels are relative to vector-transfected cells. Data are mean ± SEM, analyzed by unpaired two-sided *t*-test, NS=non-significant.

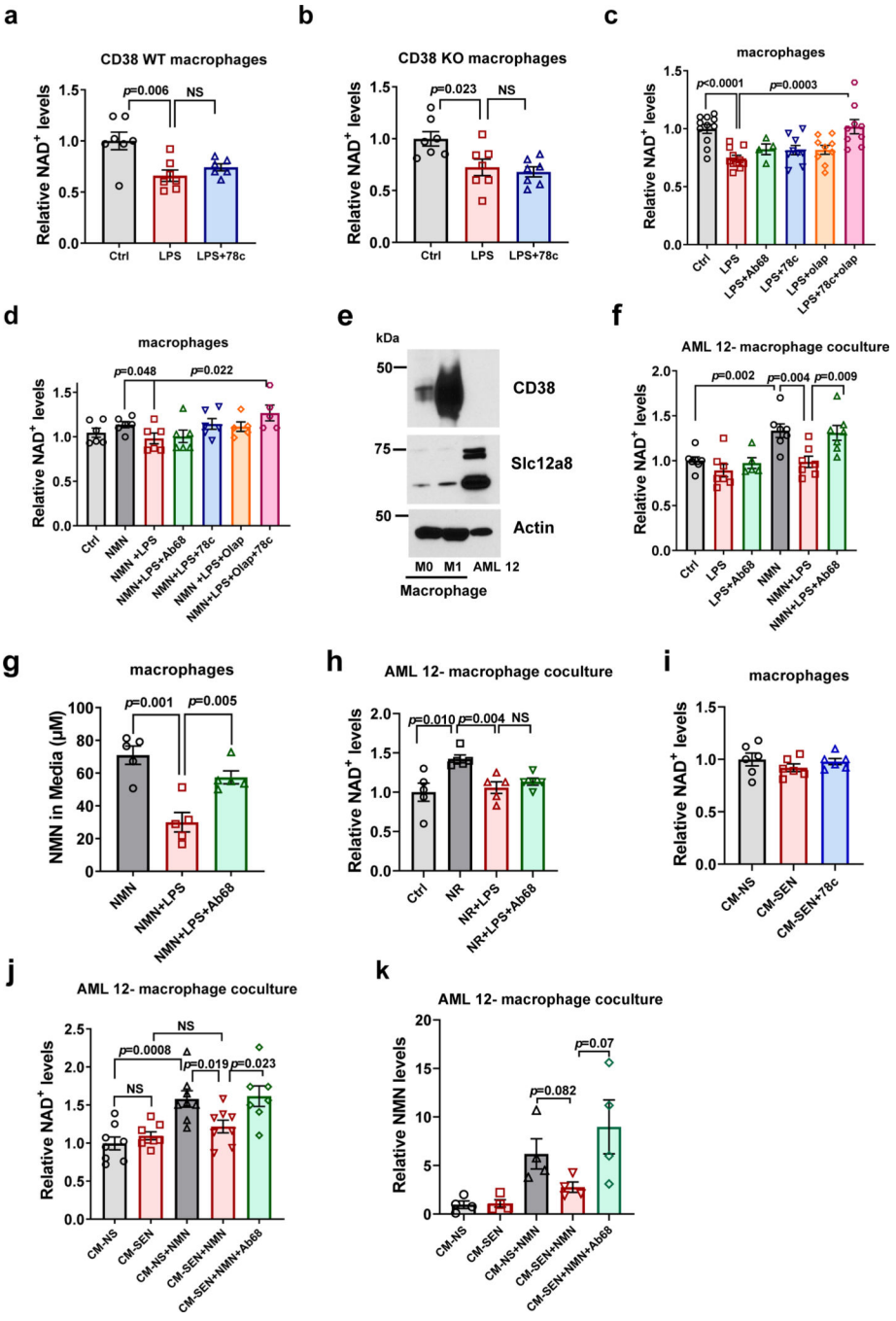

Figure 7. Regulation of NAD$^+$ and NMN levels by CD38 in macrophages.

(**a**-**b**) NAD$^+$ levels in BMDM from 3 month-old WT (**a**) and CD38 KO (**b**) mice. Macrophages were treated with vehicle (Ctrl) or LPS (100 ng/mL), with or without 78c (0.5 μM) (n=7; with exception of WT LPS+78c where n=6 biologically independent samples). (**c**-**k**) BMDM isolated from 18 month-old WT mice. (**c**) NAD$^+$ levels in macrophages treated with LPS (100 ng/mL), Ab68 (5 μg/mL), 78c (0.5 μM), and olaparib (olap, 5 μM) (Ctrl, LPS n=11; LPS+78c n=4; LPS+78c, LPS+olap, LPS+78c+olap n=9 biologically independent samples). (**d**) Macrophages were treated with LPS (100 ng/mL), Ab68 (5 μg/mL), 78c

(0.5 μM), and olaparib (olap, 5 μM). 3 hours later, 300 μM NMN was added and cells were collected 20 hours later for NAD^+ measurements (n=7 except for NMN+LPS+olap and NMN+LPS+olap+78c where n=6 biologically independent samples). (**e**) Representative immunoblotting of three biologically independent samples of M0 or M1 (LPS-treated) macrophages and AML12 lysates showing CD38 and Slc12a8. (**f**) NAD^+ levels in AML 12 cells cocultured with macrophages. Macrophages were treated with LPS (100 ng/mL), Ab68 (10 μg/mL), and NMN (200 μM) before incubation with AML 12 cells (n=7 biologically independent samples except for LPS+Ab68 where n=5). (**g**) Extracellular NMN in culture media after treatment of macrophages with 100 μM NMN, LPS (100 ng/mL), and Ab68 (5 μg/mL). LPS was given 9 hours before NMN, and Ab68 was given 3 hours before NMN. Cells were incubated with NMN for 12 hours before media was collected (n=5 biologically independent samples). (**h**) NAD^+ levels in AML 12 cells cocultured with macrophages. Macrophages were treated with LPS (100 ng/mL), Ab68 (10 μg/mL), and NR (200 μM) before incubation with AML 12 cells (n=5 biologically independent samples). (**i**) NAD^+ levels in macrophages treated with CM from non-senescent (CM-NS) or senescent mouse pre-adipocytes (CM-SEN or CM-SEN + 78c (0.5 μM)) (n=6 biologically independent samples). (**j-k**) NAD^+ (n=8 biologically independent samples except for CM SEN+NMN+Ab68 where n=7) and NMN levels (n=4 biologically independent samples) in AML 12 cells cocultured with macrophages. Macrophages were treated with CM-NS or CM-SEN from mouse preadipocytes, Ab68 (10 μg/mL), and NMN (200 μM) before incubation with AML 12 cells. All levels are relative to their respective control (Ctrl or CM-NS). Data are mean ± SEM, analyzed by unpaired two-sided t-test.

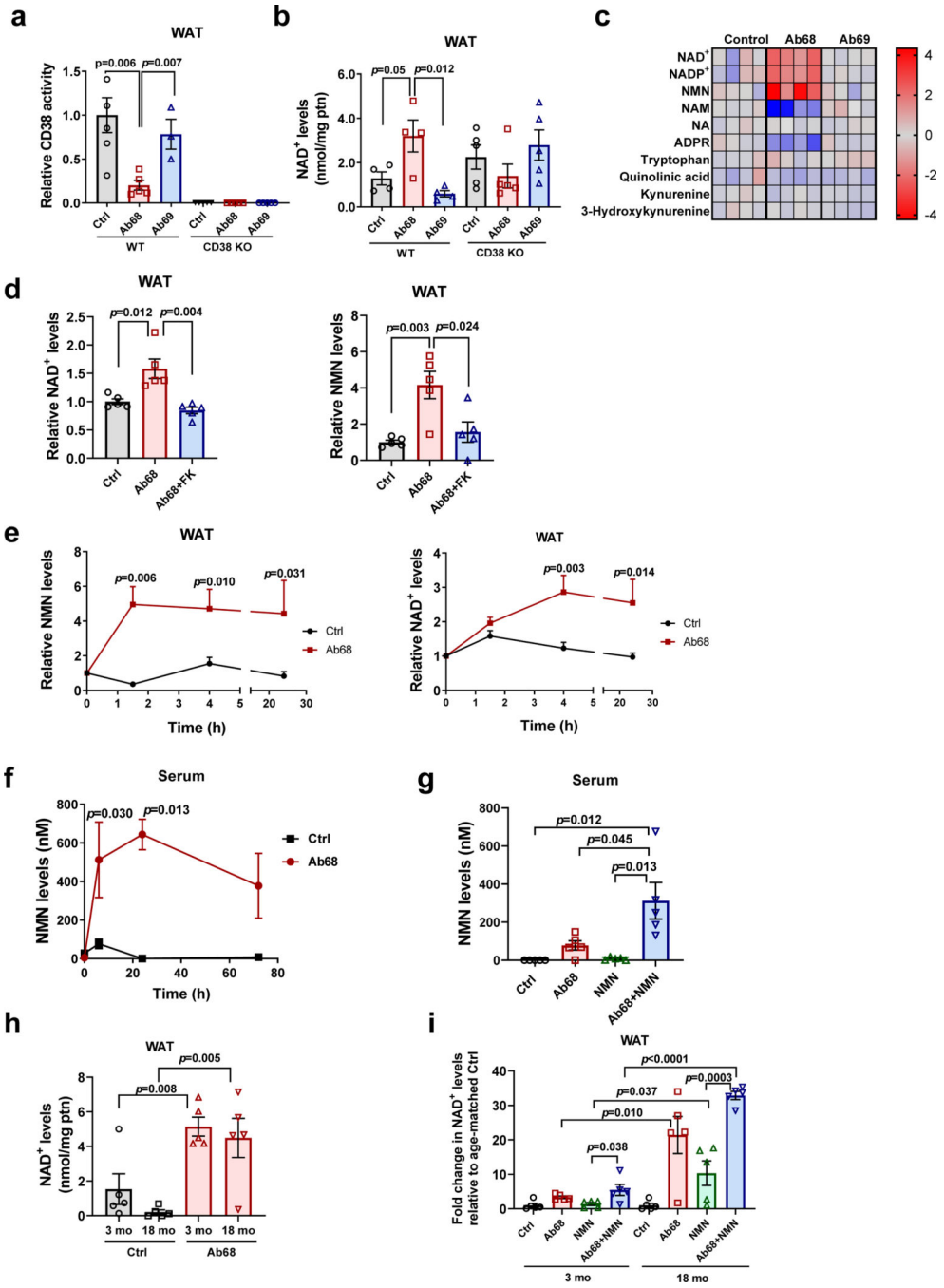

Fig. 8. Blocking CD38 extracellular enzymatic activity regulates NMN, NAD$^+$ levels, and CD38 activity *in vivo*.

(**a-c**) 4 month-old WT and CD38 KO mice were treated with vehicle (Ctrl), Ab68 (5 mg/kg), or Ab69 (5 mg/kg) by intraperitoneal (i.p.) injection on day 1 and day 5, and euthanized on day 8. (**a**) Relative CD38 activity in WAT. Levels are relative to control WT (Ctrl) (WT Ctrl n=6; WT Ab68, CD38 KO n=5; WT Ab69 n=3 mice). (**b**) NAD$^+$ levels in WAT (WT n=4 mice; CD38 KO n=5 mice). (**c**) Heat map showing levels of metabolites in WT mice treated with Ab68 and Ab69 relative to Ctrl (n=4 mice per group). (**d**) 4 month-old WT mice were

treated withFK866 (FK) (25 mg/kg) and/or Ab68 (5 mg/kg) (n=5 mice per group). NMN and NAD^+ levels were measured in WAT. Levels are relative to Ctrl. (**e**) 22 month-old WT mice were injected i.p. with a single dose of vehicle (Ctrl) or Ab68 (5 mg/kg), euthanized at different time points, and NMN and NAD^+ levels measured in WAT. Graphs show the time course of the relative increase of NMN or NAD^+ in vehicle and Ab68-treated over levels at time 0 (n=4 mice per group). (**f**) 18 month-old mice were injected i.p. with a single dose of vehicle (Ctrl) or Ab68 (5 mg/kg) and mice were euthanized at different time points. NMN levels were measured in serum (Ctrl, 0, 24, 72 hours, and Ab68 72 hours n=4 mice per group; Ab68 24 hours n=5 mice; Ctrl 6 hours n=8 mice; Ab68 6 hours n=9 mice). (**g**) 18 month-old WT mice were injected i.p. with vehicle (Ctrl, NMN groups), 5 mg/kg Ab68 (Ab68, Ab68+NMN groups), with and without 500 mg/kg NMN. Serum NMN levels were determined (n=5 mice per group). (**h**) Absolute NAD^+ levels in WAT of 3 month-old (young) and 18 month-old (old) mice were determined 3 days after treatment with a single injection i.p. injection of vehicle (Ctrl) or 5 mg/kg Ab68 (n=5 mice per group). (**i**) 3 month old and 18 month-old mice were treated with Ab68 and NMN as described in panel (**g**) and WAT levels of NAD^+ were measured. NAD^+ levels after each treatment are expressed relative to its age-matched control (vehicle treatment) (n=5 mice per group). Data are mean ± SEM, analyzed by unpaired two-sided *t*-test, except for **(e-f)** where data are analyzed by two-way ANOVA.

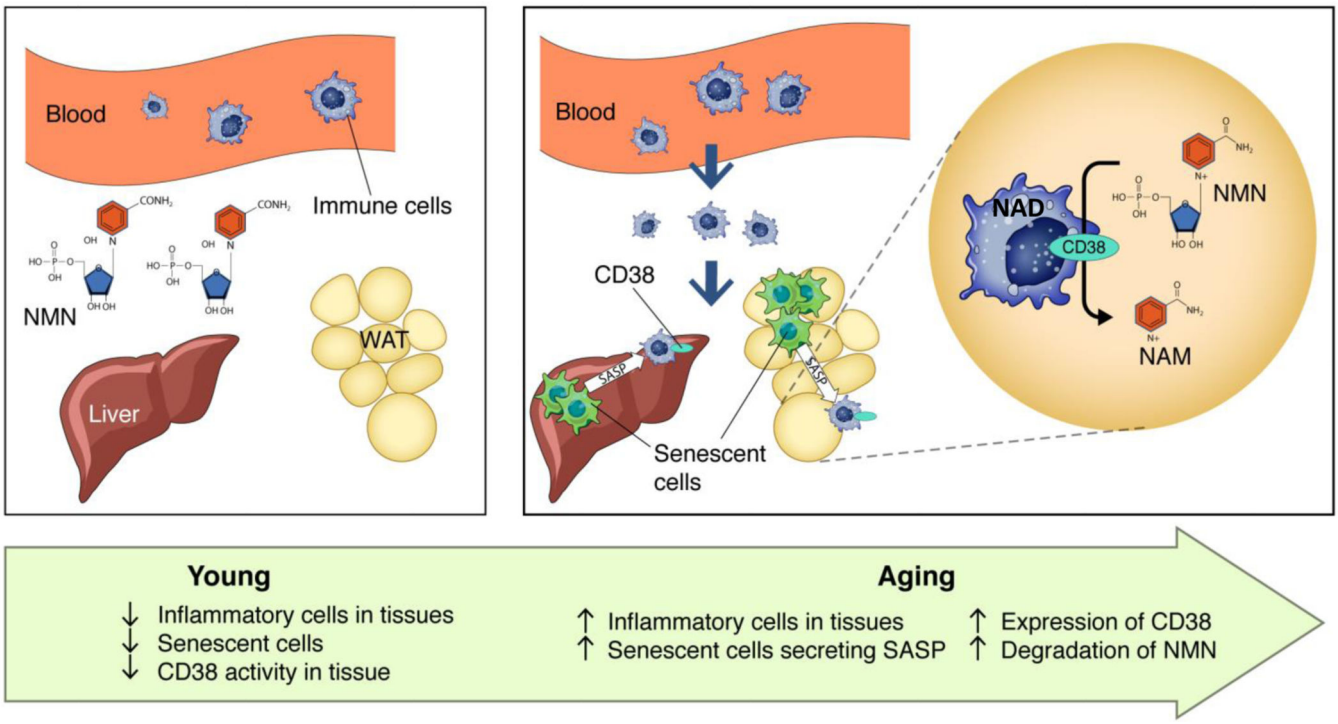

Fig. 9. Schematic representation of the role of cellular senescence and sterile inflammation in the regulation of CD38 and NMN degradation.

In young mice, levels of $CD38^+$ inflammatory cells and senescent cells in tissues are lower than older mice. During aging there is an increase in senescent cells that, at least in part, through their senescence associated secretory phenotype (SASP), promotes accumulation of $CD38^+$ immune cells. The ecto-enzymatic activity of CD38 in immune cells degrades NMN extracellularly, preventing the NMN-induced NAD^+ boosting in other cells in the tissue.